Dune dynamics in a tidal inlet channel of the Danish Wadden Sea

Dissertation zur Erlangung des Doktorgrades der Naturwissenschaften

im Fachbereich Geowissenschaften der Universität Bremen

vorgelegt von

Verner B. Ernstsen

Bremen, Dezember 2005

Tag des Kolloquiums:

17. Februar 2006

Gutachter:

1. Priv. Doz. Dr. Dierk Hebbeln

2. Prof. Dr. Burghard W. Flemming

Prüfer:

1. Prof. Dr. Gerhard Bohrmann

2. Prof. Dr. Tobias Mörz

Contents

Preface

This Ph.D. study has been carried out in the period January 2003 to December 2005 within the projects *Constructional Impacts on Coastal Dynamics* (Project D1) and *Morphodynamics and Sediment Budgets of Shallow Shelf Seas* (Project C4) at the Research Center Ocean Margins, University of Bremen, Department of Geosciences.

The work has resulted in seven papers either published in or submitted to peer reviewed journals, three papers as first author and four papers as co-author. Five of the papers summarise the results of the investigations in the Grådyb tidal inlet channel in the Danish Wadden Sea and are included in this thesis (Paper I-V in Chapter 2-6). Two papers, to which contributions have been made as co-author, presenting results from investigations in the German part of the Wadden Sea are not included in this thesis. One of these two papers is on the effect of extreme events on morphodynamics in relation to numerical model shortcomings and the other is on predicting local scour depth from dune dynamics:

Observed storm surge morphodynamics and implications to numerical modelling schemes
Winter, C., R. Riethmüller, M. Heineke, V.B. Ernstsen and R. Noormets
Proceedings of the ASCE Coastal Dynamics '05 Conference (in press)

Implications of bedform dynamics on the prediction of local scour in tidal inlets: a case study from the southern North Sea
Noormets, R., V.B. Ernstsen, A. Bartholomä, B.W. Flemming and D. Hebbeln
Geo-Marine Letters (submitted)

Acknowledgements

The projects within which the Ph.D. study was carried out are financed by the German Science Foundation. Head of the projects are Prof. Dr. Gerold Wefer, Prof. Dr. Burg W. Flemming and Priv. Doz. Dr. Dierk Hebbeln. Supervisor of the Ph.D. study was Priv. Doz. Dr. Dierk Hebbeln. In this connection thanks to Burg and Dierk for letting me pursue my ideas and for always having time when deadlines got hot.

However, several people have contributed to this study. The crew of the RV Senckenberg as well as Dr. Elke Tilch are acknowledged for assisting during the cruises. Likewise thanks to the technicians at the Senckenberg Institute, Marine Science Department for assisting with the infrastructure before and after the cruises as well as for the assistance in the laboratory.

Thanks to Erik Brenneche, Port of Esbjerg, for promptly providing tide gauge data, and for answering any questions concerning the operations related to Esbjerg Harbour.

Prof. Dr. Terry Healy is thanked for making it possible to spend a two months externship at the Coastal Marine Group, University of Waikato, Department of Earth Sciences, New Zealand. Here also thanks to Dirk Immenga and Brad Scarfe for a nice working atmosphere and inspiring discussions.

Special thanks to Dr. Alex Bartholomä and Dr. Jesper Bartholdy for inspiring discussions. We do not always agree, but that is just an additional motivation to keep going.

Dr. Christian Winter is warmly thanked for endless discussions of crazy and less crazy ideas, but most of all for a cosy, open and very inspiring working atmosphere.

In particular thanks to Dr. Riko Noormets for making the last three years a true learning process in terms of doing science, especially for guarantying high-quality data and for always giving constructive criticism of my work.

Finally, warm thanks to family and friends back home, you guys dropping by really warms. However, one is above them all, my deepest thanks to you Sonja, especially for distracting my otherwise absent mind in the last couple of months, keeping me somehow in balance despite the stress, and for giving me the most beautiful title of all.

Summary

Although flow transverse bedforms have been studied for more than a century from field studies, laboratory flume experiments and mathematical models, their initiation, development and dynamics are far from being fully understood.

The objective of this study is to investigate the dynamics of dunes on different spatial and temporal scales. The study area is in the Grådyb tidal inlet channel, which forms the navigation channel to Esbjerg, in the Danish Wadden Sea. State of the art swath bathymetry at centimetre-scale resolution and precision is applied in order to observe and quantify processes on both long-term (annual) and short-term (single semi-diurnal tidal cycle) scales. In addition, bed material samples and high-resolution measurements of the flow are obtained in order to relate the dune dynamics to the sediment dynamics and prevailing hydrodynamics. The main results from the investigations are summarised in five papers.

The precision of the applied swath bathymetry system under normal field survey conditions is determined by repetitive bathymetric measurements of a shipwreck over three years, showing a precision in all three directions on centimetre-scale (Paper I).

Large barchanoid-shaped dunes are shown to develop due to an increase in dune migration from the centre towards the sides of the channel, resulting from a decrease in dune height from the centre towards the sides of the channel. The decrease in dune height is ascribed to an equivalent decrease in grain size from the centre towards the sides of the channel, as water depth and flow velocity are uniform across the channel. Measured annual bedload transport rates are significantly over-predicted by common and widely applied bedload transport formulae (Paper II).

Quantifying sediment transport during a single semi-diurnal tidal cycle shows that bedload transport rates are higher on the crests than in the troughs of the large compound dunes. Net dune migration can be flood directed during a single tidal cycle, despite an annual net ebb-directed dune migration. Finally, measured bedload transport rates during single tidal cycles are also significantly over-predicted by common and widely applied bedload transport formulae (Paper III).

Relating dune dynamics to hydrodynamics during a single semi-diurnal tidal cycle (same as in Paper III) shows that the higher dune crest than trough mobility is due to higher flow velocities at the dune crest. In addition, bed material goes into suspension with accelerating

ebb flow and settles with decelerating ebb flow, resulting in an average erosion and accretion of the bed of ~6.5 cm. During flood tide the bed is practically stable. This results in a potential net export of sediment to the ebb tidal delta during every single semi-diurnal tidal cycle. Furthermore, the height of the compound dunes follows water depth, which acts as a limiting factor to dune growth, whereas the height of the superimposed stoss side dunes follows flow velocity, i.e. superimposed stoss side dunes are water depth-independent (Paper IV).

General statements relating dune dimensions directly to the form-corrected Shields parameter are established from the depth-independent superimposed stoss side dunes, showing that dune dimensions are primarily controlled by flow strength and grain size, and that water depth can act as an additional limiting factor to dune growth. This can be used e.g. to give a first approximation of flow conditions, as long as information on grain size and dune dimensions are available, as it is often the case in oceanographic surveys (Paper V).

The introduction of high-resolution, high-precision swath bathymetry has truly revolutionised the study of bedform dynamics. The spatial depiction and the possibility to precisely quantify dimensions and dynamics have turned field studies into quasi laboratory experiments. Although it is impossible to steer the controlling parameters (flow velocity and grain size) and limiting factors (water depth), as in flume studies, it is possible to precisely measure flow velocity, grain size and water depth as well as the related bedform dynamics. However, considerable limitations are still present in studies of bedform dynamics, e.g. the absolute quantification of suspended sediment in the water column as well as the determination of near-bed flow velocities without disturbing either the flow or the bed.

Chapter 1: General introduction

1.1 Motivation and objectives

Tidal inlet channels are narrow natural waterways that connect the open sea with a lagoon, as is generally the case in barrier-island systems; and often these waterways form the navigation channels to sheltered harbours. The narrow channels typically generate high flow velocities (>1 m/s), and accordingly the beds are generally composed of sandy material and covered with flow transverse bedforms [e.g. *Boothroyd and Hubbard*, 1975].

Flow transverse bedforms have earned a wide variety of descriptive names, e.g. ripples, ridges, dunes, megaripples, giantripples, sandwaves. However, despite the wide spectrum of morphologies (excluding antidunes), they are all located in the lower flow regime, and the wide variety of forms is simply a reflection of secondary effects such as changing water depth, unsteady flow, or reversing flow. Throughout this thesis the bedforms are described according to the classification recommended by a panel of twenty-seven scientists participating in a symposium convened in 1987 by the 'SEPM Working Group on Bedforms and Bedding Structures'. Ripples ($L < 0.6$ m) and dunes ($L > 0.6$ m) are distinguished on the basis of bedform length (L), and dunes are further divided into categories of small (L = 0.6-5 m), medium (L = 5-10 m), large (L = 10-100 m) and very large ($L > 100$ m). The size classes are not natural boundaries as the flow transverse bedforms form a continuum [*Ashley*, 1990].

Flow transverse bedforms have been studied for more than a century [*Darwin*, 1883] and since around 1960 detailed studies on their initiation, development and dynamics have been conducted both in the field [e.g. *Cartwright and Stride*, 1958], in laboratory flumes [e.g. *Simons and Richardson*, 1961] and using mathematical models [e.g. *Kennedy*, 1963]. However, their initiation, development and dynamics are far from being fully understood [*Hulscher and Dohmen-Janssen*, 2005]. Apart from a basic research interest in studying the complex interaction between flow, sediment and form, the understanding of bedform dynamics also has an increasing relevance in a socio-economic perspective. The deadweight tonnage of cargo ships, e.g. container ships and bulk carriers, is continuously increasing. This increase is accompanied by a corresponding increase in the draft of the ships, which leads to considerable increases in dredging expenses in order to maintain safe navigation depths in e.g.

tidal inlet channels. Understanding bedform dynamics in tidal inlet channels may provide possibilities to reduce maintenance costs significantly.

Studies of flow transverse bedforms in tidal inlet channels are relatively few, and can roughly be grouped in four categories based on the applied survey methods which all reflect the state of the art at that time:

1) In the 1960's and 1970's tidal inlet channel morphology was resolved two-dimensionally using single beam echo sounders. Apart from a single study in Jade Bay, Germany [*Reineck*, 1963], all other studies were conducted along the east coast of the USA, i.e. in St. Andrew Bay [*Salsman et al.*, 1966], Chesapeake Bay [*Ludwick*, 1972], Parker and Essex Estuary [*Boothroyd and Hubbard*, 1974 and 1975] and Chatham Harbor Estuary [*Hine*, 1975]. The single beam echo sounders provided the possibility to determine bedform dimensions and net migration direction from bedform asymmetry, but due to inadequate positioning migration rates were impossible to determine from sequential echo sounding profiles. Instead, bedform migration was determined from stakes installed by divers on the channel bed [*Salsman et al.*, 1966; *Ludwick*, 1972; *Boothroyd and Hubbard*, 1974 and 1975], and these diver observations actually provided very detailed information even of the dynamics of the superimposed dunes over short time scales, such as single semi-diurnal tidal cycles [*Boothroyd and Hubbard*, 1974 and 1975].

2) In the late 1970's and 1980's spatial images of tidal inlet channel morphology was achieved by applying side scan sonar technology. The line of surveys along the east coast of USA was continued in Delaware Bay Estuary [*Knebel*, 1989], and in addition, surveys were conducted on the west coast in Central San Francisco Bay [*Rubin and McCulloch*, 1979 and 1980]. Side scan sonar images gave the possibility to determine net dune migration directions in space based on dune asymmetry, revealing varying transport paths in the channels; however, inadequate positioning still made it impossible to determine accurate migration rates from sequential surveys. *Rubin and McCulloch* [1979 and 1980] got around the problem of inadequate positioning by installing a channel bed-mounted rotating side scan sonar, which made the determination of dune migration rates possible. Studies were also conducted in a tidal inlet channel in Moreton Bay, Australia [*Harris and Jones*, 1988]. They applied an alternative method to determine bedform migration, namely comparison of sequential air photos; however, this method showed to be limited to areas with water depths shallower than 10 m, i.e. inapplicable in tidal inlet channels serving as navigation channels to larger harbours.

3) In addition, during the 1990's the internal structure of the flow transverse bedforms were recorded using seismics, as done by *Harris et al.* [1992] in Moreton Bay, Australia. Furthermore, improved positioning provided the possibility to determine at least annual migration rates from sequential single beam echo sounder profiles, as shown by *Bartholdy et al.* [2002] in the Grådyb tidal inlet channel, Denmark.

4) Recently, a high-resolution acoustic ripple profiler was applied in the Barra Nova tidal inlet, Portugal, from a jack-up barge resolving two dimensional ripple dynamics over time scales of a few minutes [*Williams et al.*, 2003a and b].

To the knowledge of the author, no other detailed studies on transverse bedforms in tidal inlet channels have been conducted.

The objective of this study is to investigate dune dynamics on different spatial and temporal scales in the Grådyb tidal inlet channel, which forms the navigation channel to Esbjerg, in the Danish Wadden Sea (Fig. 1.1). State of the art swath bathymetry at centimetre-scale resolution and precision is applied and gives the opportunity to observe and quantify processes in both space and time, which were impossible to resolve applying older techniques. In addition, bed material samples and high-resolution measurements of the flow were obtained in order to relate the observed dune dynamics to the sediment dynamics and prevailing hydrodynamics.

1.2 Study area

Surveys were conducted in the Grådyb tidal inlet channel on the Danish west coast between the barrier spit of Skallingen to the northwest and the barrier island of Fanø to the southeast. The channel connects the northern-most tidal basin of the Wadden Sea with the adjacent North Sea and forms the navigation channel to Esbjerg (Fig. 1.1).

1.2.1 Earlier work in the area

Studies of the morphodynamics of the barrier system, with the main focus being on the barrier spit Skallingen, have a long tradition beginning with the pioneering work of *Nielsen* [1935]. Since then work has been conducted along the coast on cross-shore sediment transport [*Aagaard et al.*, 2002 and 2004a] and long-shore sediment transport [*Aagaard et al.*, 2004b], on the beach and in the fore dunes [*Aagaard et al.*, 1998; *Christiansen and Davidson-Arnott*, 2004], on the spit terminus and platform [*Vinther et al.*, 2004], on the tidal flats [*Bartholdy*

and Folving, 1986; *Lund-Hansen et al.*, 2004] and on the salt-marshes [*Christiansen et al.*, 2002; *Nielsen and Nielsen*, 2002; *Bartholdy et al.*, 2004]. In the Grådyb tidal inlet channel, work has been carried out on the import and export of fine-grained sediment [*Bartholdy and Anthony*, 1998], which resulted in a conceptual model describing transport, deposition and resuspension of the fine-grained material [*Bartholdy*, 2000]. The dunes in the Grådyb tidal inlet channel have been studied by *Bartholdy et al.* [2002] based on side scan sonar images and a time series (1991-1999) of single beam echosounder profiles along the centre line of the navigation channel.

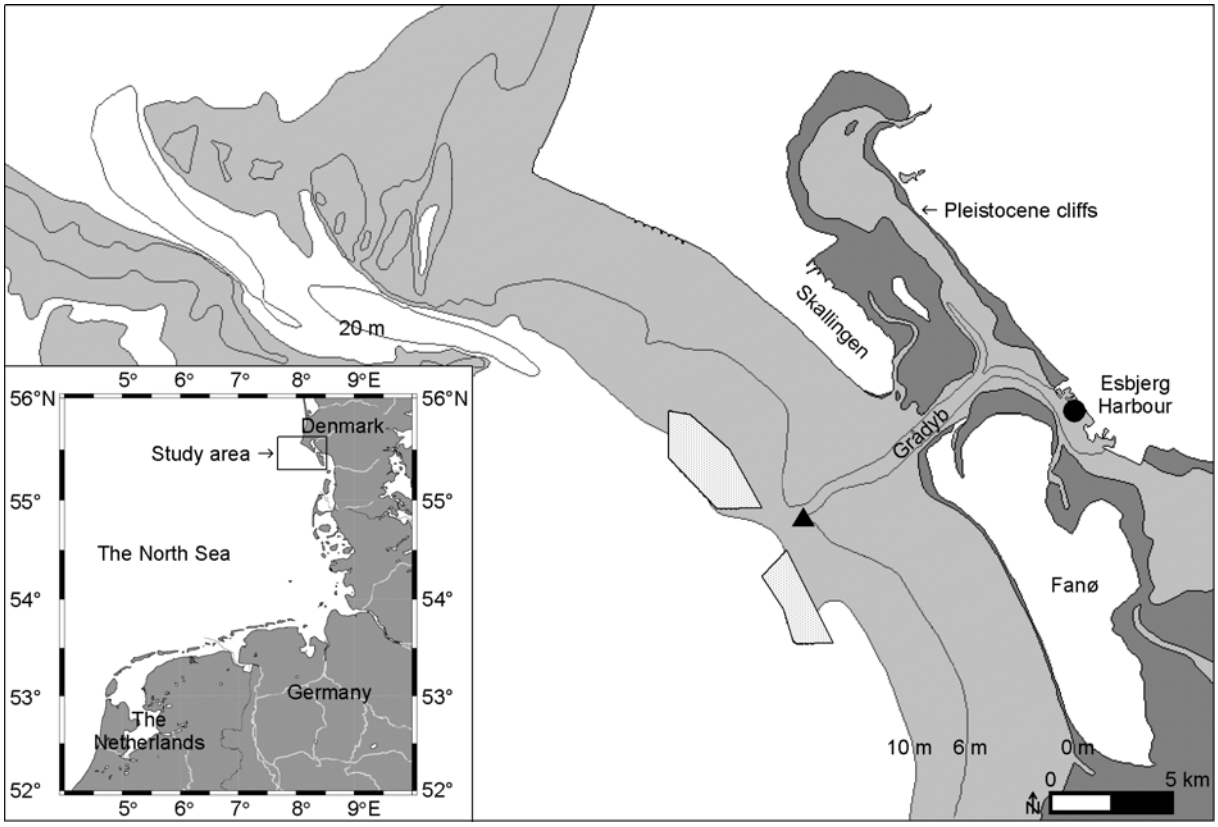

Fig. 1.1 Location of the study area in the Grådyb tidal inlet channel between the barrier spit of Skallingen and the barrier island of Fanø in Denmark. Water depths are relative to mean low water springs (MLWS). Triangle and dot mark the tide gauges at Grådyb Bar and in the Port of Esbjerg, respectively. The two encircled dotted zones are dumping sites for dredged material.

1.2.2 Physical setting

The tides in the Grådyb tidal area are semi-diurnal with a mean tidal range of about 1.5 m (1.3 m at neap tide and 1.7 m at spring tide) and a tidal prism in the order of 150 x 10^6 m^3 [*Bartholdy and Anthony*, 1998]. The width of the tidal inlet channel is roughly 1 km and the

mean depth is 10-13 m. The channel is ebb-dominated with maximum depth-averaged ebb and flood current velocities around 1.3 m/s and 1.1 m/s, respectively [*Ernstsen et al.*, 2005].

The bed of the channel is covered with large to very large compound dunes with superimposed small to medium dunes [*Bartholdy et al.*, 2002]. The bed material is composed of moderately well to well sorted medium to coarse sand with mean grain sizes ranging from 0.3 to 0.7 mm [*Bartholdy et al.*, 2002]. There are two sediment sources in the area: 1) the Pleistocene cliffs lining the mainland shore of the back-barrier tidal basin (Fig. 1.1) which supply medium to coarse sand, and 2) the near-shore region of the open coast which supplies fine sand to the tidal inlet [*Bartholdy et al.*, 2002].

On the seaward side of the tidal inlet, the channel cuts through a submerged ebb tidal delta (Fig. 1.1), which is dredged in order to maintain a minimum depth of 10.3 m MLWS in the navigation channel [*Bartholdy and Anthony*, 1998].

The average wave height in the adjacent North Sea is around 0.5 m [*Aagaard et al.*, 1995]. During storms single waves may reach a height of 4 m in deep water [*Aagaard*, 2002]. Based on numerical model results, storm waves are not expected to have a marked influence on the dominating dynamics in the tidal inlet channel; and the fact that the large to very large compound dunes in the channel can be recognised and followed for years emphasizes this [*Bartholdy et al.*, 2002].

1.3 Methods

1.3.1 Bathymetry

Bathymetry has been recorded using a SeaBat™ 8125 (RESON) multibeam echo sounder (MBES) system operating at 455 kHz and the 6042™ Version 7 (QINSY/RESON) data collecting and processing software package. The vertical resolution of the MBES system is in a sub-centimetre scale [*www.reson.com*]. The horizontal resolution is a function of water depth and vessel speed. For instance, a water depth of 15 m results in an across-track resolution of 0.13-0.51 m due to the across-track beam width of 0.5°; at a vessel speed of 2.6 m/s (5 kn) the along-track resolution is 0.10 m. The MBES system was coupled with an AQUARIUS™ 5002 MK/SK (THALES) dual frequency (L1/L2) Long Range Kinematic (LRK™) Global Positioning System (GPS). The horizontal and vertical accuracy of the positioning system is within 0.01 m at a 95% confidence interval at a range up to 40 km [*Gounon and Erceau*, 1998]. Coordinates are presented in relation to the Universal Transverse

Mercator Zone 32 (UTM32) projection with the World Geodetic System 1984 (WGS84) ellipsoid as the underlying model of the Earth. Altitudes are presented in relation to the WGS84 ellipsoid. Corrections for ship movements were applied using an OCTANS™ Surface (IXSEA OCEANO) gyrocompass and motion sensor.

The integrated MBES system possesses three major advantages in terms of studying dune dynamics. First, high-resolution swath bathymetry yields the possibility of analysing dunes in a spatial context. Second, high-resolution swath bathymetry enables the comparison of bathymetries of different times at an exact point or line, independent of the vessel track. Finally, high-resolution swath bathymetry combined with high-accuracy positioning gives the opportunity of quantifying small-scale dune dynamics over short time scales.

1.3.2 Hydrodynamics

Water level data have been extracted from the recording tide gauges at Grådyb Bar and in the Port of Esbjerg (Fig. 1.1).

Flow velocity data have been collected using a Workhorse Sentinel™ (RDI) and a BroadBand™ (RDI) acoustic Doppler current profiler (ADCP) along with the WinRiver™ (RDI) software package as well as a Niskin 6011 MKII winged current meter. The ADCPs operate at 1200 kHz. The vertical resolution of the ADCPs was set to 0.25 m and the horizontal resolution is 5-10 m at a ping rate of 0.5 Hz and a vessel speed of 2.6 m/s (5 kn). Flow velocity is measured with an accuracy of 0.3% of the water velocity relative to the ADCP ±0.3 cm/s, i.e. 0.9-1.5 cm/s assuming a vessel speed of 2.5 m/s (5 kn) and a flow velocity of 1.5 m/s in the opposite direction, and a resolution of 0.1 cm/s [*www.rdinstruments.com*]. Flow direction is measured with an accuracy of ±2°, a precision of ±0.5° and a resolution of 0.01° [*www.rdinstruments.com*]. In addition, the ADCPs measure echo intensity, which is a measure of the signal strength of the echo returning from the ADCP's transmit pulse [*RDI*, 1996]. Echo intensity is measured with a precision of ±1.5dB [*www.rdinstruments.com*]; and it has been used in several surveys to estimate the relative concentration of suspended sediment [e.g. *Reichel*, 1998; *Kostaschuk et al.*, 2005].

The Niskin 6011 MKII winged current meter measures flow velocity with an accuracy of ±1 cm/s and a resolution of 1 cm/s. Flow direction is measured with an accuracy of ±2° and a resolution of 1° [*General Oceanics Inc.*, 2000].

The major advantage of a down-looking ADCP is that a distribution (profile) in the water column is achieved without interfering with either the flow or the bed. However, the limitation of the ADCP, i.e. the fact that data from the last 6% of the range to the bed can be contaminated [*RDI*, 1996], is a considerable shortcoming, especially in the case of studying dune dynamics.

1.3.3 Bed material

Bed material was collected using a Shipek™ grab sampler. In the contest of this study, the major advantage of this sampler is that the deployment rate is high, that it only samples the uppermost sediment layer, and that it collects virtually undisturbed bed samples, thereby preserving the bed surface.

1.4 Results

The main results from the investigations in the Grådyb tidal inlet channel in the Danish Wadden Sea are summarised in five papers (Paper I-V) listed below and presented in Chapter 2-6 with three papers as first author and two papers as co-author.

1.4.1 Paper I

On the state of the art of high-accuracy bathymetric surveys in shallow coastal water: Evaluation of high-resolution multibeam echo sounding coupled with high-accuracy positioning

Ernstsen, V.B., R. Noormets, D. Hebbeln, A. Bartholomä, B.W. Flemming

Geo-Marine Letters (submitted)

The precision of the applied MBES system under normal field survey conditions has been determined by repetitive bathymetric measurements of a shipwreck over three years. The vertical precision of the MBES system is ±3.4 cm at a 95% confidence level, and during single surveys as high as ±1.9 cm. The horizontal precision is ±12.8 cm at a 95% confidence level.

1.4.2 Paper II

Development of subaqueous barchanoid-shaped dunes due to lateral grain size variability in a tidal inlet channel of the Danish Wadden Sea

Ernstsen, V.B., R. Noormets, C. Winter, D. Hebbeln,
A. Bartholomä, B.W. Flemming and J. Bartholdy

Journal of Geophysical Research, 110 (F04S08): 13 pp.

Barchanoid-shaped dunes develop due to an increase in dune migration from the centre towards the sides of the channel, resulting from a decrease in dune height from the centre towards the sides of the channel. The decrease in dune height is ascribed to an equivalent decrease in grain size from the centre towards the sides of the channel, as water depth and flow velocity are uniform across the channel. Annual measured bedload transport rates are significantly over-predicted by bedload transport formulae.

1.4.3 Paper III

Bedform dynamics and net sediment transport paths over a flood-ebb tidal cycle in the Grådyb channel (Denmark), determined by high-resolution multibeam echosounding

Bartholomä, A., V.B. Ernstsen, B.W. Flemming and J. Bartholdy

Danish Journal of Geography, 104(1): 45-55

Quantifying sediment transport during a single semi-diurnal tidal cycle shows that bedload transport rates are higher on the crests than in the troughs of the dunes. Net dune migration of single tidal cycles can be flood directed, despite an annual net ebb-directed dune migration. Measured bedload transport rates during single tidal cycles are also significantly over-predicted by bedload transport formulae.

1.4.4 Paper IV

Quantification of dune dynamics during a tidal cycle
in a tidal inlet channel of the Danish Wadden Sea

Ernstsen, V.B., R. Noormets, C. Winter, D. Hebbeln,
A. Bartholomä, B.W. Flemming and J. Bartholdy

Geo-Marine Letters (submitted)

Relating dune dynamics to hydrodynamics during a single semi-diurnal tidal cycle (same as in Paper III) shows that the higher dune crest than trough mobility is due to higher flow velocities at the dune crest. In addition, bed material goes into suspension with accelerating ebb flow and settles with decelerating ebb flow, resulting in an average erosion and accretion of the bed of ~6.5 cm. During flood tide the bed is practically stable. This results in a potential net export of sediment to the ebb tidal delta during every single semi-diurnal tidal cycle.

1.4.5 Paper V

Flow and grain size control of depth-independent simple subaqueous dunes

Bartholdy, J., B.W. Flemming, A. Bartholomä and V.B. Ernstsen

Journal of Geophysical Research, 110(F04S16): 12 pp.

General statements relating dune dimensions directly to the form-corrected Shields parameter are established from depth-independent superimposed dunes, showing that dune dimensions are primarily controlled by flow strength and grain size, and that water depth can act as an additional limiting factor to dune growth. This can be used e.g. to give a first approximation of flow conditions, as long as information on grain size and dune dimensions are available, as it is often the case in many oceanographic surveys.

Paper I

Chapter 2: Paper I

On the state of the art of high-accuracy bathymetric surveys in shallow coastal water: Evaluation of high-resolution multibeam echo sounding coupled with high-accuracy positioning

Verner B. Ernstsen[1], Riko Noormets[1], Dierk Hebbeln[1],

Alex Bartholomä[2], Burg W. Flemming[2]

[1]*Research Center Ocean Margins, University of Bremen, Leobener Str., P.O. Box 330 440, D-28359 Bremen, Germany*

[2]*Senckenberg Institute, Division of Marine Science, Suedstrand 40, D-26382 Wilhelmshaven, Germany*

Geo-Marine Letters (submitted)

Abstract

Over three years, repetitive bathymetric measurements of a shipwreck in the Grådyb tidal inlet channel in the Danish Wadden Sea were carried out using a state of the art high-resolution multibeam echosounder (MBES) coupled with a real-time Long Range Kinematic (LRK™) Global Positioning System (GPS). These surveys revealed a vertical precision of the MBES system of ±3.4 cm at a 95% confidence level. However, during a single survey the vertical precision of the MBES system was as high as ±1.9 cm at a 95% confidence level. The horizontal precision of the MBES system was determined to ±9.8 cm and ±14.9 cm in the easting and northing direction, respectively, at a 95% confidence level. However, determining the horizontal precision in the direction of the ship movement and perpendicular to it yielded values of ±12.5 and ±12.8 cm, respectively, at a 95% confidence level. The difference in horizontal precision between easting and northing is suggested to be the result of the heading of the survey lines, which were run in a NE/SW direction. Nevertheless, the achieved horizontal precision probably does not correspond to the full potential of the MBES system, as an increase in coverage density (soundings/m^2), which can be achieved by reducing the survey speed of the vessel, almost certainly would improve the precision.

2.1 Introduction

High-accuracy multibeam echo sounding coupled with high-accuracy positioning constitutes the current state of the art bathymetric survey technique [*Hughes-Clarke et al.*, 1996]. Over the last decade multibeam echosounder (MBES) surveys have become the standard in most hydrographic offices worldwide in order to produce the highest quality navigation charts to guarantee the safety of navigation. However, the use of MBES systems has also spread to other disciplines, such as offshore constructing [*Pickrill and Todd*, 2003], tracing of fish shoals [*Graham et al.*, 2004], monitoring dumping operations [*Wienberg et al.*, 2004] and studies of morphodynamics in navigation channels to determine the migration of dunes [*Ernstsen et al.*, 2005] which represent a potential navigation hazard [*Knaapen and Hulscher*, 2002].

The quality of MBES surveys is generally evaluated according to the International Hydrographic Organization's Standards for Hydrographic Surveys Special Publication No. 44 [*IHO S44*, 1998] specifying the minimum standards for hydrographic surveys, e.g. *Haga et al.*

[2003]. However, as discussed by *Wells and Monahan* [2002] and *Heaps* [2004] bathymetric surveys conducted using state of the art high-resolution MBES systems easily meet the IHO S44 Special Order Standards [*IHO S44*, 1998] questioning the applicability of the *IHO S44* [1998] as an appropriate quality control measure. In addition, there has been little independent, objective testing of positioning precision [*Edwards et al.*, 1999]. Instead, users have tended to rely on the precision estimates provided in the software developers' and instrument manufacturers' brochures [*Featherstone and Stewart*, 2001].

This study investigates the precision of high-resolution multibeam echo sounding coupled with real-time Long Range Kinematic (LRK™) positioning in shallow coastal water based on repetitive bathymetric measurements of a shipwreck in the Grådyb tidal inlet channel in the Danish Wadden Sea (Fig. 2.1). The investigations were motivated by the need of establishing the applicability of the MBES system in quantification of small-scale morphodynamics in order to adequately evaluate the determined changes.

Throughout this paper the term precision refers to the repeatability, i.e. the degree of agreement between individual measurements of a set of measurements, all of the same quantity. Accuracy refers to the reliability, and is the difference between the true value of a measured quantity and the most probable value, which has been derived from a series of measures. The true value is, of course, never known.

2.2 Study area

The shipwreck, a dinghy turned upside down [*Erik Brenneche*, Port of Esbjerg, pers. comm.], is located in the Grådyb tidal inlet on the Danish west coast between the barrier spit of Skallingen to the northwest and the barrier island of Fanø to the southeast. The Grådyb tidal inlet connects the northern-most tidal basin of the Wadden Sea with the adjacent North Sea and forms the navigation channel to Esbjerg (Fig. 2.1).

The tides are semi-diurnal with a mean tidal range of about 1.5 m and a tidal prism in the order of 150 x 10^6 m^3 [*Bartholdy and Anthony*, 1998]. The width of the channel is roughly 1 km and the mean depth is 10-13 m. The channel is ebb-dominated with maximum depth-averaged ebb and flood current velocities around 1.3 m/s and 1.1 m/s, respectively [*Ernstsen et al.*, 2005]. The bed of the channel is covered with large to very large compound dunes composed of sand with mean grain sizes ranging from 0.3 to 0.7 mm [*Ernstsen et al.*, 2005].

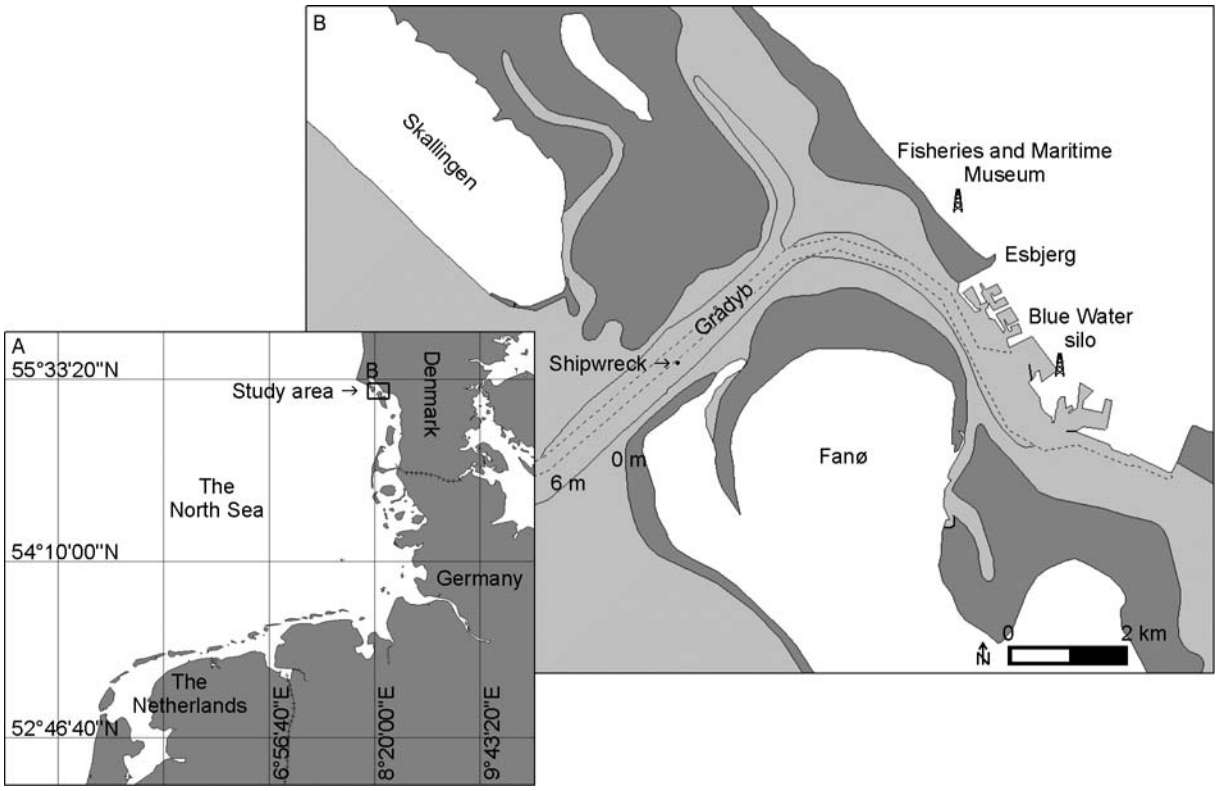

Fig. 2.1 Location of the shipwreck in the Grådyb tidal inlet between the barrier spit of Skallingen and the barrier island of Fanø in Denmark. In addition, the locations of the base station in 2002 (Fisheries and Maritime Museum) as well as in 2003 and 2004 (Blue Water silo) in Esbjerg. Dashed line marks the navigation channel. Water depths are relative to mean low water springs (MLWS).

2.3 Methods

2.3.1 Surveys

The shipwreck was surveyed ten times in total, once on the 10th of September 2002, seven times during the 15th of July 2003 and twice on the 6th of July 2004. All surveys were carried out using the same multibeam echosounder, sound velocity probe, positioning system, gyrocompass and motion reference unit. Only the location of the on-shore base station was shifted from the Fisheries and Maritime Museum during the first survey in 2002 to the Blue Water silo during the following surveys in 2003 and 2004 (Fig. 2.1).

2.3.2 Instruments

A SeaBat™ 8125 ultra high resolution focused multibeam echosounder system (RESON) was used for the surveys. This system operates at a frequency of 455 kHz. The projector arrays generate a single transmission with an along-track width of 1° and an across-track

width of 130°. Upon receive, 240 beams are formed simultaneously by the hydrophone arrays. The geometry of the receive beams is 20° along-track and 0.5° across-track which yields a swath width of 120°. The beam geometry results in an increase of the footprint from the nadir beam to the most off-nadir beams. For instance, a water depth of 15 m yields a footprint of 0.26 m along-track and 0.13 m across-track at nadir, whereas for the most off-nadir beams the footprints are 0.52 m along-track and 0.51 m across-track (Fig. 2.2). The corresponding across-track resolution of the recorded depth points ranges from 0.13 m to 0.51 m moving from the centre towards the sides of the swath (Fig. 2.2). The maximum range of detection is 120 m from the sonar head. At water depths shallower than 60 m the system measures it's maximum swath width of 3.5 times the water depth, which is the function of the swath width of 120°. Beyond depths of 60 m, the swath coverage starts decreasing as a result of the ranges of the outer beams exceeding the limited range of 120 m. The measured distances to the detected seabed are delivered with a depth resolution of 6 mm, i.e. the vertical resolution is in a sub-centimetre scale. The maximum ping rate of the system is 40 Hz, however, as only one ping is present in the water at a time, the actual rate depends on the range. The actual ping rate at a water depth of e.g. 15 m equals 25 Hz, assuming a sound velocity of 1500 m/s. At the same water depth and sound velocity with a vessel speed of 5 knots, i.e. 2.57 m/s, the along-track resolution is 0.10 m (Fig. 2.2). For further technical information on the SeaBat 8125 please refer to *RESON Inc.* [2001] and *www.reson.com*.

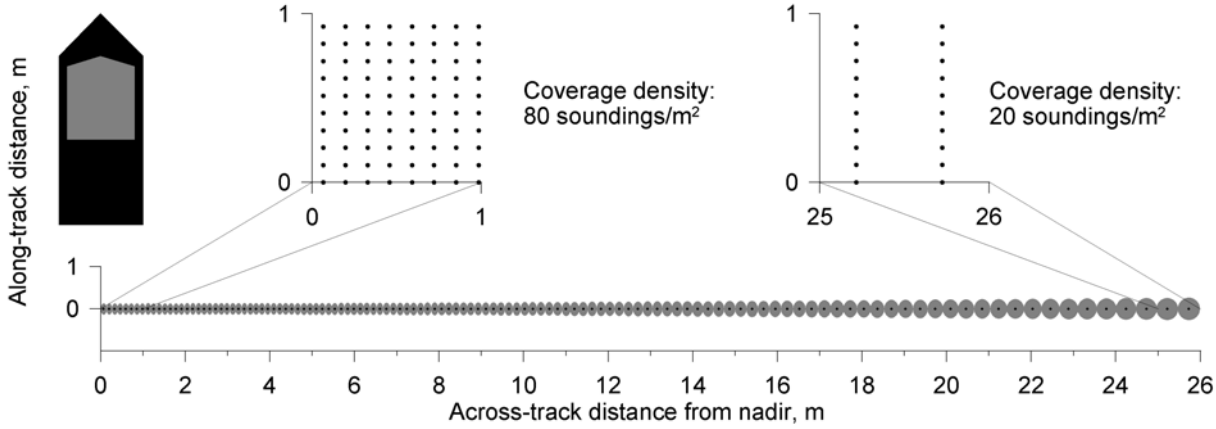

Fig. 2.2 Sketch visualizing footprint size (grey areas) and horizontal resolution of the acquired soundings (dots), assuming a water depth of 15 m, a sound velocity of 1500 m/s and a vessel speed of 5 knots.

For the focus forming process of the receive beams as well as the conversion of measured return ping times into distances, a SVP-C™/120 (RESON) sound velocity probe (SVP) was mounted close to the hydrophone. This SVP measures sound velocities in the range 1350-

1600 m/s with a resolution of 0.1 m/s and an accuracy of ±0.25 m/s. Furthermore, a portable SVP™ 15 (RESON) was used to measure sound velocity profiles through the entire water column. The portable SVP has the same parameters as the mounted SVP described above. The sound velocity is recorded at 0.5 m depth intervals. A pressure sensor determines the water depths with an accuracy of ±0.10 m + 0.2% of the measured depth. For further technical information on the SVP-C/120 and SVP 15 please refer to *www.reson.com*.

The MBES system was coupled with an AQUARIUS™ 5002 MK (THALES) Global Navigation Satellite System (GNSS) dual-frequency (L1/L2) receiver working in the Long Range Kinematic (LRK™) mode receiving differential corrections from an AQUARIUS 5002 SK GNSS L1/L2 base station over an Ultra High Frequency (UHF) radio link. In 2002 the base station was located on the roof of the Fisheries and Maritime Museum, which yielded a distance of approximately 5.4 km to the object (Fig. 2.1). In the subsequent surveys of 2003 and 2004, the base station was moved to the top of the Blue Water silo extending the baseline to approximately 6.4 km (Fig. 2.1). The LRK method achieves an optimal real-time positioning accuracy to within 0.01 m in all three dimensions at a 95% confidence interval at a range up to 40 km [*Gounon and Erceau*, 1998]. LRK technology utilizes the advantages of the two Global Positioning System (GPS) frequencies, which allow cutting down the initialization time and increasing the reliability of the initialization process as well as covering longer ranges. In practice, the range of the UHF coverage is up to 50 km assuming optimal quality of the UHF radio link, primarily depending on the transmission power and the height of the antenna. Positions and altitudes are output in World Geodetic System 1984 (WGS84) coordinates and displayed in relation to the Universal Transverse Mercator 32 (UTM32) map projection. For further technical information on the AQUARIUS 5002 MK/SK please refer to *DSNP* [1999] and *www.thalesnavigation.com*.

An OCTANS™ Surface (IXSEA OCEANO) gyrocompass and motion sensor was employed to compensate for the attitude of the vessel. The motion sensor determines heave, i.e. the accelerating vertical motion, as well as surge, i.e. the accelerating longitudinal motion, and sway, i.e. the accelerating sideways motion, with an accuracy of 0.05 m or 5%, whichever is highest. Roll, i.e. the motion about the longitudinal axis, and pitch, i.e. the motion around the transverse axis, is determined with an accuracy of 0.01°. The fibre-optic gyrocompass determines true heading with an accuracy of 0.2°. The settling time for full accuracy is less than 1 minute in static conditions and less than 3 minutes at sea. Yaw, i.e. the motion about the vertical axis, is determined from the heading with a resolution of 0.01°. For further

technical information on the OCTANS Surface please refer to *IXSEA OCEANO* [2003] and *www.ixsea-oceano.com*.

A Pulse Per Second (PPS™) Box (RESON) was used to synchronize all recoded sensor data [*RESON Inc.*, 2000a].

2.3.3 Software

The software package 6042™ Version 7 (QINSY/RESON) was used to integrate the MBES data with the information from all the auxiliary sensors during the surveys, i.e. the data acquisition and synchronization. This software was used in the real-time as well as in the post processing of the integrated data. The two main components in the post processing are the calibration of the MBES and the filtering of erroneous soundings. The calibration serves to determine four types of errors: the latency of the positioning data and the errors arising from the mounting of the echosounder – the roll angle error, the pitch angle error and finally the yaw angle error [*RESON Inc.*, 1999]. This calibration is done separately for each survey as the exact values may deviate from survey to survey. For further technical information on the software package 6042 Version 7 please refer to *RESON Inc.* [2000b] and *www.reson.com*.

2.3.4 Statistics

The precision of the MBES system was determined at a 95% confidence level from the descriptive statistics based on the conducted surveys. The system was evaluated in all three dimensions, i.e. 95% confidence intervals were determined for the easting and northing coordinates as well as for the altitude. In total, ten surveys were conducted, i.e. the sample size n was 10. Sample mean x, variance s^2 and standard deviation s are given by:

$$x = \frac{\sum x_i}{n} \tag{2.1}$$

$$s^2 = \frac{\sum \left(x_i - \bar{x} \right)^2}{n-1} \tag{2.2}$$

$$s = \sqrt{s^2} \tag{2.3}$$

Due to the small sample size the percentile value t_p for the student's t distribution with n-1 degrees of freedom f was used. The 95% confidence interval $CI_{95\%}$ (α is 0.05) is given by:

$$CI_{95\%} = \pm t_{1-\frac{\alpha}{2}}(f)\frac{s}{\sqrt{n}} = \pm t_{0.975}(9)\frac{s}{\sqrt{n}} = \pm 2.26\frac{s}{\sqrt{n}} \quad (2.4)$$

where $t_{0.975}(9) = 2.26$ was found from standard statistical tables.

2.4 Results

The MBES surveys revealed a shipwreck covering an area of approximately 6.5 m x 3.0 m and with a height of around 1.0 m above the surrounding seabed (Fig. 2.3A). In addition, pronounced local scour was observed around the object. The shape and dimensions of the object were preserved from the first survey in 2002 to the last survey in 2004 as opposed to the local scour, which underwent smaller changes over this period. Therefore, in order to give the best visualization with the highest achievable resolution of the object and the surroundings, the seven measurements from 2003 out of total ten measurements were used to create the bathymetry shown in Fig. 2.3. The wreck displayed a distinct highest point, probably the lowest point of the keel of the dinghy, which was easily located for each survey. The position of the highest point in each survey is shown in Fig. 2.3B. Note that only the average bathymetry of the surveys done in 2003 is displayed, i.e. the position of the highest point of the individual surveys cannot be related to the presented bathymetry. Based on the conducted surveys, the descriptive statistics yielded a precision of the MBES system of ±9.8 cm and ±14.9 cm in the easting and northing direction, respectively, at a 95% confidence level (Table 2.1). With the exception of the surveys 2003a and g, which were relatively distant, the determined positions were clustered around the mean value (Fig. 2.3B).

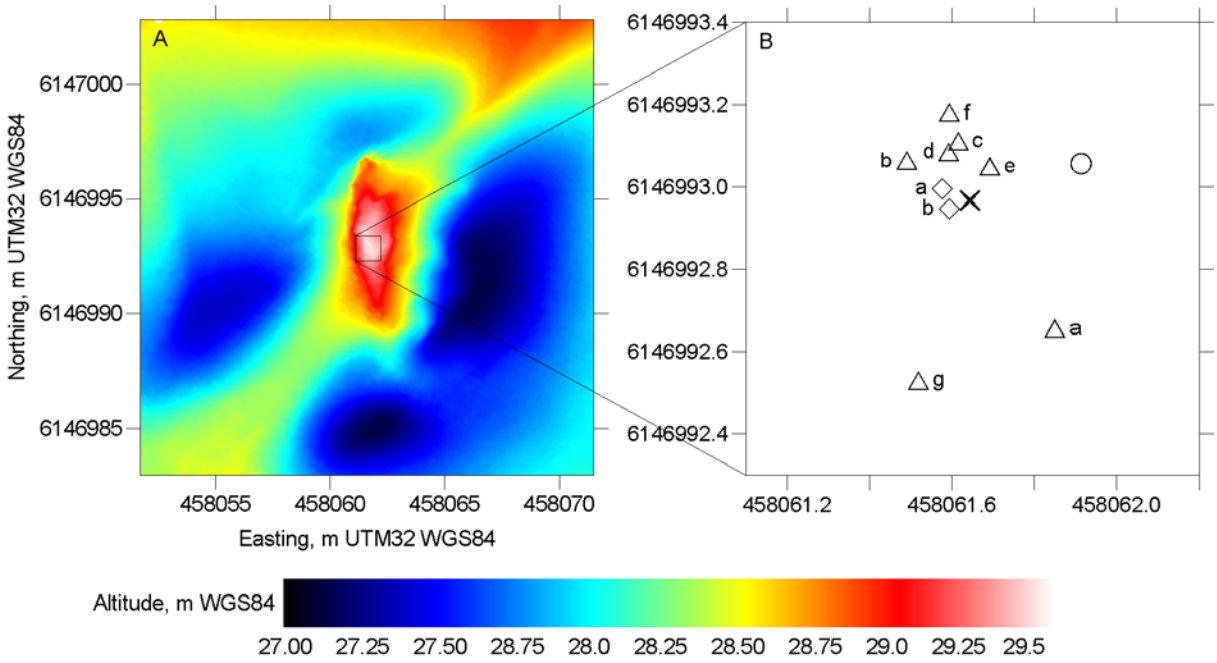

Fig. 2.3 A) Bathymetry around the shipwreck in the Grådyb tidal inlet in 2003 (for location see Fig. 2.1). The grid is 20 x 20 m with a cell size of 0.20 x 0.20 m. The bathymetry is based on the seven measurements conducted on the 15th of July 2003. B) Zoom-in around the highest point of the wreck, the grid is 1.1 x 1.1 m. The exact numerical value of the position of the highest point in each of the surveys in 2002, 2003 and 2004 is marked with a circle, triangles (a-g) and diamonds (a and b), respectively, while the mean value is shown with a cross. The exact coordinates of these positions are given in Table 2.1. Water depth relative to mean low water springs (MLWS) in relation to WGS84 altitude is given by: m MLWS = m WGS84 – 39.951 m.

The altitude of the highest point in each survey is shown in Fig. 2.4. The precision of the altitude was ±3.4 cm at a 95% confidence level based on the descriptive statistics from the conducted surveys (Table 2.1). The altitude of the point in survey 2002 falls between the surveys of 2003, all displaying higher altitudes, and the surveys of 2004, which exhibit the lowest determined altitudes of the point (Fig. 2.4). Furthermore, the difference between the two altitudes of the point in 2004 is larger than the scatter of all the altitudes of the point in 2003 (Fig. 2.4). Worth noting is that during the survey of 2003 the precision of the altitude was as high as ±1.9 cm at a 95% confidence level.

The beams describing the highest point varied from the near-centre beam as in survey 2003a (beam number 123) to the nearly outer-most beam as in survey 2004b (beam number 238) (Table 2.1). During the surveys in 2002 and 2003 the average survey speeds of the vessel varied around 5 knots or 2.57 m/s, whereas the surveys in 2004 were conducted at considerably lower speeds (Table 2.1). In 2002 and 2003 the average headings of the vessel

fluctuated around 43°N and 223°N, which were the previously planned orientations of the survey lines. In 2004 the headings were slightly different as these surveys solely had the purpose of measuring the object (Table 2.1). In 2002 and 2003 the sea was calm and accordingly the ship motions were small compared to 2004 (Table 2.1). First, the average range of roll in 2002 and 2003 was 0.85°, whereas in 2004 it was 5.36°. Second, the average range of pitch was 0.37° in 2002 and 2003, while being 3.46° in 2004. Finally, in 2002 and 2003 the average range of heave was 0.06 m, as compared to 0.43 m in 2004.

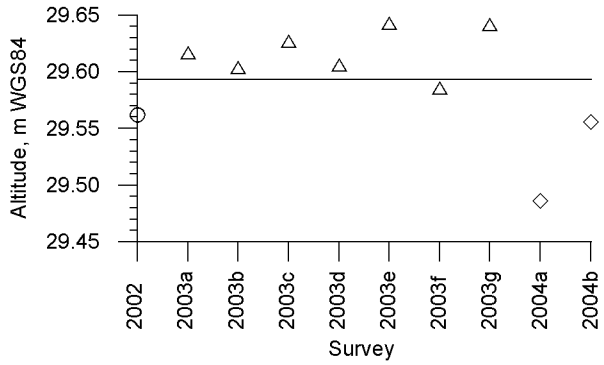

Fig. 2.4 Exact altitudes of the highest point in each of the surveys in 2002 (circle), 2003 (triangles) and 2004 (diamonds) as well as the mean value (line). The exact numerical values of the altitudes along with the corresponding coordinates are given in Table 2.1. Water depth relative to mean low water springs (MLWS) in relation to WGS84 altitude is given by: m MLWS = m WGS84 – 39.951 m.

Table 2.1 Date and time of recording of the surveys conducted in 2002, 2003 and 2004. Coordinates (m UTM32 WGS84) and altitude (m WGS84) of the highest point of the shipwreck in each of the surveys along with the resulting mean value x (m), variance s^2 (m^2), standard deviation s (m) and 95% confidence interval $CI_{95\%}$ (m) calculated from Equations (2.1)-(2.4). Corresponding number of the beam describing the highest point, ranging from 0 to 239. Finally, average speed and heading of the vessel as well as the ranges of roll, pitch and heave during each survey.

Id	Date	Time (UTC)	Easting (m)	Northing (m)	Altitude (m)	Beam no.	Speed (m/s)	Heading (°)	Roll (°)	Pitch (°)	Heave (m)
2002	10.09.2002	12:39:47 – 12:42:16	458061.913	6146993.057	29.562	94	2.82	47	0.84	0.48	0.05
2003a	15.07.2003	09:07:33 – 09:10:36	458061.850	6146992.656	29.617	123	2.87	42	0.46	0.07	0.03
2003b	15.07.2003	10:18:42 – 10:21:06	458061.490	6146993.064	29.604	205	2.79	223	0.90	0.18	0.05
2003c	15.07.2003	12:03:51 – 12:06:29	458061.616	6146993.112	29.627	105	2.64	42	0.72	0.28	0.02
2003d	15.07.2003	13:16:39 – 13:19:18	458061.592	6146993.085	29.606	222	2.56	224	0.82	0.23	0.10
2003e	15.07.2003	14:25:43 – 14:28:24	458061.692	6146993.050	29.643	134	2.81	43	0.77	0.23	0.07
2003f	15.07.2003	15:46:49 – 15:49:49	458061.594	6146993.181	29.586	176	2.58	221	1.35	1.40	0.11
2003g	15.07.2003	17:15:00 – 17:17:36	458061.519	6146992.531	29.642	129	2.34	45	0.93	0.11	0.02
2004a	06.07.2004	15:43:25 – 15:46:28	458061.577	6146992.995	29.486	192	1.54	71	6.68	2.71	0.48
2004b	06.07.2004	15:46:28 – 15:49:29	458061.594	6146992.947	29.556	238	0.77	233	4.03	4.20	0.37
Mean, x			458061.644	6146992.968	29.593						
Variance, s^2			0.019	0.044	0.002						
Standard deviation, s			0.137	0.209	0.048						
95% confidence interval, $CI_{95\%}$			±0.098	±0.149	±0.034						

Sound velocity profiles measured in the central part of the Grådyb tidal inlet in the course of 14 hours, over a tidal cycle, close to spring tide on the 11th of July 2003 are shown as an example in Fig. 2.5. Temporally, the sound velocity varied 1.8 m/s from a minimum of 1511.2 m/s measured near the bed around low water (profile 1) to 1513.0 m/s at the surface close to the successive low water (profile 7). Considering each profile vertically, however, the variation was smaller with an average range of 0.4 m/s and a maximum range of 0.5 m/s.

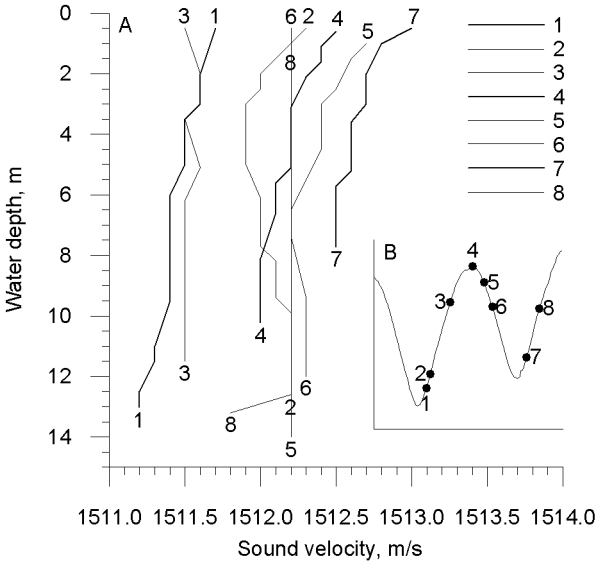

Fig. 2.5 A) Sound velocity profiles in the central part of the Grådyb tidal inlet during 14 hours, over a tidal cycle, close to spring tide on the 11th of July 2003. The profiles are labeled both at the top and bottom in order to distinguish each profile. B) Phase of the tide during the recording of the individual profiles.

2.5 Discussion

In Fig. 2.3B it was shown how the determined positions clustered around the mean value with exception of the surveys 2003a and g. The beam associated with the highest point of the shipwreck in both survey 2003a and g was close to the centre of the swath, beam number 123 and 129, respectively (Table 2.1). From measurements with a BottomChart Compact (BCC) (ELAC) MBES and a SeaBat 9001 (RESON) MBES, *Eeg* [1998] showed that the accuracy decreases from the centre to the outer beams. *Artilheiro and Pimentel* [2001] also showed this using an EM 950 (SIMRAD) MBES. Furthermore, the same trend has also been shown from error models for the SeaBat 8125 [*Hare et al.*, 2004], for that reason surveys 2003a and g should be expected to be the most accurate. However, in survey 2003e the beam associated with the highest point of the wreck is also close to the centre of the swath, beam number 134;

and this position is very close to the mean position of the point (Fig. 2.3B and Table 2.1). Furthermore, the headings of these three surveys were all the same (Table 2.1). Consequently the scatter in the horizontal positioning of the highest point of the wreck is not a systematic error arising from the post processing of the data.

The relatively large vertical difference in 2004 compared to the scatter of the altitudes in 2003 (Fig. 2.4) is suggested to be a result of the larger ship movements in 2004. In 2004 the roll was six times larger than in 2002 and 2003, the pitch was larger by a factor of nine and the heave was seven times larger (Table 2.1). A decrease in precision with an increase in ship attitude is well known from earlier studies [e.g. *Scarfe*, 2002].

Due to the small vertical variation of sound velocity through the water column (Fig. 2.4), the sound velocity measured at the sonar head was used as representative for the entire water column. A variation in sound velocity of 0.5 m/s from the surface to the bed as seen in this study (Fig. 2.5) yields a variation in water depth of 5 mm, when assuming the sound velocity variation to be from 1500.5 m/s to 1500.0 m/s along with a return time of the signal of 0.02 s from the centre beams and 0.04 s from the outer-most (60°) beams, which is equivalent to ranges of 15 m and 30 m, respectively, i.e. a water depth of 15 m. Hence the effect of the variation of sound velocity through the water column is an order of magnitude smaller than the overall precision of the MBES system (Table 2.1). Moreover, the larger temporal variation in sound velocity (Fig. 2.5) would require a larger number of sound velocity profiles to be measured in order to attain the same accuracy as achieved by continuously applying the sound velocity from the SVP fixed to the sonar head. Finally, the temporal variation in sound velocity inevitably also includes a spatial variation as the sound velocity profiles were taken in the central part of the Grådyb tidal inlet, but not at the exact same position.

To the knowledge of the authors, no data of earlier studies using a similar set up as in this study have been published, making a direct comparison of the precision of the MBES system unfeasible. However, other studies concerning either the precision of Real-Time Kinematic (RTK) or LRK positioning or of MBES soundings as well as a combination of both have been published. *Satalich and Ricketson* [1998] conducted an onshore accuracy test of a 4000 SSE (TRIMBLE) RTK GPS with maximum baseline lengths of 500 m. They found root mean square (RMS) values of the easting, northing and altitude components of ±0.85, ±0.87 and ±2.26 cm, respectively. Just as the standard deviation s, the RMS is a statistical measure of the magnitude of a varying quantity, albeit slightly different. Recalculating our measurements into RMS values yields ±13.0, ±19.8 and ±4.6 cm for the easting, northing and altitude

components, respectively, i.e. the spread of our offshore measurements is by factors 15, 23 and 2 larger than those of the onshore test. *Lutz and Gounon* [2001] also did an onshore accuracy test, but of a similar LRK GNSS as used in this study, i.e. AQUARIUS 5002™ SK/MK (THALES). At a baseline length of 4 km, which is comparable to this study, they achieved easting, northing and altitude accuracies of ±0.4, ±0.50 and ±1.0 cm, respectively, at a 95% confidence level. Even at a baseline length of 55 km the accuracy remained at the centimetre level with easting, northing and altitude values of ±1.4, ±1.8 and ±3.6 cm, respectively, at a 95% confidence level. In addition, *Lutz and Gounon* [2001] report from the offshore Yangtze River Estuary Project in China where the LRK technique had been applied, providing a horizontal accuracy of less than ±2.5 cm at baseline lengths of 20 km. Unfortunately, they leave the vertical accuracy uncommented. The LRK technique was also applied offshore on the salvage of the MV Tricoler that sank in the English Channel in 2002. The LRK GNSS used was the AQUARIUS™ 02/22 (THALES), obtaining centimetre accuracy up to baseline lengths of 50-60 km [*Berlijn*, 2003]. However, *Berlijn* [2003] gives no exact values of the obtained precision. *Eeg* [*1998*] tested the vertical precision of a BCC (ELAC) MBES and a SeaBat™ 9001 (RESON) MBES, in a very much similar way as in this study, by repeatedly surveying a field stone at a water depth of 22 m. Recalculating the measurements of *Eeg* [1998] to 95% confidence intervals yield vertical precisions of ±8.7 and ±9.3 cm for the BCC (ALLIED SIGNAL ELAC) and SeaBat 9001 (RESON) MBES, respectively. This is only by a factor of two to three larger than the vertical accuracies achieved in this study (Table 2.1). *Artilheiro and Pimentel* [2001] also conducted a test of the vertical accuracy of MBES using an EM 950 (SIMRAD). They achieved an accuracy of ±8.0 cm at a 95% confidence level at an average water depth of 10 m, i.e. also a factor two to three larger than in this study (Table 2.1). To the knowledge of the authors, the only published study combining a high-resolution MBES and a precise differential GPS is the one of *Seibt-Winckler et al.* [2002], applying an EM 3000 (SIMRAD) MBES in combination with RTK GPS (TRIMBLE). In order to evaluate the precision of their system they compared two swaths at two different locations with water depths around 11 and 8 m, respectively. The vertical mean difference between the two swaths was 5 and 13 cm at water depths around 11 and 8 m, respectively. These values, though, are difficult to compare directly to the statistics presented in this study. Furthermore, *Seibt-Winckler et al.* [2002] leave the horizontal precision uncommented. In summary, the precision achieved in this study exceeds those of

earlier offshore tests, but it is still approximately an order of magnitude lower than can be attained onshore.

The three to four times lower precision horizontally compared to vertically (Table 2.1) is most likely due to the survey technique and does not correspond to the potential precision of the MBES system. The probability of reaching the potential precision increases with the coverage density (soundings/m^2), i.e. an infinite high coverage density would reduce the precision to the theoretical precision of the MBES system. First, coverage density decreases with water depth, as the footprint of each beam - and thereby the distance between soundings perpendicular to the direction of the ship - increases with water depth. Second, an increase in vessel speed increases the distance between soundings in the direction of the ship movement, which decreases the coverage density. These effects are visualized schematically in Fig. 2.2 and in reality in Fig. 2.6 where the actual soundings of survey 2003a (dots) and 2004b (crosses) in the area around the wreck are shown. Survey 2003a was conducted at a vessel speed of 2.87 m/s, an average heading of 42°, during calm conditions and measured the object with the near centre beams (Table 2.1). By contrast, survey 2004b was done at a vessel speed of 0.77 m/s, an average heading of 233° (or 53° which is almost the same as in survey 2003a), during rougher conditions, and measuring the object with the outer-most beams (Table 2.1).

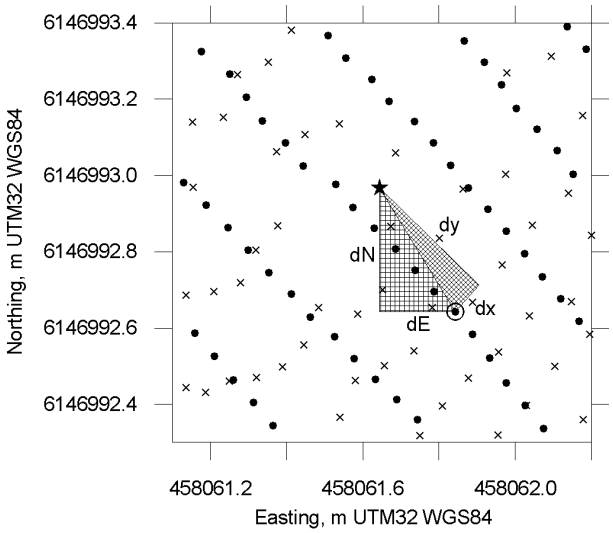

Fig. 2.6 Positions of the actual soundings in survey 2003a (dots) and 2004b (crosses) around the highest point of the wreck (area is comparable to the zoom-in in Fig. 2.3B). Star refers to the mean position of the highest point of the wreck, whereas the encircled point refers to its position in survey 2003a (the exact values are given in Table 2.1). dE and dN refer to the deviations from the position of the highest point of the wreck in survey 2003a to the mean position in the directions of easting and northing, respectively. Likewise, dx and dy refer to these deviations, but in the direction of the ship and perpendicular to the direction of the ship, respectively.

The difference in precision between easting and northing is probably a result of the heading of the survey lines. The deviations in the position from the highest point of the object in each survey to the mean position in the directions of easting (dE) and northing (dN) (example is shown in Fig. 2.6) are used in the calculations of variances (Equation 2.2). If instead, the deviations are determined in the direction of the ship (dx) and perpendicular to the direction of the ship (dy), the precisions become ±12.5 and ±12.8 cm, respectively. This is probably still not the potential precision of the MBES system, as the reductions mentioned above still apply.

2.6 Conclusions

Based on the analysis of repetitive measurements of a shipwreck in the Grådyb tidal inlet channel in the Danish Wadden Sea using a high-resolution MBES coupled with a high-accuracy GPS, the following conclusions have been reached:

1) The vertical precision of the MBES system is ±3.4 cm at a 95% confidence level (Table 2.1). However, during single surveys it is as high as ±1.9 cm at a 95% confidence level.

2) The horizontal precision of the MBES system is ±9.8 cm and ±14.9 cm in the easting and northing direction, respectively, at a 95% confidence level (Table 2.1). However, determining the deviations in the direction of the ship movement and perpendicular to it yield precisions of ±12.5 and ±12.8 cm, respectively, at a 95% confidence level. This difference in precision between easting and northing is suggested to be the result of the heading of the survey lines.

Although the achieved precision probably does not correspond to the full potential of the MBES system, as the coverage density could be increased significantly by reducing vessel speed, the precision is higher than in earlier offshore tests but, as one would expect, still lower than is attained onshore.

Acknowledgements

This study was supported by the German Science Foundation. The captain and crew of the RV Senckenberg are thanked for their expertise and unfailing good spirits during the cruises.

Paper II

Chapter 3: Paper II

Development of subaqueous barchanoid-shaped dunes due to lateral grain size variability in a tidal inlet channel of the Danish Wadden Sea

Verner B. Ernstsen[1], Riko Noormets[1], Christian Winter[1], Dierk Hebbeln[1], Alex Bartholomä[2], Burg W. Flemming[2], Jesper Bartholdy[3]

[1]*Research Center Ocean Margins, University of Bremen, Leobener Str., P.O. Box 330 440, D-28359 Bremen, Germany*

[2]*Senckenberg Institute, Division of Marine Science, Suedstrand 40, D-26382 Wilhelmshaven, Germany*

[3]*Institute of Geography, University of Copenhagen, Øster Voldgade 10, DK-1350 Copenhagen, Denmark*

Journal of Geophysical Research, 110 (F04S08): 13 pp.

Abstract

High-resolution bathymetry at centimetre-scale accuracy acquired with a multibeam echo sounder system revealed the existence of barchanoid-shaped large (i.e. length 10-100 m) to very large (i.e. length > 100 m) dunes in the Grådyb tidal inlet channel in the Danish Wadden Sea. The development of these dunes is due to an increase in dune celerity from 12 m/y in the centre of the channel to around 30 m/y at the sides. This increase in dune celerity can be explained by the fact that dune heights decrease from 3.1 m in the centre of the channel to 1.4 m at the sides, as a smaller sediment volume has to be moved per unit time for equal dune celerity. Water depth is uniform across the channel. Likewise high-resolution acoustic Doppler current profiler measurements across the channel showed a uniform distribution of both ebb and flood flow. Thus no correlation between dune dimensions and water depth or flow velocity was established. Instead, high-accuracy bed sampling along the crests of the dunes showed a decrease in mean grain size from 0.63 mm in the centre to 0.36 mm at the sides of the channel. The decrease in dune height is ascribed to this decrease in grain size, given that flow depth and flow velocity are uniform across the channel. The lateral decrease in grain size is suggested to result from sorting effects by secondary currents directed from the centre towards the sides of the channel in the trough/lee side region of the barchanoid-shaped dunes.

3.1 Introduction

Tidal inlets are narrow natural channels that connect the open sea with a lagoon, as it is often the case in barrier-island systems. The channel beds are typically covered with bedforms [*Flemming and Davis*, 1992; *Hennings et al.*, 2004], the dimensions of which are controlled by the local hydrodynamics and sediment characteristics [*Allen*, 1982; *Flemming*, 2000a and b]. Due to the generally narrow shape of tidal inlets, the flow velocities are often high (> 1 m/s) and bed material is accordingly composed of sandy material [*Flemming and Davis*, 1992]. To understand the dynamics of bedforms, numerous studies have been conducted in rivers [e.g. *Sukhodolov et al.*, 1998; *Carling et al.*, 2000a], in tidal environments [e.g. *Dalrymple et al.*, 1978; *Harbor*, 1998] and on the continental shelf [e.g. *Flemming*, 1978; *Ardhuin et al.*, 2002]. However, earlier studies have primarily been based on single longitudinal profiles [e.g. *van den Berg*, 1987; *Bartholdy et al.*, 2002], which have revealed rather little about the lateral shape of dunes. A few exceptions include the Fraser River,

Canada, where *Kostaschuk and Villard* [1996] observed dunes with a curved, concave-downstream plan form with 300 m long crest lines. *Carling et al.* [2000a] observed barchan dunes in the River Rhine, Germany, extending approximately 120 m across the channel. Recently, *Dinehart* [2002] described dunes in the San Joaquin River, USA, with crests oriented about 45° from the banks. Barchanoid-shaped dunes can also be identified on the bathymetric data presented by *Abraham and Pratt* [2002] from the Upper Mississippi River, USA. Nevertheless, these detailed field studies still focus on the longitudinal dune patterns and not on the lateral shapes of the dunes. Only one recent flume study has described the lateral flow distribution over sinuous-crested three-dimensional dunes [*Maddux et al.*, 2003a and b]. To the knowledge of the authors, no studies have dealt with lateral grain size patterns over dunes.

This study investigates the potential influence of lateral, i.e. cross-channel, variations in water depth, flow velocity and grain size patterns on the development of subaqueous barchanoid-shaped dunes in the Grådyb tidal inlet channel in the Danish Wadden Sea (Fig. 3.1). The term barchanoid is solely used to describe the lateral shape of the dunes and the net direction of migration since the flow is not unidirectional but bi-directional. In addition, there is an abundance of sediment, no lack; and the dunes are thus not migrating over firm ground.

3.2 Study area

The Grådyb tidal inlet is located on the Danish west coast between the barrier spit of Skallingen to the northwest and the barrier island of Fanø to the southeast. It connects the northern-most tidal basin of the Wadden Sea with the adjacent North Sea (Fig. 3.1).

The tides are semi-diurnal with a mean tidal range of about 1.5 m and a tidal prism in the order of 150 x 10^6 m^3 [*Bartholdy and Anthony*, 1998]. The width of the channel is roughly 1 km and the mean depth is 10-13 m. The channel is ebb-dominated with maximum ebb and flood current velocities around 1.50 m/s and 1.25 m/s, respectively [*Bartholdy and Anthony*, 1998]. The bed of the channel is composed of sand with mean grain sizes ranging from 0.3 to 0.7 mm. There are two sediment sources in the area; one being the Pleistocene cliffs lining the mainland in the landward part of the back-barrier tidal basin (Fig. 3.1), it supplies medium to coarse sand. The other, which supplies fine sand to the tidal inlet, is located in the near-shore region of the open coast [*Bartholdy et al.*, 2002].

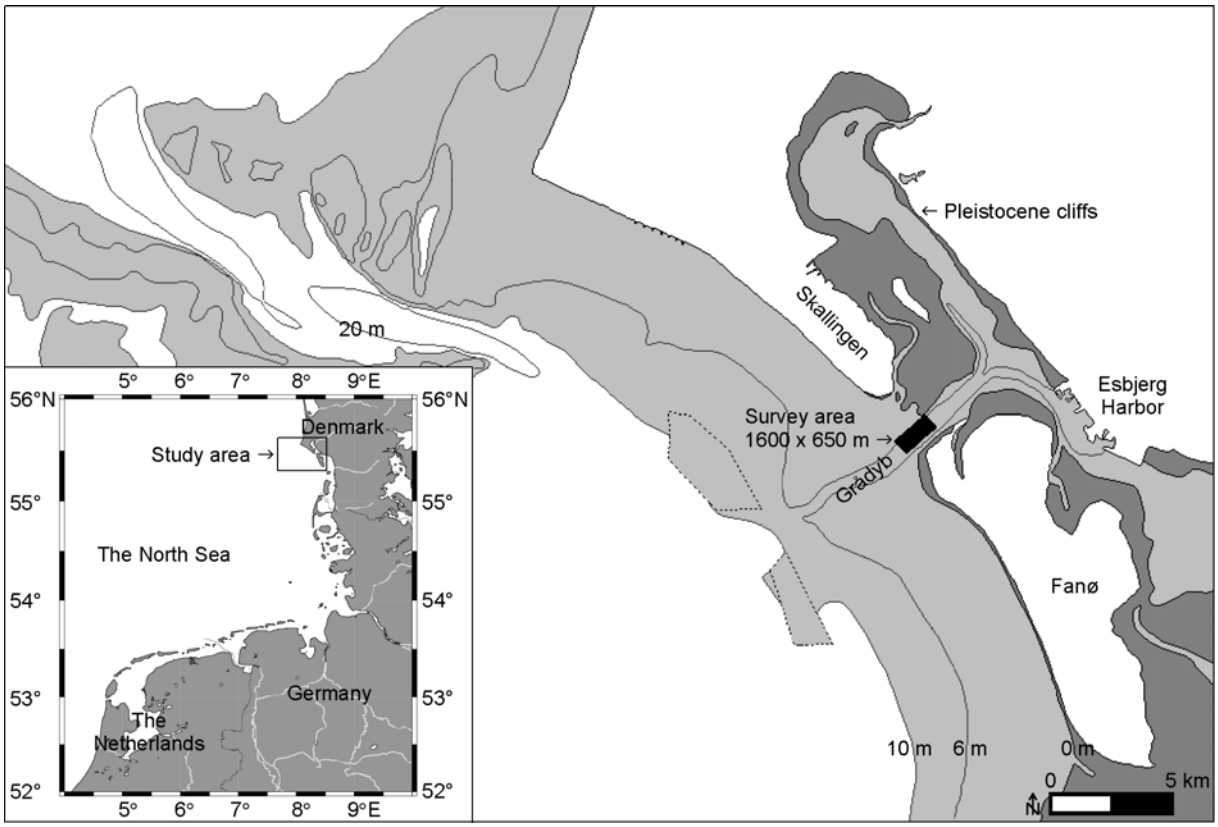

Fig. 3.1 Location of the study area in the Grådyb tidal inlet channel between the barrier spit of Skallingen and the barrier island of Fanø in Denmark. Water depths are relative to mean low water springs (MLWS). The two zones encircled by dashed lines are dumping sites for dredged material.

3.3 Methods

3.3.1 Surveys and instruments

Bathymetric surveys were conducted in a 1600 x 650 m section of the channel (for location see Fig. 3.1) on the 10th of September 2002 and the 11th of July 2003. The bathymetric data were recorded using a Seabat 8125™ (RESON) multibeam echo sounder (MBES) system operating at 455 kHz and the 6042 v. 7™ (RESON/QPS) data collecting and processing software package. The vertical resolution of the MBES system is in a sub-centimetre scale [*www.reson.com*]. The lateral resolution is a function of water depth and vessel speed. For instance, a water depth of 15 m results in an across-track resolution of 0.13-0.52 m due to the across-track beam width of 0.5°; at a vessel speed of 2.6 m/s (5 kn) the along-track resolution is 0.10 m. Therefore a cell size of 0.5 x 0.5 m was chosen for the gridding of the bathymetric data. The MBES system was coupled with an AQUARIUS 5002™ (THALES/DSNP) dual frequency (L1/L2) Long Range Kinematic (LRK™) Global

Positioning System (GPS). The vertical and lateral accuracy of the positioning system is better than 0.05 m [*Lutz and Gounon*, 2001]. Altitudes are presented in relation to UTM32 WGS84 map projections. Corrections for ship movements were applied using an Octans Surface™ (IXSEA OCEANO) gyrocompass and motion sensor.

Flow velocities were measured along cross-section NE over 10 hours of a tidal period, as well as at station C over a whole tidal period around spring tide on the 3rd of July 2004 (for locations see Fig. 3.2). Along cross-section NE, the flow velocity data were collected using a Workhorse Sentinel™ (RDI) acoustic Doppler current profiler (ADCP) operating at 1200 kHz and the WinRiver™ (RDI) software package. The vertical resolution of the ADCP was set to 0.25 m and the lateral resolution is approximately 5 m at a ping rate of 0.5 Hz and a vessel speed of 2.6 m/s (5 kn). At station C, the flow velocity data were collected using a Niskin 6011 MKII winged current meter attached to a submerged mooring system. The current meter was located approximately 4 m above the bed at a water depth varying between 10 and 12 m. Flow velocity values were recorded every 5 minutes, being averaged over 40 discrete measurements in each case.

Bed material was collected from bedform crests along the five transects N2-S2 (for locations see Fig. 3.2) on the 14th of July 2003 using a Shipek™ grab sampler. Sampling positions were determined by the high-accuracy positioning system described above. The drift of the grab sampler during lowering through the water column determines the inaccuracy in the sampling positioning, which was assessed to be better than 2 m based on the water depths and the observed cable angles.

3.3.2 Bedform dimensions and celerities

Bedform dimensions and celerities were determined from the gridded bathymetry in 2002 and 2003 along the five transects N2-S2. Only bedforms with crests extending across the entire channel in both 2002 and 2003 were considered. Bedform length L has been defined as the trough-to-trough distance with the location of a trough defined as the lowest point of the lee (or stoss) side of a bedform. Bedform height H was determined as the vertical distance from the crest to the line defining the bedform length. The location of the crest was defined as the highest point along the bedform. However, there were a few exceptions (see Fig. 3.2 and Fig. 3.3) where the determined crests differed from the highest points, but instead displayed a secondary maximum along the bedforms. These departures were due to the fact that the crests extending across the entire channel in both 2002 and 2003, in a few cases, deviated from the

highest points along the bedforms in one of the two years. The effect on the calculated bedform heights, though, was insignificant, as the deviations were small compared to the heights of the bedforms. Bedform volume per unit width V was calculated by integrating over the area above the line defining the bedform length. The bedform shape factor β was then calculated by relating the bedform volume per unit width to the product of bedform length and height ($\beta = V/LH$). Bedform celerity c was calculated for each bedform as the average movement of the troughs and the crest from 2002 to 2003. The bedform celerities are presented in meters per year although the calculations are based on two surveys only 10 months apart. The bedforms have been described according to the classification recommended in *Ashley* [1990], where ripples ($L < 0.6$ m) and dunes ($L > 0.6$ m) are distinguished on the basis of bedform length, dunes being further divided into categories of small ($L = 0.6$-5 m), medium ($L = 5$-10 m), large ($L = 10$-100 m) and very large ($L > 100$ m).

3.3.3 Water depths and flow velocities

The average water depth D relative to mean low water springs (MLWS) was also determined along transects N2-S2 based on the bathymetric grids from 2002 and 2003. Furthermore, average water depths were calculated in discrete time steps over a tidal period along the part of cross-section NE bounded by transects N2 and S2 (for location see Fig. 3.2) likewise based on the bathymetric grids from 2002 and 2003. Subsequently, the average cross-section water depths were used in the predictions of bedload transport.

Flow velocities were measured along cross-section NE at approximately half-hourly intervals. In each case, the profile was run twice (10-15 minutes in total) with the repetition serving as a quality control of the data, besides increasing the lateral resolution of data points. At each measuring point along the cross-section, the mean flow velocity (depth averaged) U was determined as the ensemble average flow velocity. These point mean flow velocities were then used to calculate the average mean flow velocity in the part of cross-section NE bounded by transects N2 and S2. Relating these average cross-section mean flow velocities to the flow velocities measured at station C revealed a significant linear correlation with the regression line $U_{NE} = 1.03u_C$ ($r = 0.992$, $n = 20$, $p < 0.0005$). This regression was used to extrapolate the 10-hour measurements along cross-section NE to cover the entire tidal period. Subsequently, the cross-section mean flow velocities were used in the predictions of bedload transport.

3.3.4 Grain size analysis

After rinsing the samples to remove salt and washing through a 4 phi (0.063 mm) wet sieve to separate sand and silt/clay, the samples were dried in the oven at 70°C and sieved at ¼-phi intervals. Where present, the mud fractions were collected, dried, and weighed to be subsequently added to the size distributions without being further analyzed.

Mean grain size d_{MZ}, phi standard deviation σ_I, phi skewness Sk_I and phi kurtosis K_G of the grain size distributions were determined on the basis of the percentile statistics described by *Folk and Ward* [1957].

3.3.5 Bedload transport based on measured bathymetry

Volumetric bedload transport q_b was too calculated along transects N2-S2 from the measured bathymetry, as well as from classical and widely applied bedload transport formulae.

Knowing bedform migration in conjunction with bedform dimensions, the volumetric bedload transport can be quantified according to the equation originally suggested by *Simons et al.* [1965]:

$$q_b = \beta cH \tag{3.1}$$

where β is the shape factor, c is bedform celerity and H is bedform height. The shape factor is equal to 0.5 in case of idealized triangular bedforms [e.g. *Simons et al.*, 1965; *Engel and Lau*, 1980]. However, in nature the shape factor often deviates from 0.5 and quite a few authors have found a value around 0.6 to be more appropriate [*van den Berg*, 1987; *Kostaschuk et al.*, 1989; *Villard and Church*, 2003]. The applicability of Equation (3.1) to quantify bedload transport has been discussed repeatedly in earlier studies [e.g. *Engel and Lau,* 1980 and 1981;*van den Berg,* 1987; *Wilbers and ten Brinke,* 2003; *Hoekstra et al.,* 2004]. The most recent review by *Hoekstra et al.* [2004] concludes that Equation (3.1) is adequate to determine bedload transport. Consequently, this approach was applied in this study, i.e. simply calculating bedload transport by inserting the appropriate values in Equation (3.1). Furthermore, as also recommended by *Hoekstra et al*. [2004], bedform-specific shape factors were used instead of a constant shape factor.

3.3.6 Prediction of bedload transport

When bedforms are present, the bed shear stress can be divided into a grain-related bed shear stress due to skin friction and a form-related bed shear stress due to form friction [e.g. *Fredsøe and Deigaard*, 1992]. The grain-related bed shear stress is the effective shear stress acting on the bed, whereas the form-related bed shear stress originates from the normal stress associated with the fluid pressure distribution upstream and downstream of the bedform crest [*van Rijn*, 1993]. Since sediment is moved by the effective shear stress and is unaffected by the normal stress, only the skin friction component of the total bed shear stress should be used [*Soulsby*, 1997]. Four bedload transport formulae were applied to calculate volumetric bedload transport: the classical *Meyer-Peter and Müller* [1948] formula and the widely applied formulae of *Engelund and Fredsøe* [1976], *van Rijn* [1984a] and *Nielsen* [1992] developed during the last three decades. According to these formulae, the dimensionless bedload transports Φ_b are given by:

Meyer-Peter and Müller [1948]:
$$\Phi_b = 8\left(\theta' - \theta_{cr}\right)^{1.5} \tag{3.2}$$

Engelund and Fredsøe [1976]:
$$\Phi_b = \frac{5}{\left[1+\frac{0.005}{\left(\theta' - \theta_{cr}\right)^4}\right]^{0.25}}\left(\sqrt{\theta'} - 0.7\sqrt{\theta_{cr}}\right) \tag{3.3}$$

van Rijn [1984a]:
$$\Phi_b = 0.053\frac{T^{2.1}}{D_*^{0.3}} \quad , \quad T < 3 \tag{3.4a}$$

$$\Phi_b = 0.1\frac{T^{1.5}}{D_*^{0.3}} \quad , \quad T \geq 3 \tag{3.4b}$$

Nielsen [1992]:
$$\Phi_b = 12\sqrt{\theta'}\left(\theta' - \theta_{cr}\right) \tag{3.5}$$

where θ' is the grain-related Shield's parameter, θ_{cr} is the threshold Shield's parameter, $T = (\theta'-\theta_{cr})/\theta_{cr}$ is the excess bed shear stress parameter and D_* is the particle parameter. The latter is defined as:

$$D_* = \left[\frac{(s-1)\,g}{\nu^2}\right]^{\frac{1}{3}} d_{50} \tag{3.6}$$

in which $s = \rho_s/\rho$ is the relative sediment density, ρ_s is the sediment density corresponding to that of quartz particles (2650 kg/m^3), ρ is the density of water (1022 kg/m^3 at a temperature of 17°C and a salinity of 31 ppt as measured on the 3rd of July 2004), g is the acceleration due to gravity (9.81 m/s^2), ν is the kinematic viscosity (1.08×10^{-6} m^2/s at the temperature and salinity mentioned above) and d_{50} is median grain size. The threshold Shield's parameter is calculated by the formula suggested by *Soulsby and Whitehouse* [1997]:

$$\theta_{cr} = \frac{0.30}{1+1.2D_*} + 0.055\left[1-\exp\left(-0.020D_*\right)\right] \tag{3.7}$$

The grain-related Shield's parameter is calculated by:

$$\theta' = \frac{u_f'^2}{(s-1)\, g\, d_{50}} \tag{3.8}$$

where u_f' is the friction velocity. For turbulent flow the friction velocity can be calculated from the Chézy equation:

$$u_f' = \sqrt{g}\,\frac{U}{C'} \tag{3.9}$$

where U is mean flow velocity (depth averaged) and C' is the grain related Chézy roughness coefficient which for rough flow is given by:

$$C' = 18\log\left(\frac{12D}{k_s'}\right) \tag{3.10}$$

in which D is water depth and k_s' is the grain roughness. *Meyer-Peter and Müller* [1948] and *van Rijn* [1984a] relate the grain roughness to the coarse 90th percentile of the grain size distribution d_{90}, i.e. for *Meyer-Peter and Müller* [1948] $k_s' = d_{90}$ whereas for *van Rijn* [1984a] $k_s' = 3d_{90}$. By contrast, *Engelund and Fredsøe* [1976] and *Nielsen* [1992] relate the grain roughness to the median grain size d_{50}, i.e. $k_s' = 2.5d_{50}$. Finally, dimensionless bedload transport is transformed to volumetric bedload transport according to:

$$\Phi = \frac{q_b}{\sqrt{(s-1)\, g\, d_{50}^3}} \tag{3.11}$$

Just as the magnitude of the flow varies during a tidal period, the direction of the flow also changes with ebb and flood. For that reason, flow velocities are considered positive

during flood and negative during ebb. Consequently, bedload transport is also positive during flood while negative during ebb.

3.4 Observations

3.4.1 Observed dune dimensions and celerities

The bed of the Grådyb tidal inlet channel is covered with large to very large compound dunes (Fig. 3.2). In total, 12 dunes extending across the channel in both 2002 and 2003 were identified along transects N2-S2 (Fig. 3.2). Following the dune crests across the channel, the dunes display barchanoid shapes (Fig. 3.2).

Bed profiles along transects N2-S2 extracted from the bathymetric grids from 2002 and 2003 are shown in Fig. 3.3. Dune dimensions and celerities have been calculated from these bed profiles.

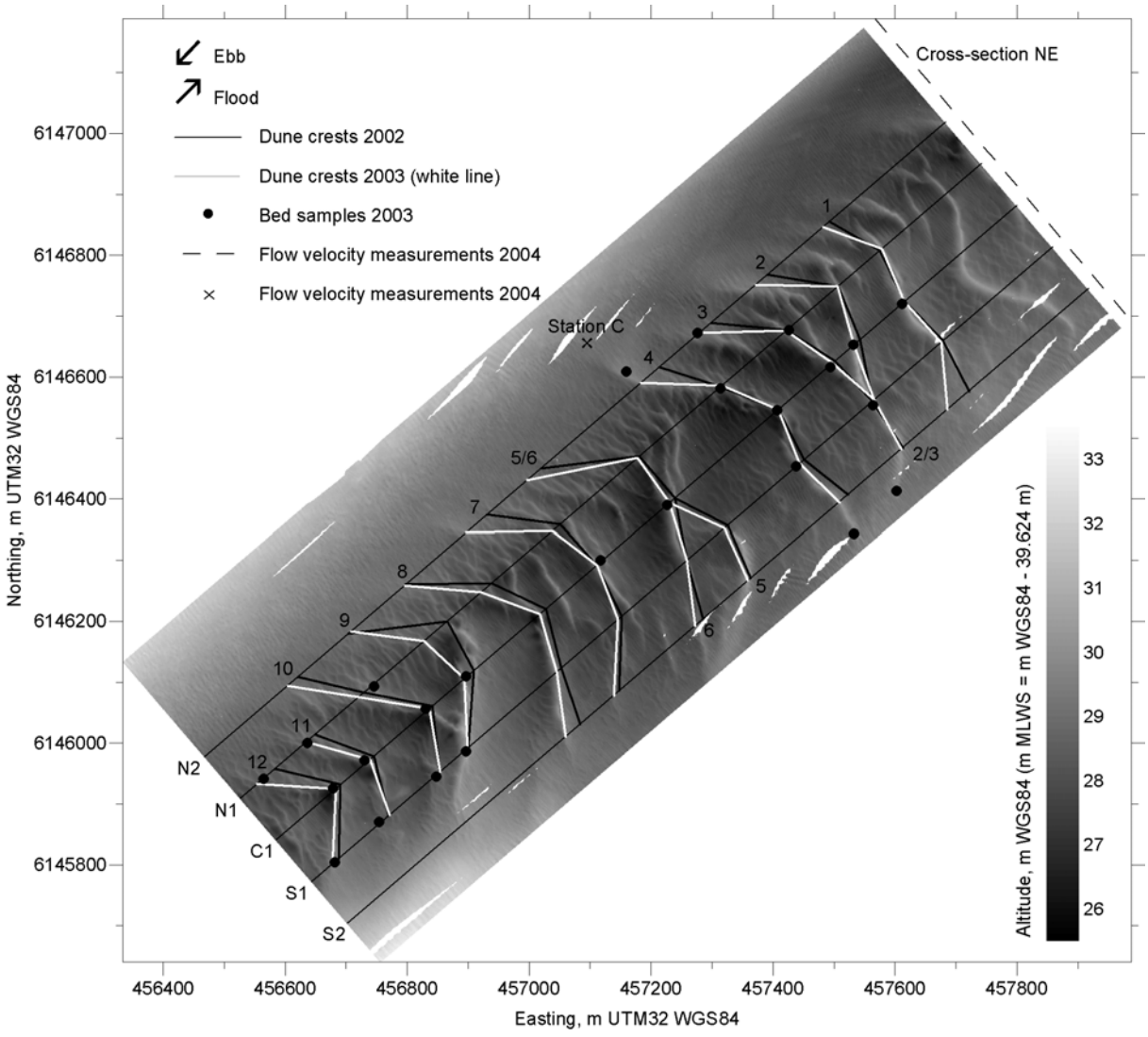

Fig. 3.2 (opposite page) Bathymetry of the Grådyb tidal inlet channel in 2003. The grid is 1600 x 650 m with a cell size of 0.5 x 0.5 m. Dune crests extending across the channel in both 2002 and 2003 are marked with black and white lines, respectively, and numbered from 1 to 12. Bed profiles were extracted along transects N2-S2 (see Fig. 3.3). Bed samples (marked with dots) were collected from dune crests along transects N2-S2 in 2003 (see Fig. 3.6 and Fig. 3.7). ADCP measurements were conducted along cross-section NE over 10 hours of a tidal period at spring tide in 2004 (see Fig. 3.4 and Fig. 3.5). Water depth relative to mean low water springs (MLWS) in relation to WGS84 altitude is given by: m MLWS = m WGS84 - 39.951 m.

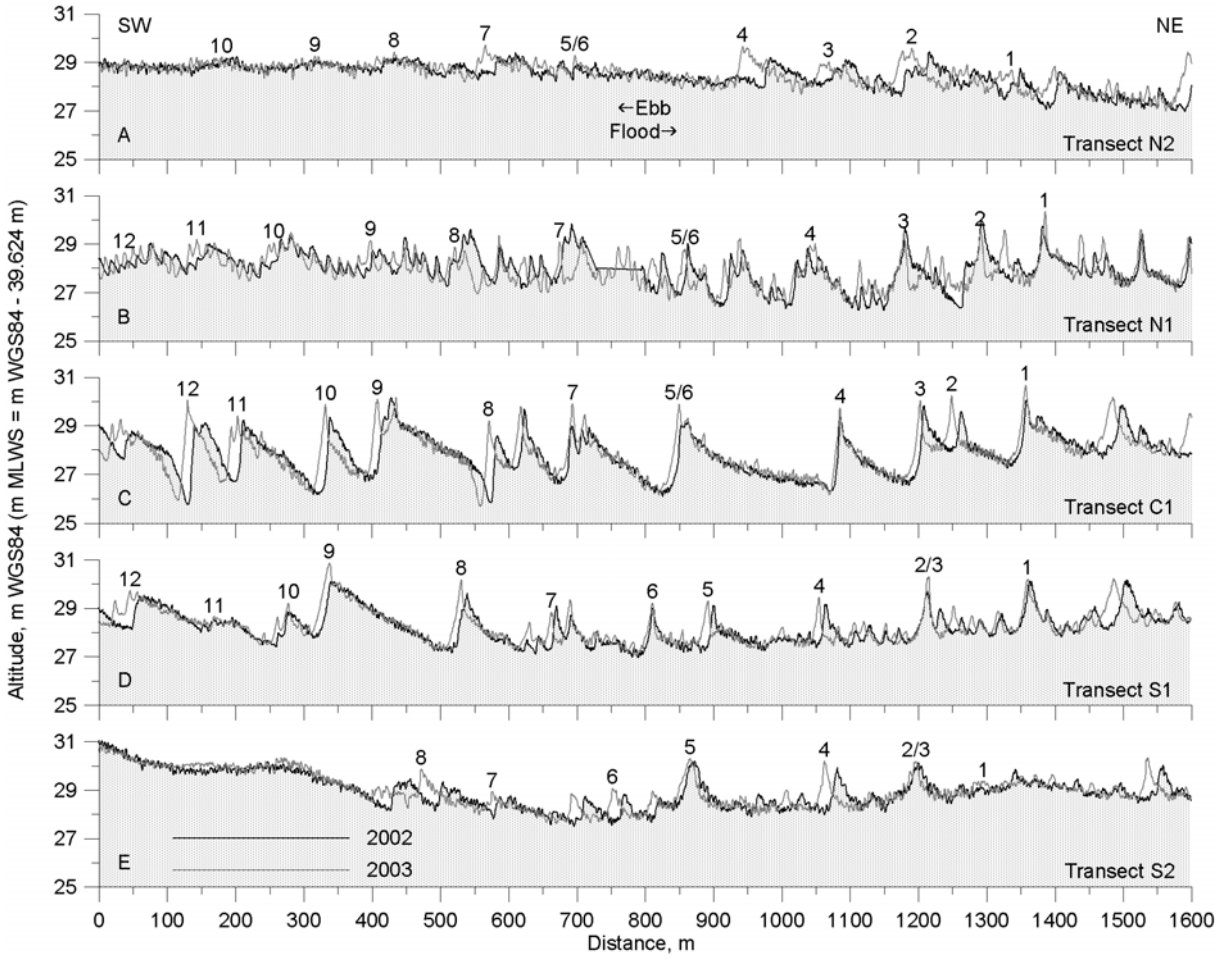

Fig. 3.3 Bed profiles along transects N2-S2 (A-E) extracted from bathymetric grids with cell sizes of 0.5 x 0.5 m from 2002 and 2003 (for locations see Fig. 3.2). Dune dimensions and celerities were determined from the identified (numbered from 1 to 12) large to very large dunes.

The average dune height decreases from 3.06 m in the centre of the channel to 1.17 m and 1.57 m at the northern and southern side of the channel, respectively (Table 3.1). The average dune length, by contrast, increases from 122 m in the centre of the channel to 149 m and 152 m at the northern and southern side, respectively (Table 3.1). The corresponding average

dune volume per unit width is 147 m^2 in the centre of the channel, whereas at the northern and southern side it is 75 m^2 and 80 m^2, respectively (Table 3.1). The average shape factors are relatively constant across the channel, ranging from 0.33 to 0.46 and displaying no clear lateral trend (Table 3.1).

Along the most southwesterly section of transects N2 and S2, large to very large compound dunes are indiscernible (Fig. 3.3A and E). The average dune length and height along the most southwesterly 100 m section of transect N2 is 7.88 m and 0.41 m, respectively (Fig. 3.3A). Along the corresponding section of transect S2, the average dune length and height is 5.16 m and 0.22 m, respectively (Fig. 3.3E).

A comparison of the identified dunes based on the bathymetric grids from 2002 and 2003 reveals a net ebb-directed dune migration (Fig. 3.2 and Fig. 3.3). In the centre of the channel the average dune celerity is 12 m/y whereas at the northern and southern side it is 31 m/y and 28 m/y, respectively (Table 3.1).

Table 3.1 Average dune length L, height H, volume per unit width V, shape factor β, celerity c, water depth D, mean grain size d_{MZ}, coarse 90th percentile of the grain size distribution d_{90}, phi standard deviation σ_I, phi skewness Sk_I and phi kurtosis K_G along transects N2-S2 (for locations see Fig. 3.2).

	N2	N1	C1	S1	S2
L, m	149	137	122	131	152
H, m	1.17	2.21	3.06	1.93	1.57
V, m^2	75	112	147	81	80
β	0.46	0.38	0.38	0.33	0.36
c, m/y	31	12	12	9	28
D, m MLWS	11.14	11.67	11.76	11.38	10.63
d_{MZ}, mm	0.357	0.441	0.629	0.460	0.362
d_{90}, mm	0.761	0.777	1.046	0.822	0.634
σ_I	0.678	0.502	0.499	0.531	0.537
Sk_I	-0.279	-0.097	-0.118	-0.121	-0.195
K_G	1.379	1.111	1.140	1.103	1.122

3.4.2 Observed water depths and flow velocities

The average water depth varies from 11.76 m MLWS in the centre of the channel to 11.14 m MLWS and 10.63 m MLWS at the northern and southern side, respectively (Table 3.1). Along the part of cross-section NE bounded by transects N2 and S2, the average water depth is 11.36 m MLWS with a standard deviation of 0.62 m.

Mean flow velocities (depth averaged) along cross-section NE at four representative stages during a tidal period around spring tide are shown in Fig. 3.4 (the exact times of the four measurements relative to the tidal period are marked with dots in Fig. 3.5). Positive

values refer to flood flow and negative values to ebb flow. Around maximum flood, the cross-section mean flow velocity in the part bounded by transects N2 and S2 is 1.04 m/s with a standard deviation of 0.10 m/s. Close to slack water at the end of the flood phase, the cross-section mean flow velocity is 0.28 m/s with a standard deviation of 0.07 m/s. At the beginning of the ebb phase, the cross-section mean flow velocity is 0.16 m/s with a standard deviation of 0.05 m/s. No measurements are available along cross-section NE around maximum ebb flow. However, the measurement closest to maximum ebb displays a cross-section mean flow velocity of 0.97 m/s with a standard deviation of 0.09 m/s. Considering the entire 10-hour measurements during the tidal period, the standard deviations of the cross-section mean flow velocities range from 0.05 m/s to 0.12 m/s with the highest standard deviations around maximum flood and ebb and the lowest close to slack water.

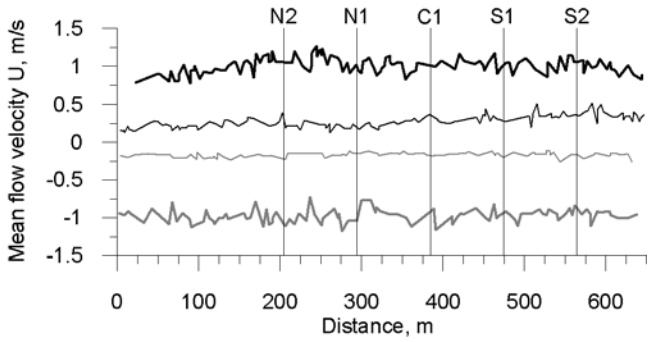

Fig. 3.4 Mean flow velocity (depth averaged) U along cross-section NE (for locations see Fig. 3.2) around spring tide just about maximum flood (bold black line), close to slack water flood (black line) and ebb (gray line) and the available measurement closest to maximum ebb (bold gray line). The exact times of the measurements relative to the tidal period are shown with dots in Fig. 3.5.

The average mean flow velocities and corresponding average water depths in the part of cross-section NE bounded by transects N2 and S2 over a tidal period around spring tide are shown in Fig. 3.5. Cross-section mean flow velocities calculated from the cross-section measurements are shown with circles and dots. The extrapolation of the curve is determined from the measurements at station C. The cross-section mean flow velocities during flood and ebb reach maximum values of 1.08 m/s and 1.32 m/s, respectively.

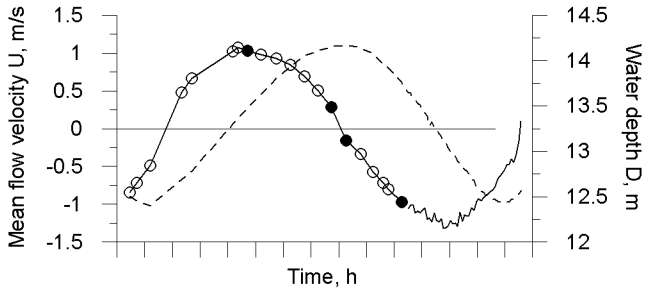

Fig. 3.5 Cross-section mean flow velocities U (line) and corresponding average water depths D (dashed line) in the part of cross-section NE bounded by transects N2 and S2 (for location see Fig. 3.2) over a tidal period around spring tide. Circles and dots mark the times of the ADCP measurements. The extrapolation of the ADCP measurements is determined from the measurements at station C (for location see Fig. 3.2).

3.4.3 Observed grain sizes

Statistics of the bed material collected from dune crests along transects N2-S2 are presented in Fig. 3.6. As examples, the frequency curves of the grain size distributions from the crests of dune 4 and 12 along transects N2-S2 are shown in Fig. 3.7, being representative of grain size distributions across the entire dune field. The average mean grain size decreases from 0.629 mm in the centre of the channel to 0.357 mm and 0.362 mm at the northern and southern side of the channel, respectively (Fig. 3.6A and Table 3.1). In addition, there is a decrease in mean grain size along the channel from northeast to southwest (Fig. 3.6A). The phi standard deviation, i.e. sorting, of the grain populations across the channel is relatively uniform (Fig. 3.7A and B and Table 3.1), whereas it decreases along the channel from northeast to southwest (Fig. 3.6B and Fig. 3.7A and B), i.e. changing from moderately well sorted to well sorted [after *Folk*, 1974]. The phi skewness, i.e. sorting in the tails of the grain population, varies from near symmetrical to negative (coarse) skewed [after *Folk*, 1974], showing signs of increasing negative skewness from the centre towards the sides of the channel (Fig. 3.6C and Table 3.1). The phi kurtosis, i.e. degree of sharpness or peakedness, of the grain size distributions is relatively uniform both across and along the channel (Fig. 3.6D and Table 3.1).

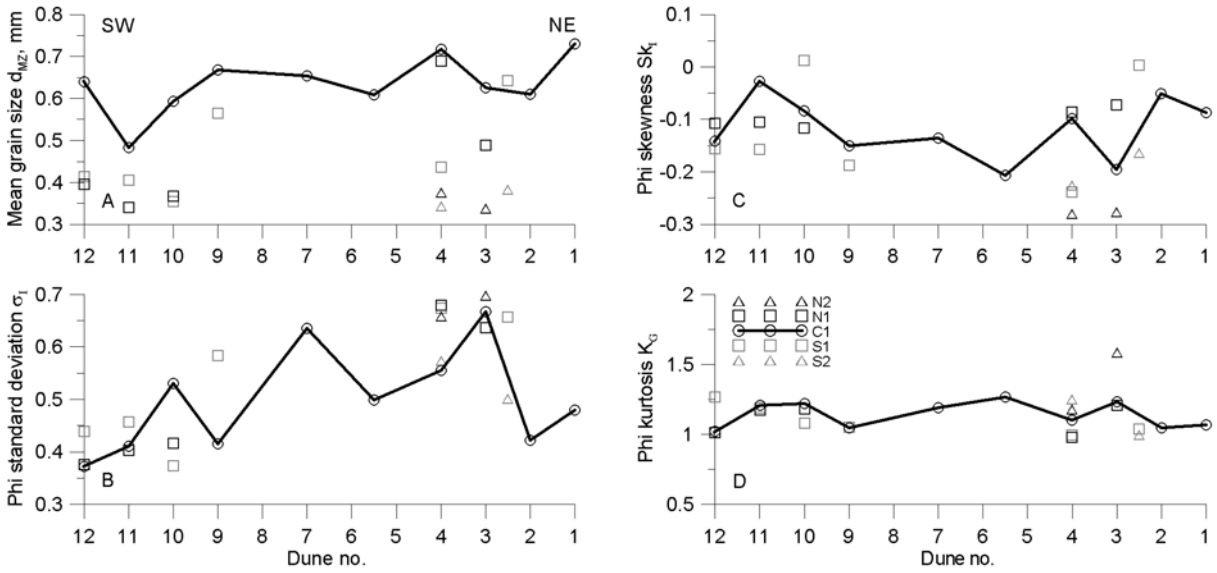

Fig. 3.6 Mean grain size d_{MZ} (A), phi standard deviation σ_I (B), phi skewness Sk_I (C) and phi kurtosis K_G (D) at dune crests along transects N2-S2 (for locations see Fig. 3.2).

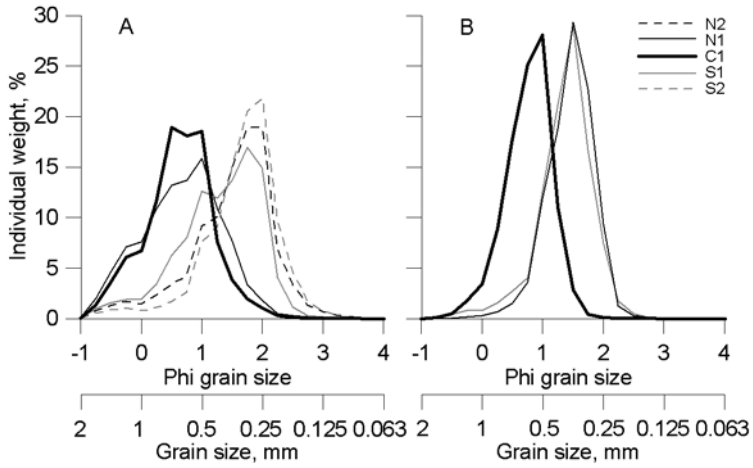

Fig. 3.7 Frequency curves of the grain size distributions along the crests of dunes 4 (A) and 12 (B) at the intersections with transects N2-S2 (for locations see Fig. 3.2).

3.5 Dune dynamics

3.5.1 Development of barchanoid-shaped dunes

The observed dune migration in the survey area reveals an increase in dune celerity from the centre towards the sides of the channel (Table 3.1). This inevitably results in the development of barchanoid-shaped dunes as also observed in the dune field (see Fig. 3.2). Furthermore, a decrease in dune height (size) was observed from the centre towards the sides of the channel (Table 3.1). This suggests that the increase in dune celerity from the centre towards the sides of the channel is a result of the decrease in dune height (size) away from the

centre of the channel. This can be explained by the fact that a smaller volume of sediment has to be moved at the sides per unit time for equal dune celerity. Plotting dune celerity against dune height (Fig. 3.8) confirms this yielding significant logarithmic relationships when using both single values for individual dunes ($r = 0.560$, $n = 49$, $p < 0.0005$) as well as average values for transects N2-S2 as given in Table 3.1 ($r = 0.813$, $n = 5$, $p < 0.05$). The regression line of the logarithmic relationship when using single values for individual dunes is shown in Fig. 3.8, i.e. $c = -14.83\ln H+26.68$ with H in m and c in m/y.

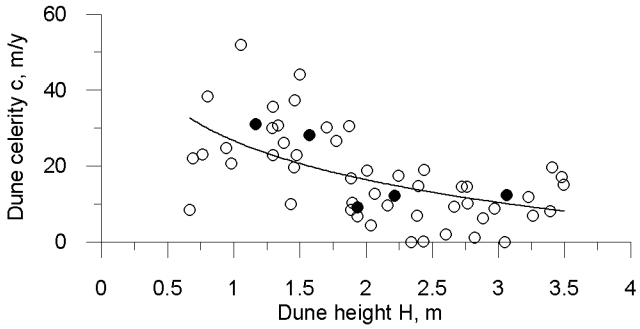

Fig. 3.8 Scatter diagram of dune celerity c against dune height H. Circles refer to the individual dunes whereas the dots refer to the average values in transects N2-S2 as given in Table 3.1 (for locations see Fig. 3.2). The line shows the regression line of the logarithmic relationship when using single values for individual dunes ($c = -14.83\ln H+26.68$ with H in m and c in m/y, $r = 0.560$, $n = 49$, $p < 0.0005$).

3.5.2 Factors controlling dune size

The scaling factors controlling the size of dunes have been argued to be grain size and flow velocity dependent, along with water depth as a limiting factor assuming an abundance of sediment [*Flemming*, 2000a]. The dunes in the Grådyb tidal inlet channel are not starved and there is a general abundance of sediment in the area [*Bartholdy et al.*, 2002]. The water depth across the channel is nearly uniform, as illustrated by the observed average water depths in transects N2-S2 (Table 3.1). In addition, the standard deviation of the water depths along the part of cross-section NE bounded by transects N2 and S2, i.e. 0.62 m is low. The flow velocity across the channel during both ebb and flood is also practically uniform. This is demonstrated by the low standard deviations of the cross-section mean flow velocities in the part of cross-section NE bounded by transect N2 and S2, i.e. 0.05-0.12 m/s, based on the 10-hour measurements during a tidal period. This implies that the decrease in dune height from the centre towards the sides of the channel (Table 3.1) is a result of the decrease in mean grain size away from the centre of the channel (Table 3.1). This is confirmed by plotting dune

height against mean grain size (Fig. 3.9) which yields significant linear relationships, both when using single values for individual dunes ($r = 0.798$, $n = 25$, $p < 0.0005$) and when using average values for transects N2-S2 as given in Table 3.1 ($r = 0.958$, $n = 5$, $p < 0.01$). The regression line of the linear relationship when using single values for individual dunes is shown in Fig. 3.9, i.e. $H = 4.70d_{MZ}-0.12$ with d_{MZ} in mm and H in m.

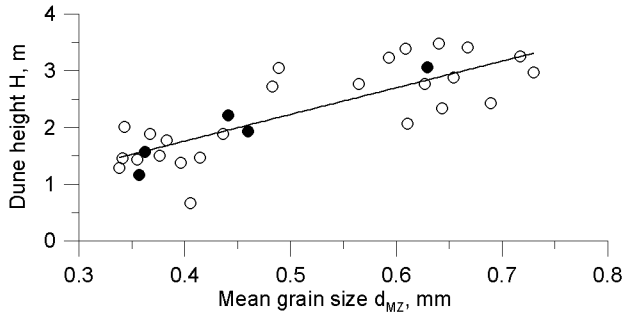

Fig. 3.9 Scatter diagram of dune height H against mean grain size d_{MZ} at the dune crests of the large to very large compound dunes (for locations see Fig. 3.2). Circles refer to the individual dunes whereas the dots refer to the average values in transects N2-S2 as given in Table 3.1 (for locations see Fig. 3.2). The line shows the regression line of the linear relationship when using single values for individual dunes ($H = 4.70d_{MZ}-0.12$ with d_{MZ} in mm and H in m, $r = 0.798$, $n = 25$, $p < 0.0005$).

3.5.3 Factors controlling grain size variability

The bathymetric data reveal asymmetric small to large dunes located in the trough/lee side region of the large to very large dunes, indicating the existence of secondary sediment transport paths as a result of secondary currents directed from the centre towards the sides of the channel (Fig. 3.10).

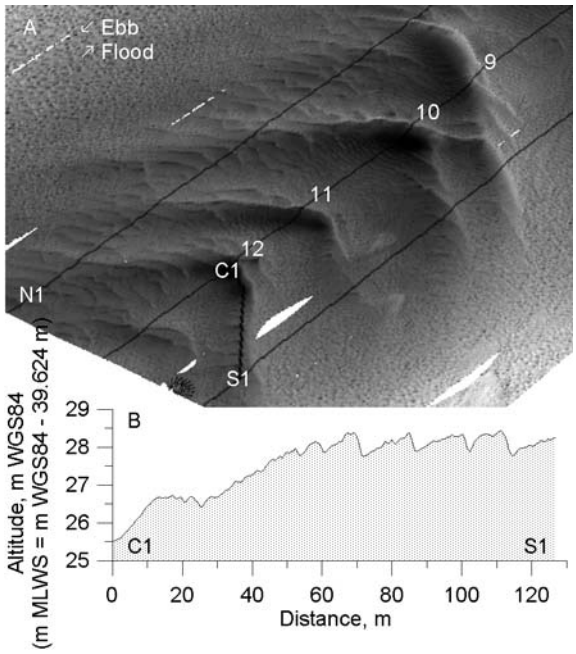

Fig. 3.10 A) Bathymetry of the southwestern part of the Grådyb tidal inlet channel in 2002 (for location see Fig. 3.2). B) Bed profile in the trough/lee side region parallel to the crest of dune 12 from the centre (C1) towards the southern side (S1) of the channel. The bed profile has been extracted from a bathymetric grid with a cell size of 0.5 x 0.5 m.

According to *McLaren* [1981] and *McLaren and Bowles* [1985] sediment in transport will decrease in mean grain size, i.e. become finer, decrease (or not increase) in standard deviation, i.e. become better sorted, and become more negatively skewed, i.e. coarse tailed, in the direction of transport. In the ebb-dominated Grådyb tidal inlet channel this model applies well with mean grain size and standard deviation decreasing in the direction of ebb flow as well as the distributions being primarily negatively skewed (Fig. 3.6 and Fig. 3.7). Laterally from the centre towards the sides of the channel there is also a decrease in mean grain size, a constant or decreasing standard deviation and a primarily increasing negative skewness (Fig. 3.6, Fig. 3.7 and Table 3.1). Applying the McLaren model laterally moreover supports the existence of secondary currents resulting in a secondary sediment transport directed from the centre towards the sides of the channel.

As already mentioned, medium to coarse sand is supplied to the system from the Pleistocene cliffs lining the mainland in the landward part of the back-barrier tidal basin (see Fig. 3.1), whereas fine sand is brought in from the near-shore region of the open coast [*Bartholdy et al.*, 2002]. This setup provides the components needed for the lateral grain size pattern observed in the Grådyb tidal inlet channel. The Pleistocene cliff sand may be transported seawards in bedload by the dominating ebb flow [*Bartholdy et al.*, 2002] resulting

in a fining, better sorting, and negatively skewing of the grain population. In addition the finer fractions of the Pleistocene cliff sand may be transported laterally in bedload or intermittent suspension from the centre towards the sides of the channel by the suggested secondary currents. The near shore fine sand introduced to the system by each flood may undergo a similar transport mechanism.

3.5.4 Dune splitting

The average dune dimensions in the centre of the channel follow the height-length relationship suggested by *Flemming* [1988] (Fig. 3.11). However, this is not the case closer to the channel sides where the dunes get lower and longer (Table 3.1). The dune dimensions along the most southwesterly 100 m section along transects N2 and S2, where the large to very large compound dunes were indiscernible, again follow the relationship suggested by *Flemming* [1988] (Fig. 3.11). This implies that the large to very large dunes at the sides of the channel are adjusting to the decrease in mean grain size by splitting up into smaller dunes.

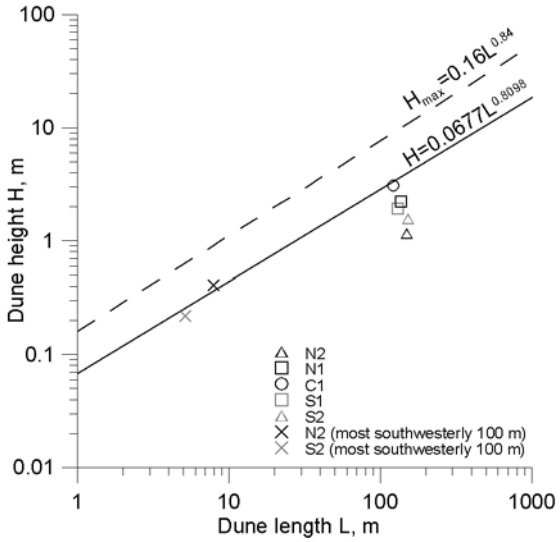

Fig. 3.11 Average dune height H against average dune length L in transects N2-S2 (for locations see Fig. 3.2). The black and gray crosses refer to the most southwesterly 100 m sections along transects N2 and S2 (for locations see Fig. 3.2). Line and dashed line show the global and upper height limit relationship, respectively, according to Flemming [1988].

3.6 Bedload transport

Average volumetric bedload transport along transects N2-S2, calculated by insertion of measured dune dimensions and celerities in Equation (3.1), are shown in Table 3.2. In the centre and along the sides of the channel, the bedload transport is practically equal with an

average value of 16 m^2/y, whereas along transect N1 and S1 it only amounts to 50% of this value with an average around 8 m^2/y (Table 3.2).

Table 3.2 Volumetric bedload transport q_b along transects N2-S2 (for locations see Fig. 3.2) calculated by insertion of measured dune dimensions and celerities in Equation (3.1) as well as predicted from the bedload transport formulae in Equations (3.2)-(3.5).

		q_b (m^2/y)				
Bedload transport formula	Equation	N2	N1	C1	S1	S2
Measured						
Simons et al. [1965]	(3.1)	17	9	15	6	15
Predicted						
Meyer-Peter and Müller [1948]	(3.2)	77	75	79	76	74
Engelund and Fredsøe [1976]	(3.3)	126	143	162	146	127
van Rijn [1984a]	(3.4)	106	110	118	113	101
Nielsen [1992]	(3.5)	126	132	143	134	126

As shown above, water depth as well as flow velocity during both ebb and flood are practically uniform. Bedload transport was predicted along transects N2-S2 at discrete time steps by insertion and substitution in Equations (3.2)-(3.11) using the cross-section mean flow velocities and water depths shown in Fig. 3.5 together with the grain size values given in Table 3.1. Integrating over the tidal period and calculating the difference by subtraction yields the net bedload transport as well as the transport direction. In Fig. 3.12, the prediction of bedload transport along transect C1 using the classical formula of *Meyer-Peter and Müller* [1948] (Equation (3.2)) is shown as an example of this procedure. In addition, the net ebb-directed bedload transport (Fig. 3.12B) documents the ebb dominance, i.e. the asymmetry and migration direction of the dunes in the Grådyb tidal inlet channel are the result of the higher flow velocities during the ebb (Fig. 3.5).

Assuming that the tidal period at spring tide on the 3rd of July 2004 is representative of an entire year, the predicted bedload transport over the tidal period was extrapolated to a yearly budget using a tidal period duration of 12 hours and 25 minutes. Predicted volumetric bedload transport along transects N2-S2 ranges from 75 m^2/y to 162 m^2/y according to the various bedload transport formulae (Table 3.2). The *Meyer-Peter and Müller* [1948] formula predicts a practically uniform bedload transport across the channel ranging from 74 m^2/y to 79 m^2/y (Table 3.2). By contrast, the formulae of *Engelund and Fredsøe* [1976], *van Rijn* [1984a] and *Nielsen* [1992] predict an increase in bedload transport from the centre towards the sides of the channel (Table 3.2). Furthermore, all bedload transport prediction formulae over-estimate the bedload transport calculated by insertion of measured dune dimensions and celerities in

Equation (3.1) (Table 3.2), the over-estimates ranging from a factor 4 in the best case to 24 in the worst case.

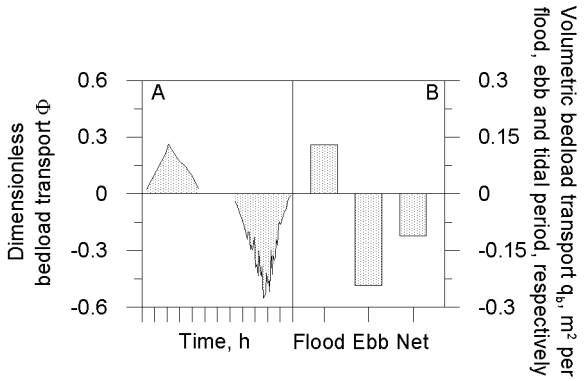

Fig. 3.12 Example schematizing the prediction of net volumetric bedload transport over a tidal period. A) Dimensionless bedload transport Φ along transect C1 (for location see Fig. 3.2) at discrete time steps according to Meyer-Peter and Müller [1948] (Equation 3.2) during a tidal period around spring tide. B) The corresponding volumetric bedload transport during flood and ebb along with the resulting net bedload transport over the tidal period.

3.7 Discussion

The development of barchanoid-shaped dunes in the Grådyb tidal inlet channel has been shown to be the result of higher dune celerities along the sides of the channel due to smaller dunes along the sides. A similar conclusion of an increase in dune celerity as a result of a decrease in dune height (size) and, hence, smaller sediment volumes that have to be moved was also reached by e.g. *Dinehart* [2002].

The decrease in dune height here being a function of the decrease in mean grain size is in conflict with the classical concept of factors controlling dune size. Commonly, dune height is considered to scale with water depth [*Yalin*, 1977; *van Rijn*, 1984b]. This is not the case in the Grådyb tidal inlet channel where the decrease in dune height from the centre towards the sides of the channel occurs at practically uniform water depths. The formulae predicting dune height to scale with water depth such as those of *Yalin* [1977] and *van Rijn* [1984b] are primarily based on data derived from flume studies where water depths are typically small compared to those in natural systems. This introduces an artificial dependency because the water depth is an upper boundary acting as a limit for dune growth. *Carling et al.* [2000a] observed this mechanism in the River Rhine where a water depth limitation on dune heights was seen at shallow water depths. However, in natural systems where water depths are

generally much larger than dune height no dependency of water depth on dune height is observed [*Kuijpers et al.*, 2002].

Dunes varying in height have been observed side by side in situations where the flow is characterized by lateral flow velocity gradients [*Flemming*, 2000b]. In the Grådyb tidal inlet channel, mean flow velocity is laterally uniform both during ebb and flood making this argument inapplicable in this environment.

However, a decrease in dune height due to a decrease in mean grain size is in accordance with *Flemming* [2000a] who theoretically shows that the larger the grain size, the larger the maximum potential dune size. *Flemming* [2000a] argues that dune growth will terminate once flow acceleration above the dune crest reaches a grain size dependent critical suspension velocity. This relation is confirmed by the observations in the Grådyb tidal inlet channel where dune height decreases with decreasing mean grain size. Though, near-bed flow velocity measurements at the crests of the dunes are required to confirm whether the suspension of bed material is the reason for the termination of dune growth.

It has been shown that the relationship between dune height and mean grain size in the Grådyb tidal inlet channel is significantly positively correlated and can be described by a linear relationship. Earlier, *Bartholdy et al.* [2002] likewise established a significant positively correlated relationship, but expressed by a power function based on two separate bed sample sets taken with a Van-Veen grab from the same study area in 1992 and 1999. The power function was derived from randomly positioned samples with mean grain sizes ranging from 0.33 mm to 0.56 mm, whereas the linear function established in this study is based solely on crest samples with mean grain sizes covering the range from 0.33 mm to 0.73 mm. The importance of sampling position may be exemplified by additional bed samples collected from the troughs and backs of 3 dunes in transect C1. These samples revealed an average mean grain size in the troughs, on the backs and on the crests of 0.488 mm, 0.523 mm and 0.629 mm, respectively, which illustrates the importance of comparable sampling positions when analyzing the data. The shift in the descriptive relationship, from a power function to a linear function, can be explained by the inaccuracy in sampling positioning during earlier surveys, since *Bartholdy et al.* [2002] most likely underestimated the related mean grain size due to the low probability of a randomly positioned sample to be located at the dune crest. The physical explanation of why the relationship is linear is currently unknown to the authors.

Concerning cross-channel distributions in grain size no earlier studies have been found. The observations from the Grådyb tidal inlet channel showing a lateral variability in grain

sizes along the dune crests is, to the knowledge of the authors, the first time that such patterns have been documented.

Recently, however, *Maddux et al.* [2003a and b] conducted a series of detailed measurements of unidirectional turbulent open-channel flow over fixed, artificial, sinuous-crested three-dimensional (3D) dunes in a laboratory flume. They found that the flow was topographically steered by the 3D features and that the largest measured cross-stream flow velocities were in the troughs with most of the cross-stream flow occurring close to the bed. Although the flume experiments were carried out in clear water without moveable bed material, they nevertheless show the existence of secondary currents in the troughs of barchanoid-shaped dunes and thereby support the suggestion of the existence of secondary transport paths in the troughs.

Dune splitting as an adjustment process to changing conditions has earlier been observed in the course of the flow velocity reduction from spring to neap tide where larger dunes split up into smaller ones with the larger spring-tide dunes still being discernible at neap tide [*Flemming and Davis*, 1992]. Likewise the large to very large dunes along the sides of the Grådyb tidal inlet channel are adjusting by splitting up into smaller dunes, however, in this case due to a decrease in mean grain size.

Concerning the discrepancy between measured and predicted bedload transport, part of the over-estimation is certainly due to the fact that the tidal period around spring tide on the 3rd of July 2004 is unrepresentative of the general dynamics in the Grådyb tidal inlet channel, seeing that the predicted bedload transport around spring tide undoubtedly exceeds the corresponding transport around neap tide considerably. An additional reason for the over-estimation is probably that transport processes in nature are not always well described by the currently available bedload transport prediction formulae, which have all been calibrated on the basis of flume studies. *Soulsby* [1997] earlier emphasized the fact of transport formulae being based on incorrect assumptions and found discrepancies up to a factor of four when using various published equations. He further argues that although bedload transport responds quickly to changes in, e.g., flow velocity and water depth, and hence justifying an approach based on quasi-equilibrium transport, a calculation based on dune dimensions and celerities is recommended, especially in unsteady flows as found in tidal environments. The lateral distribution of bedload transport with lower values between the centre and along the sides of the channel may be an effect of the suggested secondary currents and related transport from the centre towards the sides of the channel. Nonetheless, a higher measuring frequency with

better resolved near bed dynamics is needed to shed more light on these processes occurring oblique to the main current and at a lower order of magnitude in flow velocities.

3.8 Conclusions

Based on the analysis of bathymetry, flow velocity and grain size in a dune field section of the Grådyb tidal inlet channel in the Danish Wadden Sea, the following conclusions are reached:

1) Dune migration is net ebb-directed and increases from the centre towards the sides of the channel resulting in the development of barchanoid-shaped dunes.

2) The increase in dune celerity is a result of the corresponding decrease in dune height (size) from the centre towards the sides of the channel, because smaller volumes of sediment have to be moved at the sides per unit time for equal dune celerity.

3) The decrease in dune height is due to an equivalent decrease in grain size from the centre towards the sides of the channel, in view of the fact that water depth and flow velocity during both ebb and flood are practically uniform across the channel. The grain size control on dune height may be due to the fact that flow velocities at the dune crests reach the suspension criteria of the bed material which then terminates further dune growth as theoretically proposed by *Flemming* [2000a]; but near-bed flow velocity measurements at the crests of the dunes are required to test this hypothesis.

4) The decrease in grain size is suggested to be the sorting effect of secondary currents in the trough/lee side region directed from the centre towards the sides of the channel, supporting the transport of the finer sediment fractions.

5) The more rapidly migrating flanks of the barchanoid-shaped dunes seems to be an adjustment to the decrease in grain size from the centre towards the sides of the channel, causing the dunes to split up into smaller forms.

6) The net ebb-directed bedload transport, calculated from dune dimensions and celerities, is lower between the centre and along the sides of the channel. This lateral distribution of bedload transport is unresolved by the classical *Meyer-Peter and Müller* [1948] and the widely applied formulae of *Engelund and Fredsøe* [1976], *van Rijn* [1984a] and *Nielsen* [1992]. In addition, these bedload transport formulae over-predict the bedload transport as calculated from dune dimensions and celerities.

Notation

c Bedform celerity, m/y.

C' Grain related Chézy roughness coefficient, $m^{0.5}/s$.

d_{MZ} Mean grain size, m (or mm).

d_{50} Median grain size, m (or mm).

d_{90} Coarse 90^{th} percentile of the grain size distribution, m (or mm).

D Water depth, m

D_* Particle parameter

g Acceleration due to gravity, m/s^2.

H Bedform height, m.

k_s' Grain roughness, m.

K_G Phi kurtosis.

L Bedform length, m.

q_b Volumetric bedload transport, m^2/y.

s Relative sediment density

Sk_I Phi skewness.

T Excess bed shear stress parameter.

u_f' Friction velocity, m/s.

U Mean flow velocity (depth averaged), m/s.

V Bedform volume per unit width, m^2.

β Shape factor.

θ' Grain-related Shield's parameter.

θ_{cr} Threshold Shield's parameter.

ρ Water density, kg/m^3.

ρ_s Sediment density, kg/m^3.

σ_I Phi standard deviation.

ν Kinematic viscosity, m^2/s.

Φ_b Dimensionless bedload transport.

Acknowledgements

This study was supported by the German Science Foundation. The captain and crew of the RV Senckenberg are thanked for their expertise and unfailing good spirits during the

cruises. Appreciated is also the field assistance of Elke Tilch and Anders Bartholdy. Nicol Mahnken-Roetzer, Sonja Heinrich and Wolfgang Nenno are thanked for assisting in the laboratory. Finally, the quality of the manuscript improved from valuable comments and suggestions by two anonymous reviewers, the Associate Editor and the Editor, who are all thanked for their thorough and engaged reviews.

Paper III

Chapter 4: Paper III

Bedform dynamics and net sediment transport paths over a flood-ebb tidal cycle in the Grådyb channel (Denmark), determined by high-resolution multibeam echosounding

Alex Bartholomä[1], Verner B. Ernstsen[2], Burg W. Flemming[1], Jesper Bartholdy[3]

[1]*Senckenberg Institute, Division of Marine Science, Suedstrand 40, D-26382 Wilhelmshaven, Germany*

[2]*Research Center Ocean Margins, University of Bremen, Leobener Str., P.O. Box 330 440, D-28359 Bremen, Germany*

[3]*Institute of Geography, University of Copenhagen, Øster Voldgade 10, DK-1350 Copenhagen, Denmark*

Danish Journal of Geography, 104(1): 45-55

Abstract

High-resolution bathymetric surveys were carried out by means of a high-frequency (455 kHz) multibeam echosounder (MBES) to determine the total volumetric sediment transport over a tidal period in a tidal channel at the Danish west coast. With the high repetition rate and high accuracy of the MBES, a simple comparison of morphological changes recorded at short time intervals allows an accurate calculation of dune heights and migration rates, the main parameters required for realistic approximations of volume budgets in tidal channels. The net sediment volume of 0.061 m^3/m^2 over one tidal period is ebb-orientated, which means an annual net volume export of 44.5 m^3/m^2 per year. The general ebb-oriented export trend recorded for the large, compound dune system is contrasted by a net flood-oriented transport in the 'active zone' involving smaller superimposed dunes, which amounts to 0.6 m^2 per flow phase on top of the large dunes, and 0.15 m^2 per flow phase on the slopes and in the troughs. This gives a mean volumetric sediment transport rate of 0.7697×10^{-5} m^2/s for the ebb flow, and 1.059×10^{-5} m^2/s for the flood flow, strongly deviating from earlier calculated transport rates.

4.1 Introduction

Tidal inlets like the Grådyb channel on the west coast of Denmark are natural waterways connecting the open sea with back-barrier tidal basins. The channel beds are typically covered with large bedforms [e.g. *Allen*, 1968; *Flemming and Davis*, 1992], the dimensions of which are controlled mainly by the local hydraulic regime and sediment composition, and the general morphological setting [e.g. *Allen*, 1982; *Flemming*, 2000a]. Studies of bedform migration and associated variations in sediment composition have focussed largely on fluvial regimes, amongst others, also in central Europe [e.g. *Carling et al.*, 2000a, 2000b]. Dimensional adjustments of subaqueous dunes in response to changing flow conditions have been reviewed by *Flemming* [2000b], whereas short-term time-lag effects of dune adjustments have been discussed by *Allen* [1976] for tidal flow regimes. However, the general problem of the effects of unsteady flow on bedform behaviour over short time periods, e.g. over individual tidal cycles, has thus far only been assessed rather imprecisely on the basis of various sediment transport equations [e.g. *Soulsby*, 1997].

The simplest approach to reliably estimate sediment transport rates in confined channels is the combination of high-resolution bathymetric surveys with rapid scan repetitions. This

procedure allows an accurate calculation of dune heights and migration rates, the main parameters required to determine the total volumetric transport over a tidal period. Such accuracy can be achieved only with high-frequency echosounding equipment coupled with very precise position referencing.

In the course of longer-term bathymetric, hydrological and sedimentological studies of the Grådyb channel, an annual bedform migration rate of 32 m was deduced [*Bartholdy et al.*, 2002]. Although such annual surveys covering periods of ten years and more can yield good results of overall net transport rates on the basis of conventional echosounding, they are unsuitable for assessing how this longer-term net transport has evolved when considering shorter tidal time scales, such as individual tidal cycles or spring-neap cycles. In addition, the effect of storm surges is not resolved either.

The main aim of the present study, therefore, was to investigate the short-term dynamics of bedforms and associated transport rates over individual ebb-flood tidal periods in the same tidal channel as before, this time using a high-frequency multibeam echosounder (MBES) with a height resolution of a few millimetres, coupled with centimetre-scale position referencing.

4.2 Study site and physiographical setting

The survey was carried out in September 2002 in the Grådyb channel, the main navigation channel to the harbour of Esbjerg (Fig. 4.1), from aboard the RV Senckenberg. The Grådyb tidal inlet, which connects the northernmost tidal basin of the Wadden Sea with the adjacent North Sea, is located on the Danish west coast between the barrier spit of Skallingen and the barrier island of Fanø. The survey area was located in the centre of the Grådyb channel, between 08°18'500E and 08°21'000E, and covered a distance of approximately 3 km and a width of 650 m.

The tides are semi-diurnal with a local mean tidal range of ca. 1.5 m and a tidal prism of the order of 150×10^6 m^3. The width of the channel is ca. 1 km and the mean depth varies in the range 10-13 m. The channel is ebb-dominated, with maximum ebb and flood current velocities of ca. 1.50 and 1.25 m/s, respectively [*Bartholdy and Anthony*, 1998]. The bed of the channel is composed of sandy material, mean grain size decreasing from 550 µm in the landward section (northeast) to 300 µm in the seaward section (southwest). The bed is covered with very large compound dunes and superimposed, medium-sized simple dunes [cf.

classification of *Ashley*, 1990]. The local spectrum of dune dimensions and their genesis have been assessed in detail by *Bartholdy et al.* [2002].

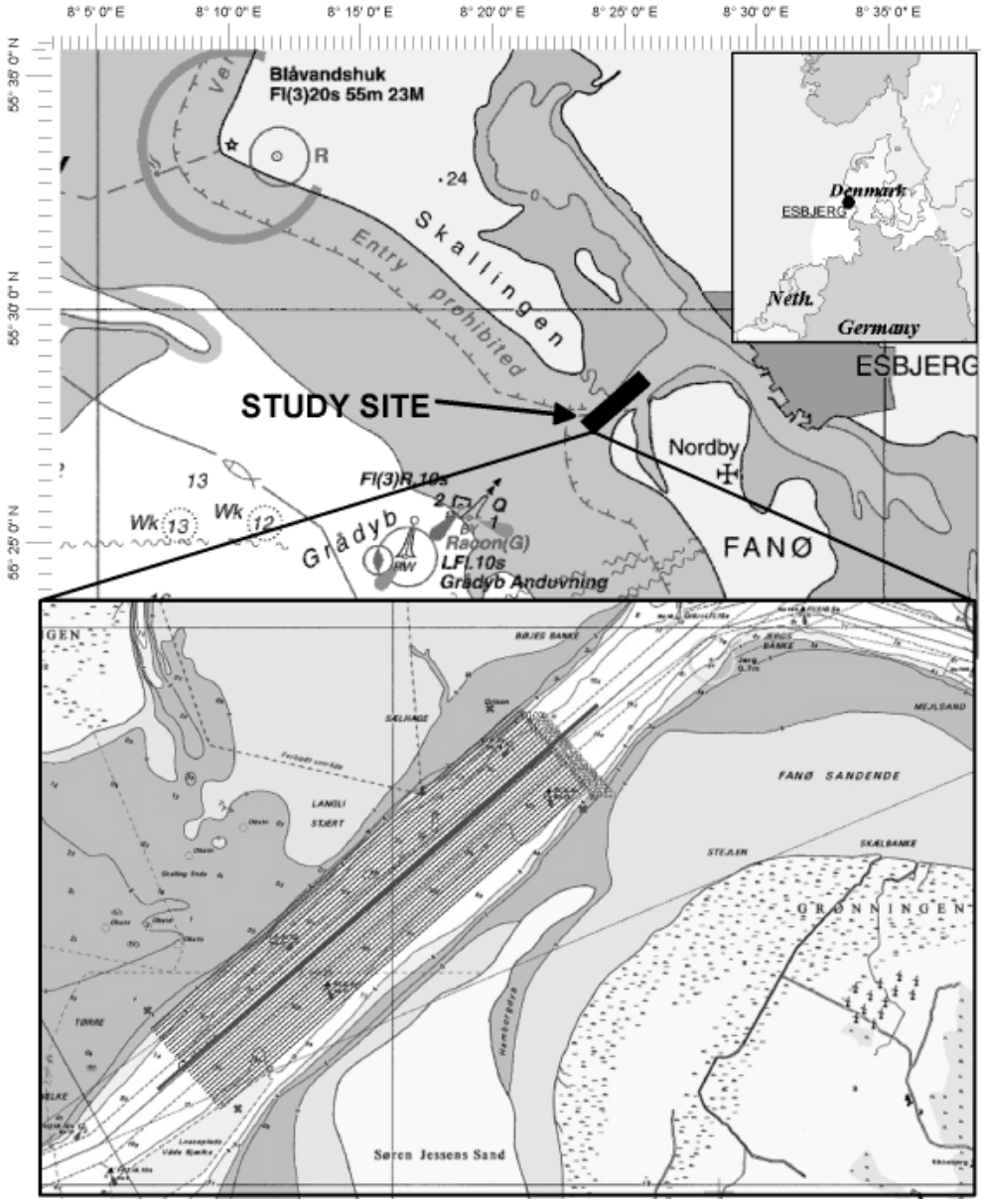

Fig. 4.1 Location of the study area in the Gådyb tidal inlet between the barrier spit Skallingen and the barrier island Fanø in Denmark, also showing the study site of the MBES surveys in 2002 (3000x650 m) in the central sector of the Gådyb channel. The thick line in the centre of the track map indicates the 12-h survey track along the central navigation lane during spring tide in September 2002.

4.3 Materials and methods

High-resolution elevation scans of large, highly dynamic bedforms were carried out over a tidal cycle by means of a high-frequency multibeam (455 kHz) RESON 8125 bathymetric system having 240 hard beams and along- and across-track beam angles of 1° and 0.5°, respectively, thus yielding a swath coverage of 120°. The ping rate was set at 40 Hz. With an internal height resolution of 0.6 cm, the system achieves a real-time height accuracy of 2.5 cm. All data sets were collected and processed by means of the Software 6042 v. 7 (™RESON/QPS).

The multibeam was coupled with an AQUARIUS 5002 (THALES/DSNP) dual-frequency (L1/L2) long-range kinematic (LRK) global positioning system (GPS). The vertical and lateral accuracy of this system is better than 0.05 and 0.03 m respectively [*Lutz and Gounon*, 2001]. Flow velocity data were collected simultaneously by means of a BB1200 (RDI) acoustic Doppler current profiler (ADCP) operating at 1200 kHz. The vertical resolution is 25 cm per cell and, at a vessel speed of 2.5 m/s (5 knots), a repetition rate at 5-10 m intervals is achieved. The resolution of the flow velocity is 1 mm/s, the accuracy being 0.25% of the flow velocity relative to the ADCP velocity of 2.5 mm/s. Velocities are based on the mean ensemble average flow velocity, which is directly given by the ADCP data.

In order to gain an overview of the study area, the central part of the Grådyb channel (2 km^2) was surveyed along 27 parallel tracks using a 30 m swath coverage (Fig. 4.1 and Fig. 4.2). The resulting lateral track resolution of nearly 30 m is a function of flow depth and vessel speed. At a water depth of 15 m, the across-track resolution is 0.13-0.52 m due to the across-track beam width of 0.5°. A vessel speed of 2.5 m/s (5 knots) results in an along-track resolution of 0.10 m. Therefore, a cell size of 0.5 m was chosen for grid analysis of the bathymetric data.

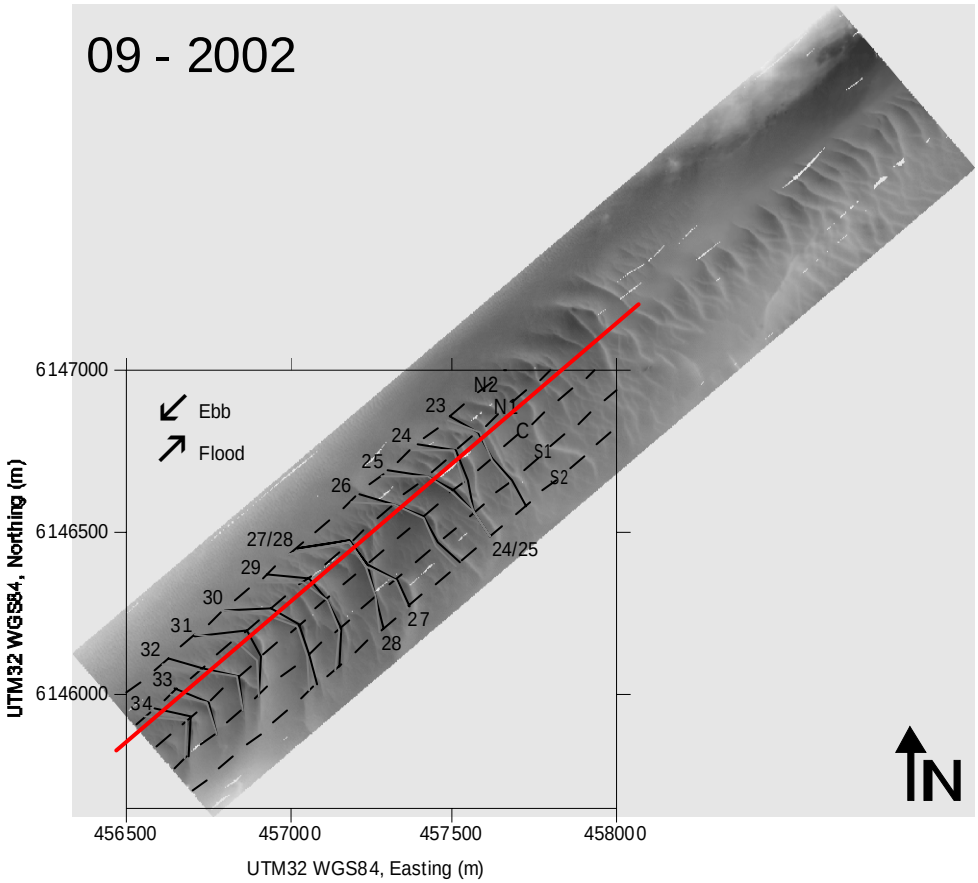

Fig. 4.2 Grey-scale topographic map of the total survey area in 0.5 x 0.5 m grid size (based on 27 tracks of 25-m distance intervals; total area = 3000 m x 675 m = 2.025 km^2), showing large bedforms in the south-western sector and smaller dunes in the north-eastern sector. The red line indicates the back-and-forth survey track over the 12-h tidal period in September 2002. The dashed lines indicate the subsections N2, N1, C, S1 and S2 (see Table 4.1). Numbered cross sections are identified dune crests. The subsection selected for the present study includes the crest numbers 30 and 31.

In order to quantify bedform dynamics over a spring tidal cycle, the central track line of the navigation channel was scanned 18 times, which corresponds to the former survey of *Bartholdy et al.* [2002; cf. Figs 1 and 2]. The mean travel time for one scan was about 20 min. During the 12-h measuring period on 11 September 2002, high tide was at 07h00 and 19h30, low tide at 13h15. The survey started at 07h53, the first profile being completed at 08h16, the last at 17h45.

Table 4.1 Average dune lengths (L), heights (H), areas (A), celerities (c), and mean flow velocities (V) at the dune crests along lines N2, N1, C, S1 and S2, and over a dune back along the intersections of cross section SW with lines N2, N1, C and S1 (for locations see Fig. 4.2 and Fig. 4.3). Average bed level (h) is in relation to WGS84. Mean grain size (d_{50}) is given in millimetre [after Ernstsen et al., 2004].

Profile	N2	N1	C	S1	S2
L (m)	149	137	122	131	152
H (m)	1.16	2.21	3.06	1.93	1.57
A (m^2)	75	112	147	81	80
c (m/year)	26	10	10	8	23
V (m/s) dune crests	-	0.93	1.02	0.95	-
V (m/s) dune backs	0.84	0.76	0.88	0.81	-
h (m, WGS84)	28.62	28.27	28.25	28.56	28.89
d_{50} (mm)	0.369	0.442	0.478	0.427	0.404

In the course of the survey it was noted for the first time that the central track line did not coincide with the centre line of the dune crests, which was found to be slightly displaced towards the south, i.e. outside the official navigation channel (Fig. 4.2 and Fig. 4.3). This can be ignored in the present case, because the data for the various subsections constituting the total survey area showed only slight fluctuations in dune geometry, mean flow velocity and mean grain size (Table 4.1).

For a better visualisation of bedform changes over one tidal period, a section of the centre profile was selected which was representative of the elementary inventory of the dune types in the Grådyb channel. This subsection is located in the south-western quarter of the central line track, and represents the most seaward and most exposed set of large dunes found in the entire channel (Fig. 4.3). Dune geometry, area and volume calculations are based on the dune geometry data, which were digitised from the centre beam profile of the MBES data (see below). The absolute values of the area-below-curve were calculated by means of the trapezoidal integration method, which is related to the zero-base level. The volume calculation is based on a swath area of 130 m x 27 m (= 3510 m^2), corresponding to the swath range of a given range of water depths between 10 and 12 m at a 120° beam angle.

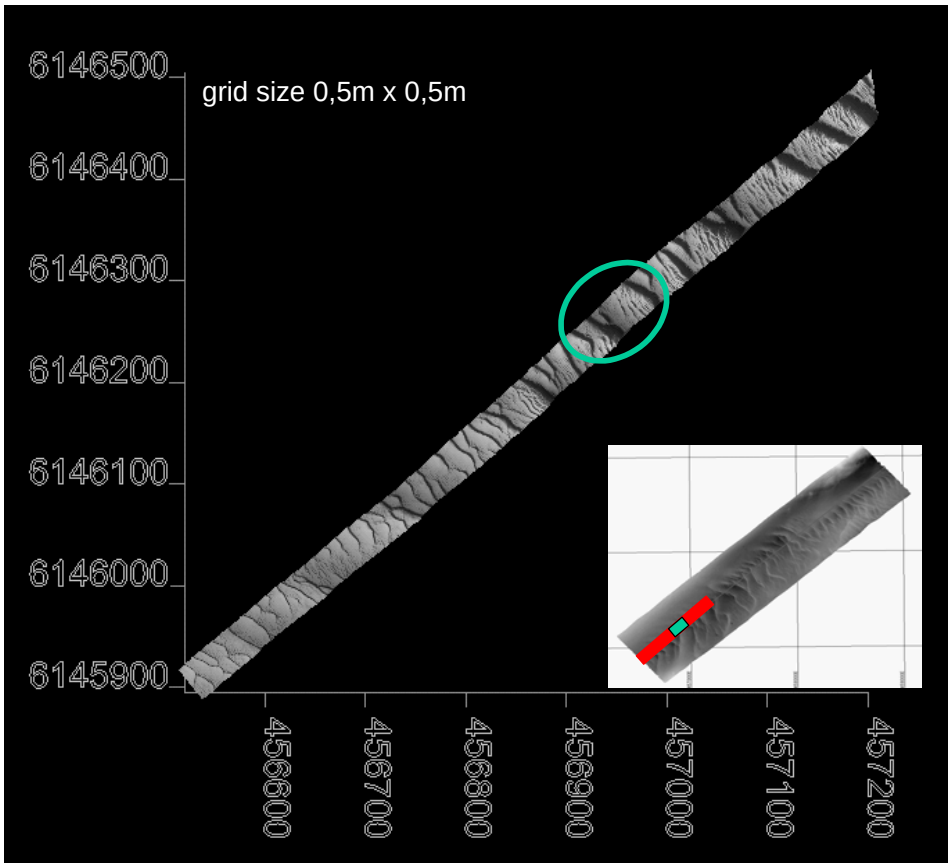

Fig. 4.3 Subsection of the central line track in the Grådyb channel (length 130 m, width 27 m; total coverage ca. 3500 m^2, shown as oval-marked area) selected for visualisation of bedform changes.

The bedload transport rate was calculated by means of the software SandCalc, following the procedure recommended by *Soulsby* [1997]. Bedload transport can be expressed in terms of the volumetric transport rate q_b (in m^2/s), which is the volume of grains moving per unit time per unit bed width. The equation of *Nielsen* [1992], which strictly applies to unidirectional flows only, was used because the influence of waves in an ebb flow-dominated tidal channel can hardly be estimated, and the dune geometry did not reflect any typical wave effects in the present case:

$$\Phi = 12\theta^{0.5}\left(\theta - \theta_{cr}\right) \tag{4.1}$$

where θ is the total Shields parameter and $\theta_{cr} = 0.05$ [after *Nielsen*, 1992].

Considering the ebb and flood flow, and the problem of the different migration velocities of the large compound dunes and the superimposed dunes, the volumetric transport rate can be calculated by the equation [e.g. *van den Berg*, 1987; *Soulsby*, 1997]:

$$q_b = \rho_s\left(1-\varepsilon\right)\psi HU_b = \sigma_s\psi HU_b \tag{4.2}$$

where ρ_s is sediment density, ε is porosity of the sediment, ψ is a bedform shape factor (set to 0.5), H is bedform height, U_b is bedform migration velocity and σ_s is sediment density corrected for porosity. For bedforms composed of medium to coarse sand, a sediment density corrected for porosity of approximately 1.7 kg/m^3 is realistic [cf. *Bartholdy et al.*, 1991; *Carling et al.*, 2000a].

4.4 Results

Over one tidal period, the record of the bedform geometry in the Grådyb channel reflects the general morphological characteristics of an ebb-dominant system (Fig. 4.2 and Fig. 4.4). The channel bed is covered by large compound dunes of coarse sand, which are mainly confined to the SW sector. The heights of these large dunes generally range between 1.5 and 3 m. In the study area as a whole, dune length can reach up to 100 m (Fig. 4.2), which classifies them as large to very large dunes following *Ashley* [1990]. In the selected subsection, the mean dune length is nearly 60 m and maximum heights nearly 2.5 m (Fig. 4.4). The tidally active part of the bedforms, which has a maximum reworking depth of 0.5 to 0.8 m, includes two generations of dunes, one composed of smaller, superimposed dunes, the other of the crests of large dunes, composed of fine to medium sand.

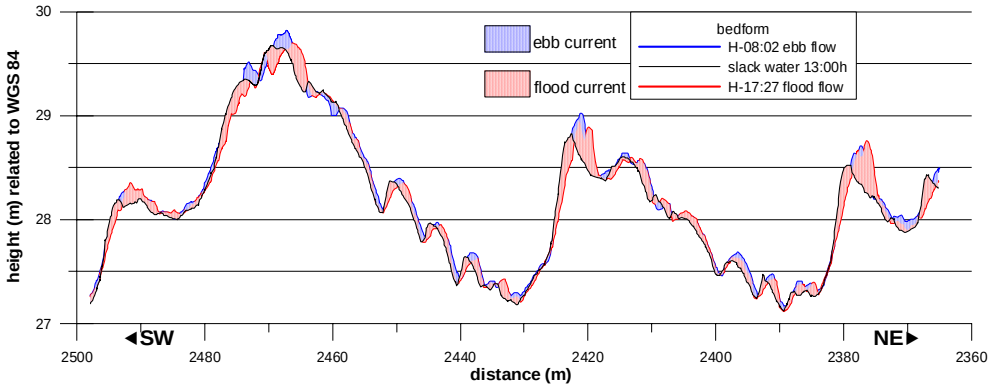

Fig. 4.4 The SW subsection of the central line over one tidal period. Lines indicate individual bedform stages over the tidal period, and shaded areas the lateral shift with time. The large dunes are always ebb-dominated; the flood cap active zone is approx. 0.8 m.

Over the entire ebb cycle, a total sediment volume of around 290 m^3 was exported seawards out of the subsection. Of this, nearly 74% of the total displaced volume moved seawards in the accelerating phase of the ebb flow up to maximum flow (Table 4.2). The MBES data clearly show that in this phase of the ebb flow the bedforms became steeper, adjusting their heights slightly downwards (Fig. 4.5). By contrast, only about 25% of the total

displaced volume moved seawards in the decelerating phase of the ebb current up to slack water (Table 4.2).

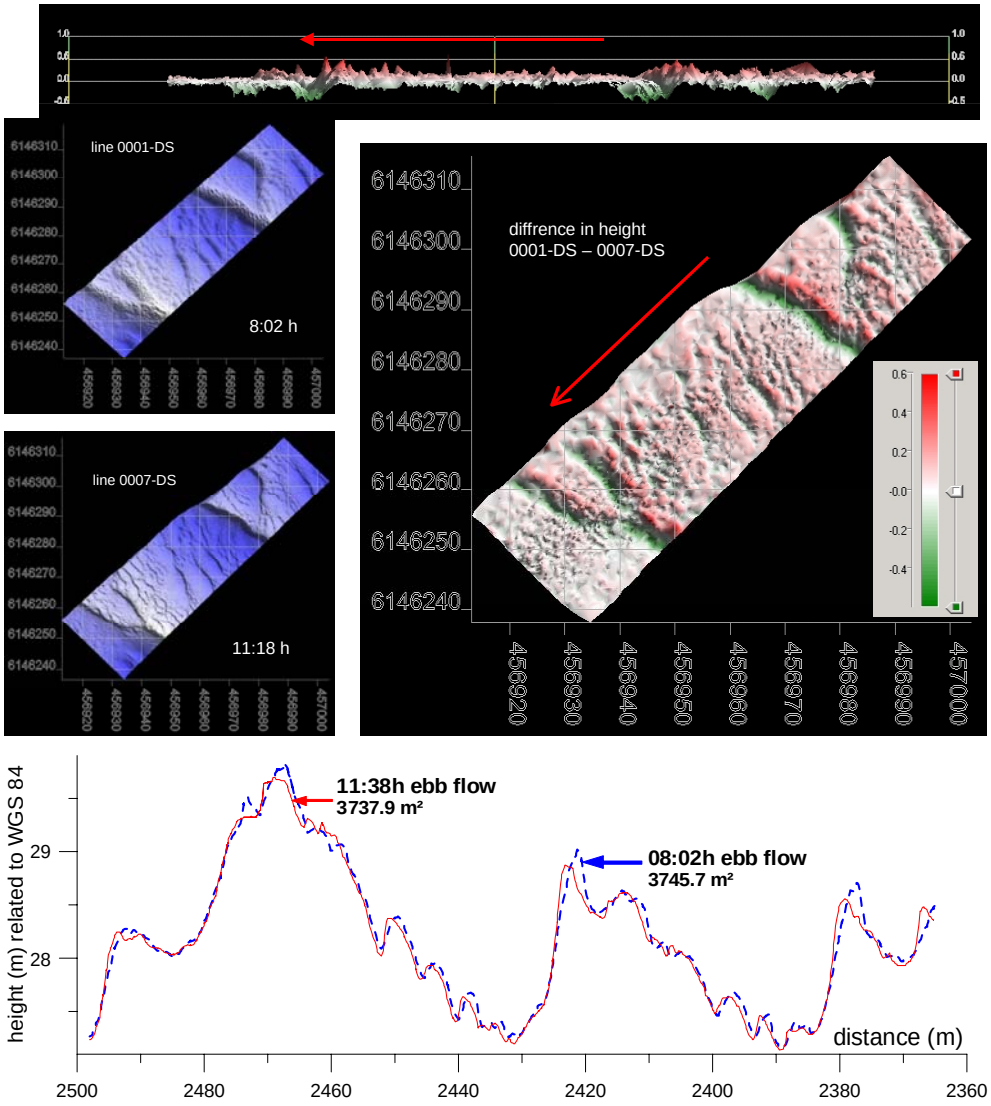

Fig. 4.5 Ebb flow phase in the selected subsection. The left-hand sections of the three-dimensional plot show the transformation into darkly shaded, ebb-orientated dune crests. The change in height over time is given in the right-hand upper section of the total subsection area (green areas denote increase in height, red areas decrease in height). The centre line with area-below-curve values is given in the two-dimensional plot.

During the flood phase, typical flood caps of finer sand developed on top of the crest, which is recorded as a shape smoothing in the MBES three-dimensional plot (Fig. 4.6). The reason for this effect is documented in the two-dimensional profile in Fig. 4.6. With increasing flood flow, the finer material of the superimposed dunes is transported over the crests of the large dunes, i.e. from the lee-side to the stoss-side. The smaller superimposed dunes appear to act as a carpet for the large compound dunes [*Bartholdy et al.*, 2002]. The

intensity of this effect varies with the geometry of the large dunes. Thus, the upper 1.2 m of the lee-side (slip face) of the largest dune (height nearly 3 m) splits up into three to four smaller dunes (Fig. 4.6). The smaller ones of these relatively large bedforms have heights of 1.5-2.0 m and an active reworking depth of only 0.3-0.4 m in their crest region. Superimposed on these are poorly developed small dunes. This effect increases in the course of the flood phase, and leads to the crest smoothing of the large dunes mentioned above (red line in Fig. 4.7).

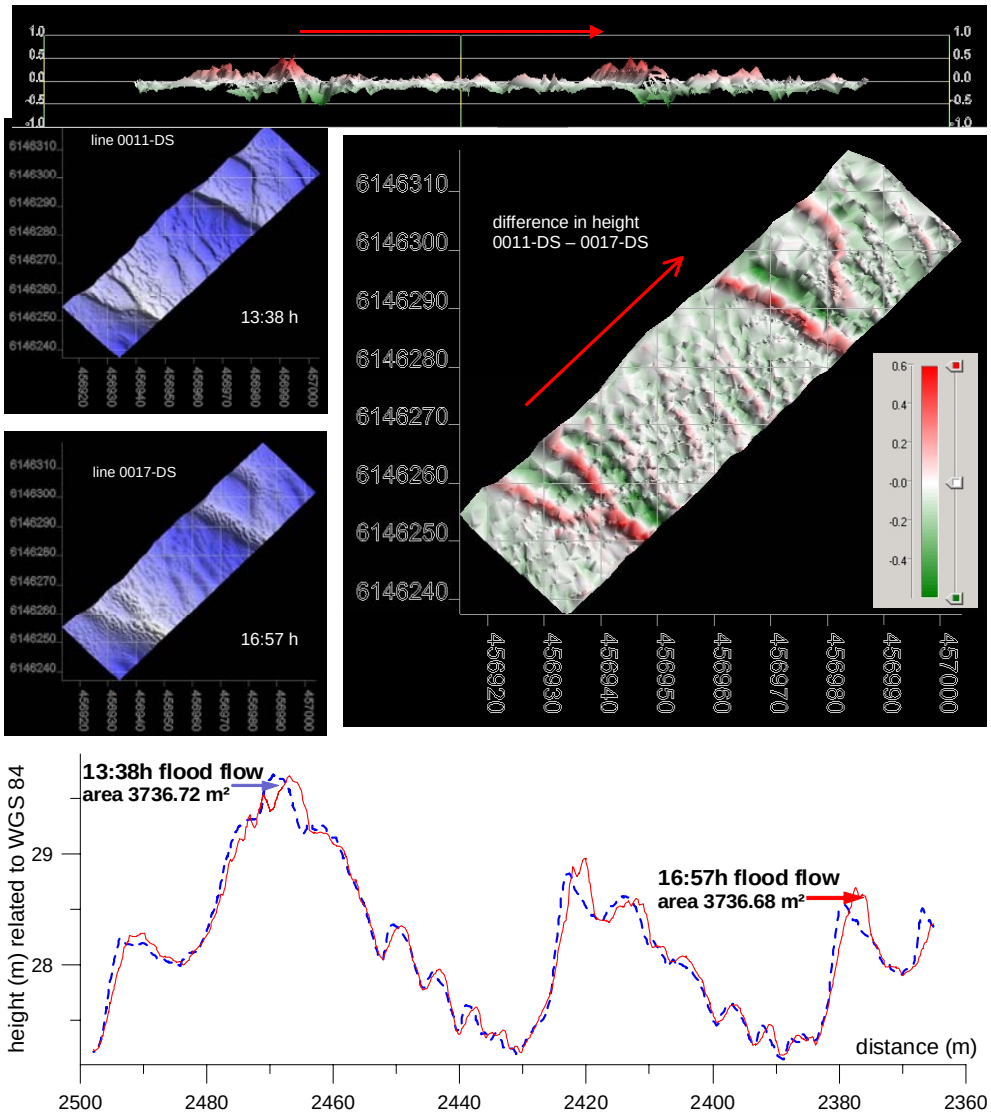

Fig. 4.6 Flood flow phase in the selected subsection. The left-hand sections of the three-dimensional plot show the beginning of transformation into ebb-orientated dunes with flood caps. The change in height over time is given in the right-hand upper section of the total subsection area (green areas denote increase in height, red areas decrease in height). The centre line with area-below-curve values is given in the two-dimensional plot.

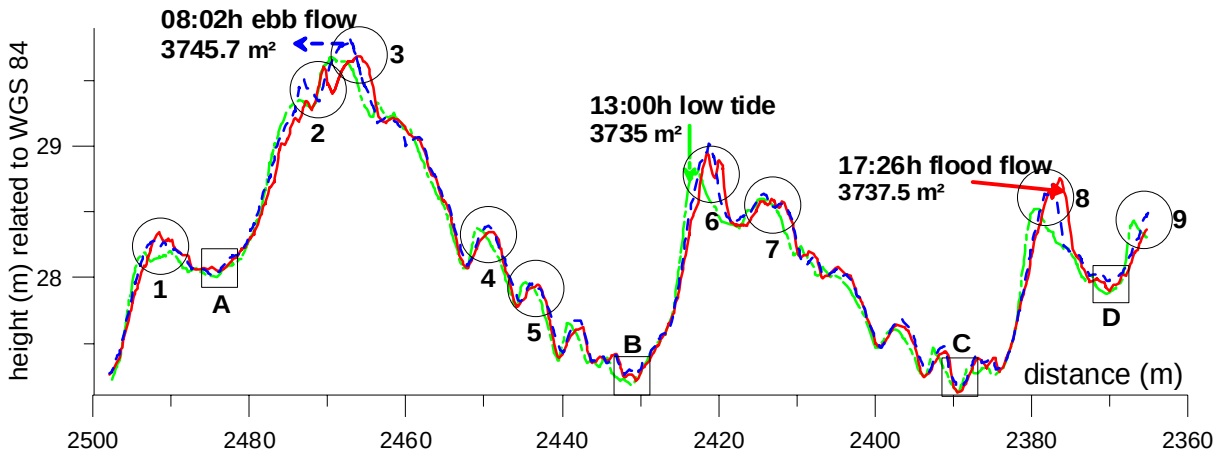

Fig. 4.7 The bedform changes of three scans over the tidal period. Positions labelled with numbers (1 to 9) and letters (A to D) are the base for the height lateral-shift calculation for the dune crests and dune troughs, respectively.

During the flood phase a volume of only 73 m^3 of sediment is imported (Table 4.2), indicating that a very subordinate amount of sediment, equivalent to 20% of the entire sediment turnover over the tidal period, is transported back into the system from the seaward side.

Table 4.2 Variation of transport volume with time and flow direction over a tidal period on 11 September 2002. Area = calculated area-be-low-curve of the height-distance plots. Volume calculations are related to a subsection area of 3564 m^2. Positive values denote accumulation, negative values erosion.

Time	Flow dir.	Area (m^2)	Area diff. (m^2)	Vol. diff. (m^3)	Vol. diff. Ebb/flood (m^3)
08:02 h	Ebb	3,745.77			
11:38 h	Ebb	3,737.85	8:02–11.38=–7.92	–213.84	Vol. diff. ebb flow = – 290.25
13:02 h	Low tide	3,735.02	11:38–13:02=–2.83	–76.41	
13:38 h	Flood	3,736.72	13:02–13:38=+1.83	+49.41	
16:57 h	Flood	3,736.68	13:38–16:57=+0.04	+1.08	Vol. diff. flood flow = +73.13
17:26 h	Flood	3,737.50	16:57–17:26=+0.82	+22.14	
Difference start to end of the tidal period			-8.06	-217.12	

The volume calculations clearly document an export tendency over the tidal period during spring tide. On the other hand, the dune geometry, and the dune crests in particular, show only slight net changes (Fig. 4.8). With mobility rates of up to 2.5 m during the ebb flow, and 3.0 m during the flood flow in the inverse direction, the dune crests are actually displaced by as much as 0.8 m landwards, i.e. in the flood direction, when integrated over the entire tidal cycle (Fig. 4.8).

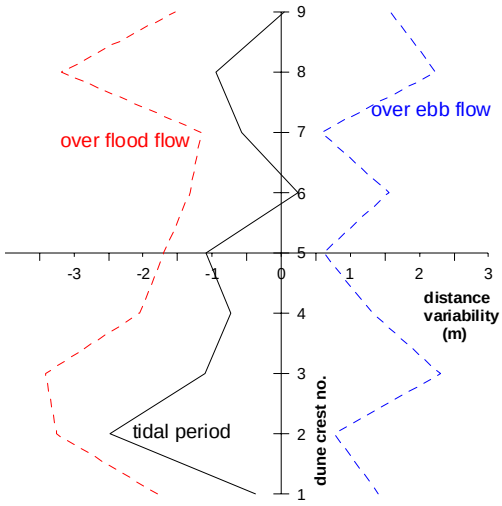

Fig. 4.8 Dune crest mobility over one tidal period cycle related to the entire dune geometry.

Dune heights show considerable variation over the tidal period (Fig. 4.9). In dependence of the celerity of the superimposed dunes in the 'active' crest zone, heights vary up to 0.5 m over the ebb flow, whereas over the flood flow height variations barely reach 0.1 m. When considering the entire tidal period, the height evolution thus appears to be controlled by the ebb flow.

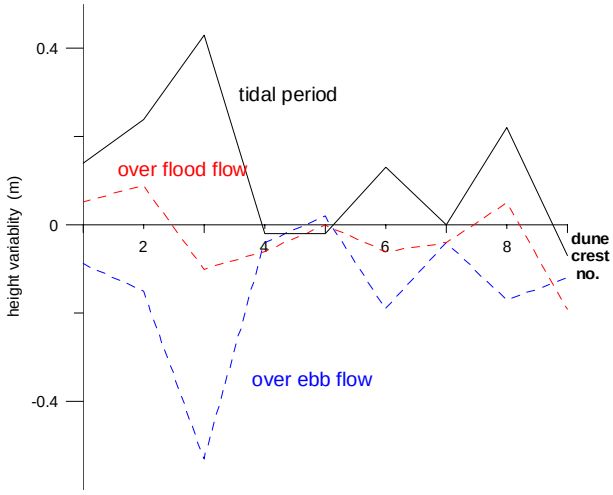

Fig. 4.9 Dune height variation over one tidal period related to the entire dune geometry.

In contrast to the mobility of the dune crests, the position and geometry of the dune troughs are relatively stable over the entire tidal period (Fig. 4.7). The overall height variation is less than 0.1 m and lateral shifts are generally less than 1 m (Table 4.3). Contrary to the dune crest geometry, the troughs of the large compound dunes show no significant change over the tidal period, their elevations fluctuating by a few centimetres only.

The net sediment volume transported over one tidal period for a swath area of 3510 m^2 amounts to 217 m^3 (Table 4.2). This, in turn, amounts to an average net volume of

0.061 m^3/m^2. Assuming that the spring tide represents a mean value for the whole semi-diurnal tidal period, the annual net volume would be 44.5 m^3/m^2 per year.

Table 4.3 Positions and heights of the dune troughs over the tidal period on 11 September 2002. Max. diff. denotes the maximum variation in position (pos.) and height (D) over the entire tidal period.

	Time							
	08:02 h, ebb flow		13:00 h, slack water		17:26 h, flood flow		Max. diff.	
Dune trough	Pos. (m)	D (m)	Pos. (m)	D (m)	Pos. (m)	D (m)	Pos. (m)	D (m)
A	2,484.61	28.0	2,484.35	28.0	2,483.83	28.05	0.78	0.05
B	2,430.57	27.25	2,431.07	27.18	2,430.56	27.21	0.51	0.07
C	2,389.29	27.17	2,389.42	27.12	2,389.25	27.13	0.17	0.05
D	2,370.13	27.98	2,370.30	27.97	2,369.96	27.90	0.37	0.08

4.5 Discussion and conclusions

Our annual rates are almost certainly an overestimation because the survey was restricted to a single tidal cycle at spring tide. In this tidal phase, higher water levels and slightly longer high-velocity flow events with correspondingly higher transport rates must be expected. Under these conditions, a total volume of 360 m^3 of transported sediment was measured over the tidal period. This amounts to a net volume export of approximately 220 m^3 out of the study area (3500 m^2). Only one third of the total sediment turnover was thus imported during the flood phase.

During the ebb tidal phase, the calculated transport rate obviously reveals the same basic tendency, since the flow velocities are correspondingly higher. Based on a maximum ebb flow velocity of 1 m/s, the volumetric sediment transport rate amounts to 2.156×10^{-5} m^2/s during the ebb phase. During the flood phase, by contrast, the peak flow velocity is 0.74 m/s and the volumetric sediment transport rate amounts to 6.73×10^{-6} m^2/s. These calculations are valid for a median grain size of 318 µm, a water temperature of 19°C, and an average water depth of 11 m [cf. *Nielsen*, 1992].

Based on the calculated annual net volume transport and the transport rates for both tidal phases, the bedform stability criterion for large dunes after *van den Berg and van Gelder* [1993] gave a straight-line relationship between the particle parameter and the mobility parameter, as discussed in *Bartholdy et al.* [2002]. However, this does not reflect the complex situation on the large compound dunes observed in the present study. Indeed, *Bartholdy et al.* [2002] have criticized that too little distinction is being made between compound and simple dunes. In the MBES data the 'active zone' of the superimposed dunes can be clearly separated from the much larger stable zone characterizing the large, compound dunes as a whole.

Although the reworking depth in the 'active zone' on the crests of the large dunes increases with the height of the large dunes, it remains steady in each case over the entire flow phase (Fig. 4.10). For short periods such as a single tidal cycle, sediment transport is controlled by this 'active zone' alone, and with it the bedform transport rate. *Bartholdy et al.* [2002] pointed out that the superimposed dunes, which are composed of finer grain sizes, did not follow the standard dune dimension versus water depth relationship. This means that standard transport equations [e.g. *van Rijn*, 1984a or *Nielson*, 1992] should be applied only in the case of constant dune heights and migration rates. This contrasts sharply with the strong differentiation in dune heights and lengths of the superimposed dunes observed during both the ebb and the flood phases in the Grådyb tidal channel.

It is interesting to note that the general ebb-oriented export trend recorded for the large, compound dune system is contrasted by a net flood-oriented transport in the 'active zone' involving the smaller superimposed dunes, which amounts to 0.6 m^2 per flow phase on top of the large dunes, and 0.15 m^2 per flow phase on the slopes and in the troughs (Fig. 4.10). For the ebb and flood flow a mean volumetric sediment transport rate of 0.7697×10^{-5} m^2/s and 1.059×10^{-5} m^2/s, respectively, is calculated (Fig. 4.10). This strongly deviates from the rates calculated on the basis of the equations recommended by *Nielsen* [1992], which predict transport rates of 2.156×10^{-5} m^2/s for the ebb flow and 6.73×10^{-6} m^2/s for the flood flow.

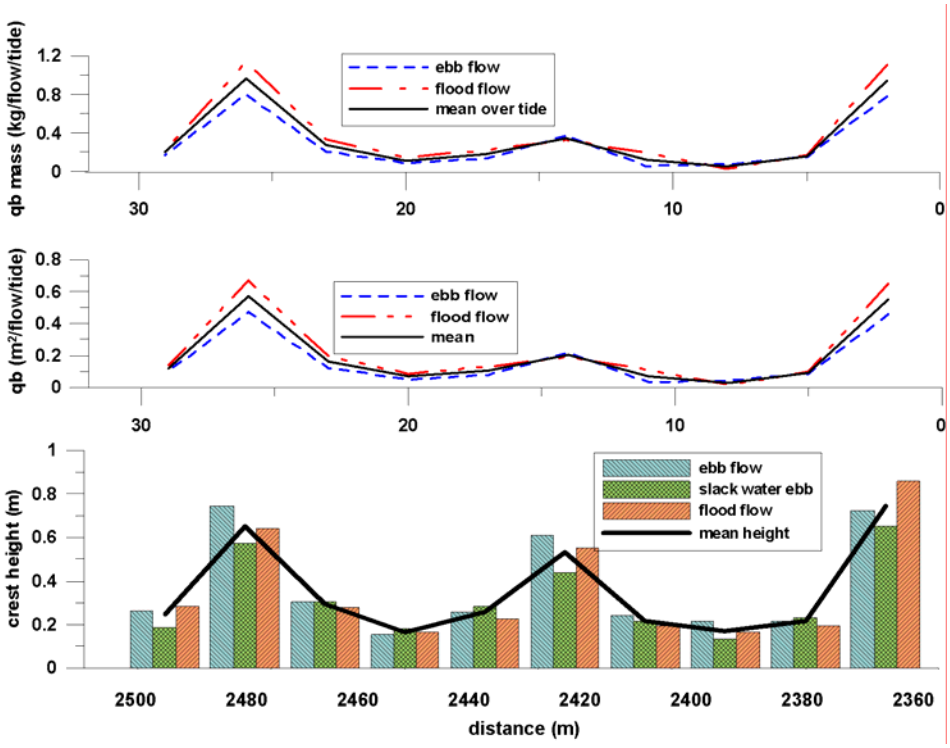

Fig. 4.10 Dune crest height variation and total sediment volume transport in the 'active zone' over one tidal period.

The discrepancy between the much lower transport rates calculated from high-resolution bathymetric surveys in the present study and the unrealistically high values calculated on the basis of published transport equations can be explained only by the latter being based on incorrect assumptions concerning "real world" conditions. This problem has also been emphasised by *Soulsby* [1997] who addressed the large discrepancies (factor 4) obtained when using various published transport equations. He also recommended calculation of bedload transport rates by measuring mean dune migration rates, especially in unsteady flows like tidal currents, as we did for the present paper.

In our case we have demonstrated that the smaller, superimposed dunes control the transport processes, rather than the large, compound ones. This was possible only by using a high-resolution MBES system with ping rates of up to 40 pings per second, thereby achieving the required lateral resolutions along track in the order of centimetres in dependence of the vessel speed. The high accuracy of the system avoids the problem of overlapping footprints common to all standard echosounder systems, which give mixed and partly duplicated information about the same morphology at different survey positions. Calculated transport rates have a time-limited validity only because of the unsteady flow conditions of the tidal current. With the high repetition rate and high accuracy of the MBES, a simple comparison of morphological changes recorded at short time intervals allows realistic approximations of volume budgets in tidal channels.

On the basis of the present findings we conclude that, in future studies, the relationship between the more dynamic, finer-grained superimposed dunes and the more static, coarser-grained compound dunes should be investigated over complete neap-spring tidal cycles and during high-energy events. This should enable better understanding of the environmental conditions, which control the long-term net migration and sediment transport rates in the Grådyb channel.

Acknowledgements

The authors wish to heartily thank the captain and crew of the RV Senckenberg for their help and expertise during the September 2002 cruise period. We are indebted for the international cooperation to the harbour authority of Esbjerg, to the Royal Danish Administration of Navigation and Hydrography (Farvandsvæsnet), Copenhagen, and to the Institute of Geography, University of Copenhagen. The referees are acknowledged for their constructive review comments. Finally, the Senckenbergische Naturforschende Gesellschaft

and the Research Centre of Ocean Margins, University of Bremen, is thanked for providing the financial assistance to realise this study.

Paper IV

Chapter 5: Paper IV

Quantification of dune dynamics during a tidal cycle in a tidal inlet channel of the Danish Wadden Sea

V. B. Ernstsen[1], R. Noormets[1], C. Winter[1], D. Hebbeln[1],

A. Bartholomä[2], B. W. Flemming[2], J. Bartholdy[3]

[1]Research Center Ocean Margins, University of Bremen, Leobener Str., P.O. Box 330 440, D-28359 Bremen, Germany (E-mail: ernstsen@uni-bremen.de, Tel.: +49 421 218 65675, Fax: +49 421 218 65505)

[2]Senckenberg Institute, Division of Marine Science, Suedstrand 40, D-26382 Wilhelmshaven, Germany

[3]Institute of Geography, University of Copenhagen, Øster Voldgade 10, DK-1350 Copenhagen, Denmark

Geo-Marine Letters (submitted)

Abstract

High-resolution swath bathymetry measurements at centimetre-scale precision conducted during a tidal cycle in the Grådyb tidal inlet channel in the Danish Wadden Sea reveal the short-term dynamics of a medium sand-sized large ebb-directed compound dune with superimposed small to medium dunes. Dune dynamics are related to simultaneous measurements of flow derived by an acoustic Doppler current profiler. Spatially, dune crests migrate more than dune troughs due to higher flow velocities at the crests than in the troughs. Temporally, superimposed lower lee side dunes migrate more during the flood than the ebb tide due to higher near-bed trough flow velocities during the flood phase, as a result of varying exposure to the flow. Net dune migration is flood-directed over the tidal cycle, despite the fact that annual net migration is ebb-directed; hence, extrapolation of short-term migration rates is impossible. The superimposed dunes reverse direction during each half tidal cycle, whereas the compound dune only develops a flood cap during flood tide, i.e. the response time of the compound dune in order to transport the required volume of sediment to reverse direction is longer than a half tidal cycle. Over a tidal cycle the bed level is stable, but significant erosion and accretion occurs during the tidal phases. During the ebb tide, bed material goes into suspension with accelerating flow and settles with decelerating flow, resulting in an average erosion and accretion of the bed of 6.5 cm. During the flood tide, the bed of the compound dune is overall practically stable; however, bed material is eroded from the exposed lower lee side and partly transported to the crest in bedload and partly brought into suspension. In general, dune height changes during the tidal cycle, whereas dune length remains stable. The height of the compound dune follows water depth, which acts as a limiting factor to dune growth, whereas the height of the stoss side dunes follows flow velocity, i.e. the stoss side dunes are water-depth independent.

5.1 Introduction

Tidal inlet channels are generally narrow with high flow velocities (>1 m/s) and composed of sandy bed material. In addition, the beds are typically covered with dunes [e.g. *Boothroyd and Hubbard*, 1974 and 1975]. Very few studies have investigated the dynamics of dunes in tidal environments on time scales as short as single tidal cycles [*Hawkins and Sebbage*, 1972; *Boothroyd and Hubbard*, 1974 and 1975; *Fenster and FitzGerald*, 1996; *Bastos et al.*, 2004; *Hoekstra et al.*, 2004; *Kostaschuk and Best*, 2005]. Due to instrumental

limitations, most studies primarily had a qualitative approach, the most recent study by *Kostaschuk and Best* [2005], who to some extent were able to quantify changes in dune dimensions, being a lone exception. High-resolution swath bathymetry, on the other hand, now provides the opportunity to compare morphology along the exact same channel reach at different times. In combination with high-accuracy positioning, horizontal and vertical changes at centimetre-scale can be resolved [*Ernstsen et al.*, submitted, Paper I].

This study investigates the dynamics of a large compound dune with superimposed small to medium dunes over a semi-diurnal tidal cycle in the Grådyb tidal inlet channel in the Danish Wadden Sea (Fig. 5.1).

5.2 Study area

The large compound dune is located in the Grådyb tidal inlet on the Danish west coast between the barrier spit of Skallingen to the northwest and the barrier island of Fanø to the southeast. The Grådyb tidal inlet connects the northern-most tidal basin of the Wadden Sea with the adjacent North Sea, forming the navigation channel to Esbjerg (Fig. 5.1).

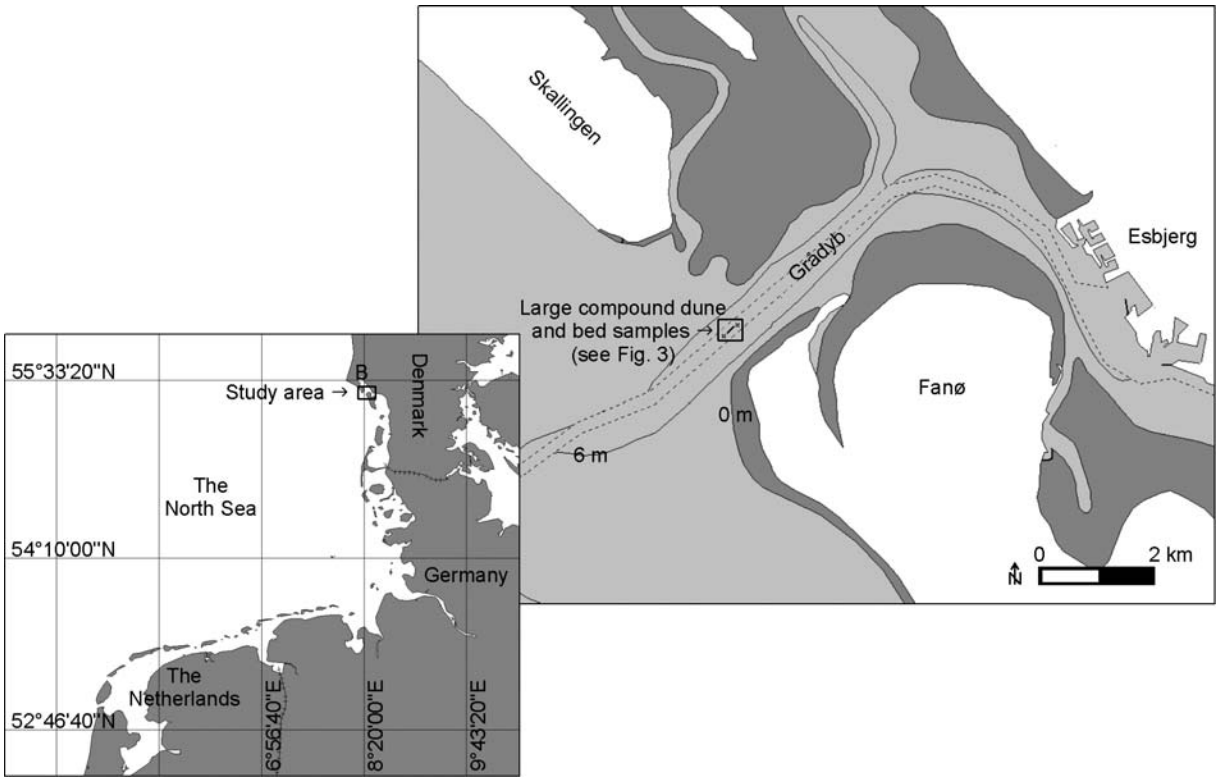

Fig. 5.1 Location of the large compound dune (line) and the collected bed samples (crosses) in the Grådyb tidal inlet between the barrier spit of Skallingen and the barrier island of Fanø in Denmark. Dashed line marks the navigation channel to Esbjerg. Water depths are relative to mean low water springs (MLWS).

The tides are semi-diurnal with a mean tidal range of about 1.5 m and a tidal prism in the order of 150 x 10^6 m^3 [*Bartholdy and Anthony*, 1998]. The width of the channel is roughly 1 km and the mean depth is 10-13 m. The channel is ebb-dominated with maximum ebb and flood current velocities around 1.50 m/s and 1.25 m/s, respectively [*Bartholdy and Anthony*, 1998]. The bed of the channel is covered with large to very large barchanoid-shaped compound dunes composed of sand with mean grain sizes ranging from 0.3 to 0.7 mm [*Ernstsen et al.*, 2005]. There are two sediment sources in the area: 1) the Pleistocene cliffs lining the mainland shore of the back-barrier tidal basin which supply medium to coarse sand, and 2) the near-shore region of the open coast which supplies fine sand to the tidal inlet [*Bartholdy et al.*, 2002].

5.3 Methods

5.3.1 Surveys and instruments

Surveys along the large compound dune (Fig. 5.1) were conducted thirteen times in the course of 8 hours and 45 minutes of a tidal cycle on the 11th of September 2002 (Fig. 5.2). In the following, time is presented in Central European Time (CET), which is equal to Coordinated Universal Time (UTC) + 1 hour. The first survey was done around 07:14, about 1 hour and 39 minutes after high water and 4 hours and 11 minutes before low water, whereas the last survey was carried out around 15:59, about 4 hours and 34 minutes after low water and 1 hour and 46 minutes before the succeeding high water. Subsequently the survey period is referred to as a tidal cycle, despite the fact that in reality only 75% of the tidal cycle was covered.

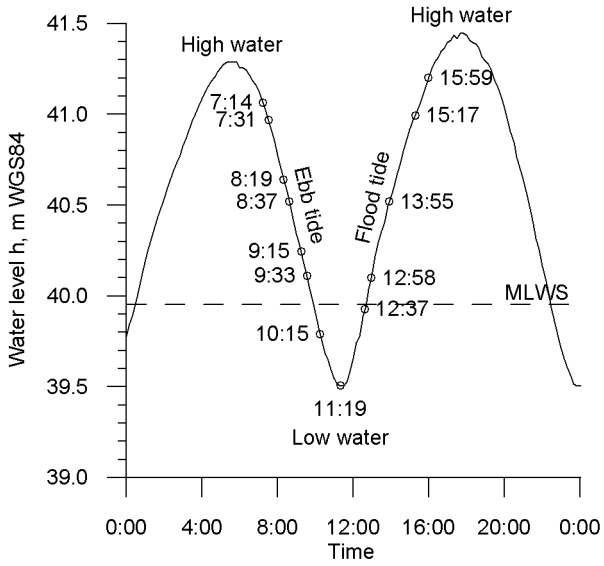

Fig. 5.2 Times of the thirteen MBES and ADCP surveys during the tidal cycle on the 11th of September 2002. Water depth relative to mean low water springs (MLWS) in relation to WGS84 altitude is given by: m MLWS = m WGS84 - 39.951 m.

Bed material was collected at two locations near the compound dune (Fig. 5.1 and Fig. 5.3) on the 9th of September 2002 using a Shipek™ grab sampler.

Flow velocities and echo intensities were measured using a BroadBand™ (RDI) acoustic Doppler current profiler (ADCP) operating at 1200 kHz and the WinRiver™ (RDI) software package. Echo intensity, a measure of the signal strength of the echo returning from the ADCP's transmit pulse [*RDI*, 1996], has been used in several surveys to estimate the relative concentration of suspended sediment [e.g. *Reichel*, 1998; *Kostaschuk et al.*, 2005]. The vertical resolution of the ADCP was set to 0.25 m and the lateral resolution is 5-10 m at a ping rate of 0.5 Hz and a vessel speed of 2.6 m/s (5 kn).

Bathymetry was recorded using a SeaBat™ 8125 (RESON) multibeam echo sounder (MBES) system operating at 455 kHz and the 6042™ Version 7 (QINSY/RESON) data collecting and processing software package. The vertical resolution of the MBES system is in a sub-centimetre scale [*www.reson.com*]. The lateral resolution is a function of water depth and vessel speed. For instance, a water depth of 15 m results in an across-track resolution of 0.13-0.51 m due to the across-track beam width of 0.5°; at a vessel speed of 2.6 m/s (5 kn) the along-track resolution is 0.10 m. As the outermost beams were not used in the analysis, a cell size of 0.2 x 0.2 m was chosen for the gridding of the bathymetric data. The MBES system was coupled with an AQUARIUS™ 5002 MK/SK (THALES) dual frequency (L1/L2) Long Range Kinematic (LRK™) Global Positioning System (GPS). The horizontal precision of the

MBES system is ±13.0 cm at a 95% confidence level, while the vertical precision during single surveys, as it is the case in this study, is as high as ±1.9 cm at a 95% confidence level [*Ernstsen et al.*, submitted, Paper I]. Coordinates are presented in relation to the Universal Transverse Mercator Zone 32 (UTM32) projection with the World Geodetic System 1984 (WGS84) ellipsoid as the underlying model of the Earth. Altitudes are presented in relation to the WGS84 ellipsoid. Corrections for ship movements were applied using an OCTANS™ Surface (IXSEA OCEANO) gyrocompass and motion sensor. For more detailed information on the MBES system see *Ernstsen et al.* [submitted, Paper I].

5.3.2 Grain size analysis

Initially the collected bed samples were rinsed to remove salt. The desalted samples were then washed through a 4 phi (0.063 mm) sieve to separate sand and mud (silt/clay), before being dried overnight in an oven at 70°C. Finally, splits of the dried sand samples were analysed in a MacroGranometer™ settling tube [*Brezina*, 1979]. Subsequently, mean grain size, standard deviation, skewness, and kurtosis of the grain size distributions were determined on the basis of the percentile statistics described by *Folk and Ward* [1957].

5.3.3 Hydrodynamic parameters

Flow velocities were measured along the span of the compound dune. At each measuring point, the mean flow velocity (depth averaged) U was determined as the ensemble average flow velocity. These point mean flow velocities were then used to calculate the average mean flow velocity along the compound dune. Average near-bed flow velocities $u_{0\text{-}1\ m}$ (0-1 m above the bed) were calculated in a similar way. In addition, near-bed flow velocities $u_{0\text{-}3\ m}$ (0-3 m above the bed) were determined over the crest and troughs of the compound dune.

Correspondingly, average mean echo intensities EI and average near-bed echo intensities $EI_{0\text{-}1\ m}$ were calculated.

Average water depth D along the compound dune during the tidal cycle was determined by subtracting the average bed level of the compound dune, derived from the bathymetric grids, from the tidal curve (Fig. 5.2).

5.3.4 Bedform dimensions

Bedform dimensions were determined from the gridded bathymetry. Bedform length L has been defined as the trough-to-trough distance (baseline) with the location of a trough

defined as the lowest point of the lee (or stoss) side of a bedform. Bedform height H was determined as the vertical distance from the crest to the line defining the bedform length. The location of the crest was defined as the highest point along the span of the bedform. Bedform asymmetry is described by the symmetry ratio, which is the relation between flood side length L_{flood} and ebb side length L_{ebb}. Flood side length is the part of the bedform length exposed to the flood flow, whereas ebb side length is the part exposed to the ebb flow. Flood side slope φ_{flood} is the angle of the flood side with the base line, and likewise ebb side slope φ_{ebb} is the angle of the ebb side with the base line. A definition sketch visualizing the bedform dimensions is shown in Fig. 5.3.

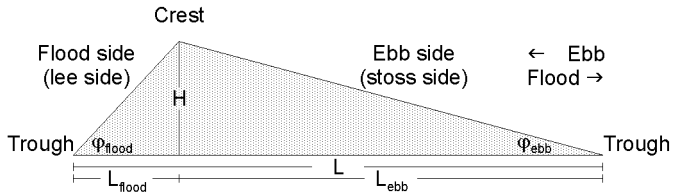

Fig. 5.3 Definition sketch visualizing bedform dimensions according to a triangular description.

The bedforms have been described according to the classification recommended in *Ashley* [1990], where ripples (L < 0.6 m) and dunes (L > 0.6 m) are distinguished on the basis of bedform length, dunes being further divided into categories of small (L = 0.6-5 m), medium (L = 5-10 m), large (L = 10-100 m) and very large (L > 100 m).

5.4 Results

A bathymetric image of the large barchanoid-shaped compound dune and the surrounding area on the 10th of September 2002 is shown in Fig. 5.4. Marked are the locations of the bed samples (Fig. 5.4A) as well as the line along which the thirteen MBES and ADCP surveys were conducted during the tidal cycle on the 11th of September 2002 (Fig. 5.4B)

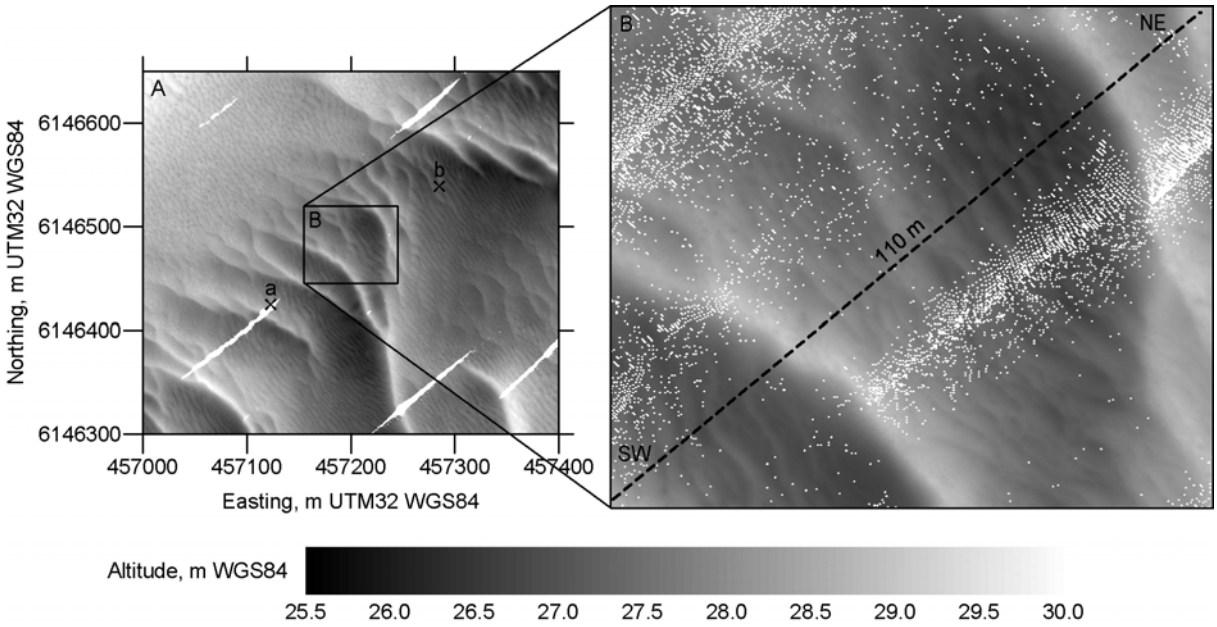

Fig. 5.4 A) Bathymetry around the large barchanoid-shaped compound dune in the Grådyb tidal inlet channel on the 10th of September 2002 (for location see Fig. 5.1). The grid is 400 x 350 m with a cell size of 0.4 x 0.4 m. Crosses mark the locations of the bed samples collected on the 9th of September 2002. B) Zoom-in of the compound dune. The grid is 90 x 75 m with a cell size of 0.2 x 0.2 m. The thirteen MBES and ADCP surveys during the tidal cycle on the 11th of September 2002 were conducted along the dashed line, and accordingly bed profiles for determination of dune dimensions were extracted along the dashed line. Water depth relative to mean low water springs (MLWS) in relation to WGS84 altitude is given by: m MLWS = m WGS84 - 39.951 m.

5.4.1 Grain size and hydrodynamics

Mean grain size close to the compound dune is 0.407 mm. The grain size distributions display phi standard deviations close to 0.50, i.e. according to *Folk* [1974] well sorted/moderately well sorted. The skewness, i.e. sorting in the tails of the grain population, of sample a is near-symmetrical, whereas of sample b it is negatively (coarse) skewed [after *Folk*, 1974]. The average kurtosis, i.e. degree of sharpness or peakedness, of the grain size distributions is 1.222.

Mean flow velocity over the compound dune displays a rather stepped temporal trend over the tidal cycle (Fig. 5.5). During the ebb tide, the mean flow velocity increases rapidly to relatively constant values around 0.80-1.00 m/s before decreasing just as abruptly towards low water (Fig. 5.5). The pattern during the flood tide is much the same with an initial abrupt increase to constant values around 0.80-1.00 m/s (Fig. 5.5). Mean echo intensity along the compound dune is characterized by a sharp increase early in the ebb phase, followed by a

progressive decrease towards low water (Fig. 5.5). A similar pattern is observed during the flood tide, a relatively early and abrupt increase being followed by a progressive decrease towards the succeeding high water (Fig. 5.5). Note the significantly lower echo intesities during the flood phase as compared to the ebb phase (Fig. 5.5). Furthermore, mean echo intensity displays a low peak shortly after low water, while the lowest value is reached with a time delay of about one hour after low water (Fig. 5.5).

Near-bed flow velocity over the compound dune displays a similar trend as the mean flow velocity, except that near-bed flow velocities on average are about 0.19 m/s lower during the ebb phase and 0.27 m/s lower during the flood phase (Fig. 5.5). Near-bed echo intensity follows a pattern similar to the near-bed flow velocity, e.g. during the flood phase a local minimum is observed in flow velocity as well as in echo intensity (Fig. 5.5).

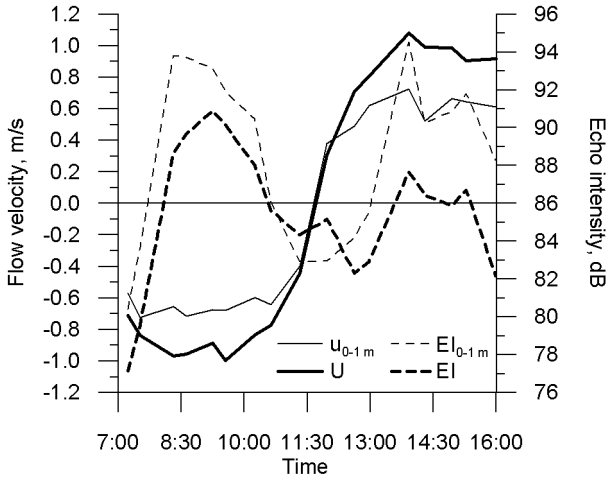

Fig. 5.5 Average mean (depth-averaged) flow velocity U (m/s) (thick line) and mean echo intensity EI (dB) (thick dashed line) along the large compound dune during the tidal cycle as well as average near-bed flow velocity $u_{0\text{-}1\,m}$ (m/s) (thin line) and echo intensity $EI_{0\text{-}1\,m}$ (dB) (thin dashed line).

Flow velocity over the compound dune not only varied vertically and temporally, but also spatially. On average the near-bed (0-3 m above the bed) flow velocity is 0.27 m/s higher at the crest than in the troughs of the compound dune (Fig. 5.6). Near-bed flow velocities at the crest were comparable during ebb and flood tide; however, distinct maximum near-bed crest flow velocities were reached in the middle of the ebbing tide (Fig. 5.6). Moreover, the near-bed trough velocities were generally higher during flood than ebb tide, and a distinct local minimum was reached in the middle of the ebb tide, which coincided with the maximum near-bed flow velocities at the crest (Fig. 5.6).

As expected, average water depth over the compound dune decreased during the ebb tide and increased during the flood tide (Fig. 5.6).

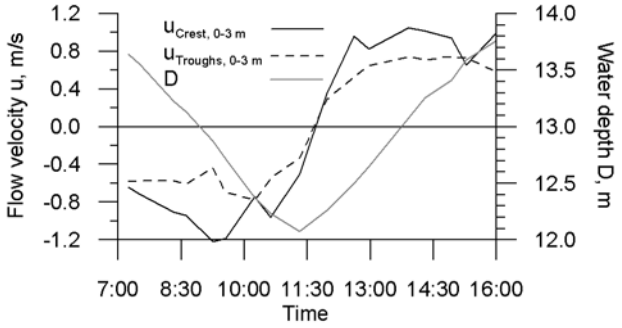

Fig. 5.6 Near-bed average flow velocity $u_{0\text{-}3\,m}$ (m/s) at the crest (black line) and in the troughs (black dashed line) of the large compound dune during the tidal cycle. Also shown is the average water depth D (m) along the compound dune (grey line).

5.4.2 Dune dynamics

Bed profiles were extracted from the bathymetric grids along the centre of the large barchanoid-shaped compound dune perpendicular to the crests of the superimposed small dunes (dashed line in Fig. 5.4). Trough and crest positions of the compound dune and the superimposed dunes (dune-a to -n in Fig. 5.7A) during the tidal cycle were determined from the extracted bed profiles, the crest of dune c being equivalent to the crest of the compound dune (Fig. 5.7B). Subsequently, average reach-values are presented for the lower lee side, crest, upper stoss side, and lower stoss side. In case of considering points and not reaches, the troughs and the crest of the compound dune are also presented.

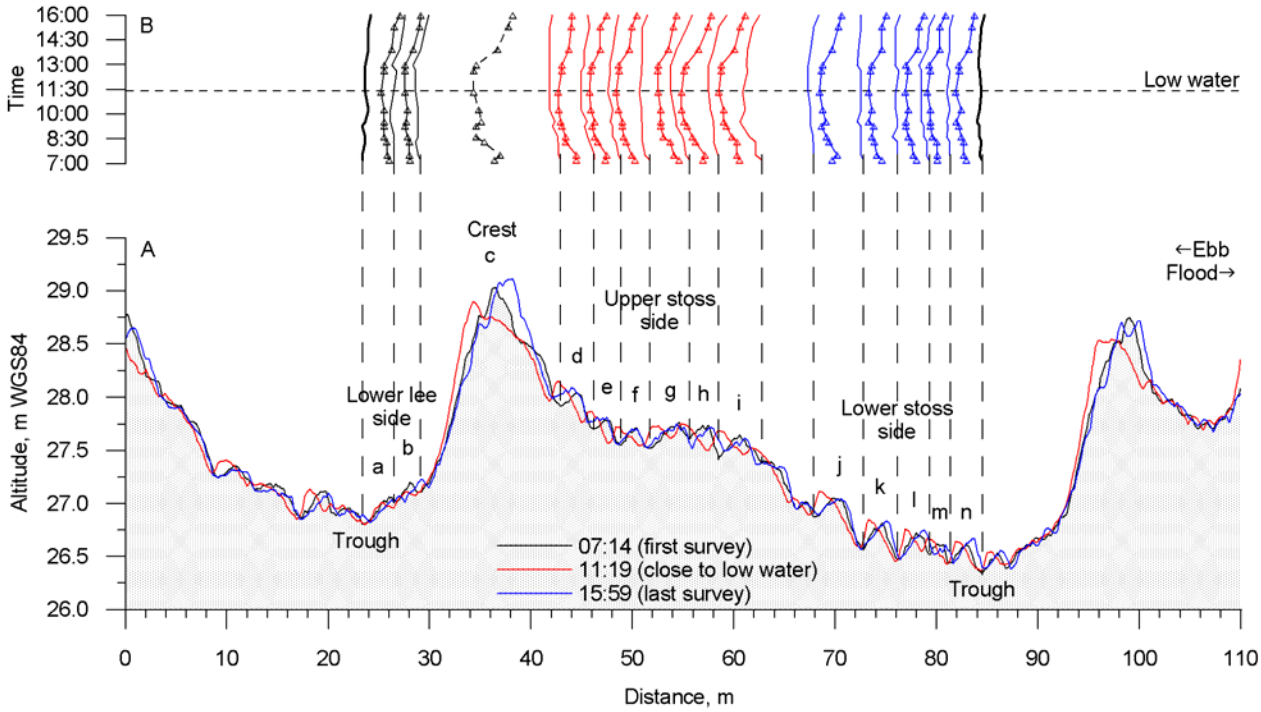

Fig. 5.7 A) Bed profiles along the compound dune at the first survey, close to low water and at the last survey during the tidal cycle extracted from bathymetric grids with cell sizes of 0.2 x 0.2 m (for location see Fig. 5.1 and Fig. 5.3). B) Trough and crest positions of the compound dune and of the superimposed dunes during the tidal cycle.

Dune migration

Temporally, dune migration is more pronounced during the accelerating flow phase than during the decelerating flow phase of the ebb tide, the only exception being the compound dune troughs (Table 5.1). During the flooding tide, troughs migrate more during the decelerating flow phase, whereas crests migrate more during the accelerating flow phase (Table 5.1). Overall, dune migration is more pronounced during the flood than the ebb tide. This results in a net flood-directed migration over the tidal cycle, the only exception being the troughs of the upper stoss side dunes (Table 5.1).

Spatially, dune crests migrate more than dune troughs, e.g. lower lee side crests migrate more than lower lee side troughs etc. (Table 5.1). Furthermore, in general trough and crest migration decreases from the crest towards the troughs of the compound dune, both during the ebb and the flood tide, i.e. the compound dune crest migrate more than the crests of the upper stoss side dunes which, in turn, migrate more than the crests of the lower stoss side dunes etc. (Table 5.1). However, there are a few exceptions. With decelerating flow during the ebb tide, the compound dune crest migrates less than the upper stoss side crests, and the compound dune troughs migrate more than both the lower stoss side troughs and lower lee side troughs

(Table 5.1). Note that the considerable migration of the compound dune troughs during decelerating ebb flow is actually flood-directed, resulting in a net flood-directed migration over the ebb phase (Table 5.1). Furthermore, with accelerating flow during the flood tide, the lower lee side troughs migrate more than the stoss side troughs, and, with decelerating flow during flood tide, the lower lee side dunes migrate more than the lower stoss side dunes, resulting in the lower lee side troughs migrating more than the stoss side troughs over the flood phase (Table 5.1).

Table 5.1 Dune migration with accelerating and decelerating flow during both ebb and flood tide based on the changes in horizontal position of the troughs and crests of the compound dune and the superimposed dunes during the tidal cycle (shown in Fig. 5.7B). In addition, net dune migration over the tidal cycle. – and + denote ebb- and flood-directed migration, respectively.

	Ebb tide			Flood tide			Tidal cycle
	Acc. flow (m)	Dec. flow (m)	Net (m)	Acc. flow (m)	Dec. flow (m)	Net (m)	Net (m)
Troughs	-0.17	+0.25	+0.08	+0.05	+0.38	+0.43	+0.51
Lower lee side troughs	-0.26	-0.03	-0.29	+0.55	+0.65	+1.20	+0.91
Lower lee side crests	-0.52	-0.13	-0.65	+0.91	+0.78	+1.69	+1.04
Crest	-1.82	-0.26	-2.08	+2.34	+1.56	+3.90	+1.82
Upper stoss side troughs	-1.01	-0.34	-1.35	+0.38	+0.80	+1.18	-0.17
Upper stoss side crests	-1.44	-0.48	-1.92	+1.28	+0.80	+2.08	+0.16
Lower stoss side troughs	-0.26	-0.18	-0.44	+0.18	+0.52	+0.70	+0.26
Lower stoss side crests	-0.88	-0.25	-1.13	+1.27	+0.60	+1.87	+0.74

The compound dune remains ebb-directed throughout the tidal cycle, although its crest and the smaller stoss side dunes reverse direction from flood-directed (or symmetric) to ebb-directed during the ebb tide and vice versa during the flood tide (Fig. 5.8). Overall, the lower lee side dunes change from a pronounced flood-asymmetry to an almost symmetric shape during the ebb tide and vice versa during the flood tide (Fig. 5.8). Note the increase in symmetry ratio of the lower lee side dunes in the middle of the ebb tide (Fig. 5.8), predominantly ascribed to flood-directed displacement of the crests of the lower lee side dunes (Fig. 5.7B).

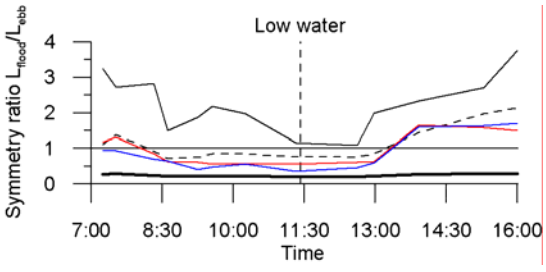

Fig. 5.8 Symmetry ratio of the compound dune (thick black line) and the superimposed dunes, i.e. lower lee side (black line), crest (black dashed line), upper stoss side (red line) and lower stoss side (blue line). Unity corresponds to symmetric, while below and above unity corresponds to asymmetric ebb- and flood-direction, respectively.

Bed erosion and accretion

By comparing bed volumes (areas) per unit width relative to a fixed altitude (e.g. the WGS84 ellipsoid) along a fixed reach, erosion and accretion along the compound dune during the tidal cycle can be approximated. Temporally, 3.9 m^3/m of the compound dune (total volume ~52 m^3/m), i.e. 7.5%, erodes with accelerating ebb flow and accretes with decelerating ebb flow (Fig. 5.9A and Table 5.2). During flood tide the compound dune, in general, undergoes only little erosion and accretion, resulting in an overall accretion of the compound dune of 0.7 m^3/m over the tidal cycle, i.e. a volume change of 1% of the total compound dune volume. The compound dune volume is hence practically constant over a tidal cycle (Fig. 5.9A and Table 5.2). Spatially, the pronounced erosion and accretion during ebb tide occurs on the stoss side and crest of the compound dune.

Table 5.2 Volumetric erosion (-) and accretion (+) per unit width along the compound dune with accelerating and decelerating flow during both ebb and flood tide. In addition, net erosion or accretion over the tidal cycle.

	Ebb tide		Flood tide		
	Acc. Flow (m^2)	Dec. flow (m^2)	Acc. flow (m^2)	Dec. flow (m^2)	Net
Compound	-3.918	+3.889	+0.720	+0.004	+0.695
Lower lee side	-0.245	+0.171	-0.015	-0.061	-0.149
Crest	-0.837	+0.931	+0.251	-0.163	+0.182
Upper stoss side	-1.136	+1.177	+0.270	-0.101	+0.210
Lower stoss side	-0.807	+0.829	-0.006	+0.184	+0.199

Dividing the volume changes with the fixed lengths of the reaches yield the changes in volume per square meter bed, which is equivalent to erosion or accretion in meters. The overall pattern is, of course, the same, but the spatial distribution along the compound dune is better visualised. During ebb tide, 6.5 cm is eroded and accreted on average. However, the degree of erosion and accretion generally decreases from the crest towards the troughs of the compound dune (Fig. 5.9B, C and Table 5.3). During flood tide, the compound dune on average experiences insignificant erosion and accretion, as the changes are within the range of precision of the MBES system (see error bars Fig. 5.9B and Table 5.3). On the other hand, it can be expected that a potential deviation at each point is actually levelled out, as the visualised changes are based on volumetric calculations and the overall alternating trend of erosion and accretion is found at both the stoss side and the crest (Fig. 5.9B). Nevertheless, since the changes are at the limit of the precision of the MBES system, the compound dune as a whole is considered to be stable during flood tide, with exception of the substantial accretion on the crest and the corresponding erosion on the lower lee side, as shown by the dashed line and the black line, respectively, in Fig. 5.9B.

Table 5.3 Volumetric erosion (-) and accretion (+) per square meter along the compound dune with accelerating and decelerating flow during both ebb and flood tide. In addition, net erosion or accretion over the tidal cycle.

	Ebb tide		Flood tide		
	Acc. Flow (m)	Dec. flow (m)	Acc. flow (m)	Dec. flow (m)	Net
Compound	-0.066	+0.065	+0.012	-	+0.012
Lower lee side	-0.064	+0.044	-0.004	-0.016	-0.039
Crest	-0.070	+0.078	+0.021	-0.014	+0.015
Upper stoss side	-0.064	+0.067	+0.015	-0.006	+0.012
Lower stoss side	-0.055	+0.056	-	+0.013	+0.014

The higher erosion and accretion on the crest (~25 cm) as opposed to the troughs (≤5 cm) of the compound dune is even more clearly visualised by the vertical movement of the trough and crest positions during the tidal cycle (Fig. 5.9). Furthermore, the erosion and accretion of the crest (point) is much higher than the average volumetric erosion and accretion per square meter of the crest (reach), indicating a considerable sediment turnover within the crest dune. Moreover, the dune forming the crest of the compound dune displays erosion and accretion with accelerating and decelerating ebb flow, respectively, and an alternating pattern of erosion and accretion during flood tide (Fig. 5.9B), whereas the crest itself generally decreases in altitude during the ebb tide and accretes during the flood tide (Fig. 5.9C). Minor local accretion also occurs around low water (Fig. 5.9C).

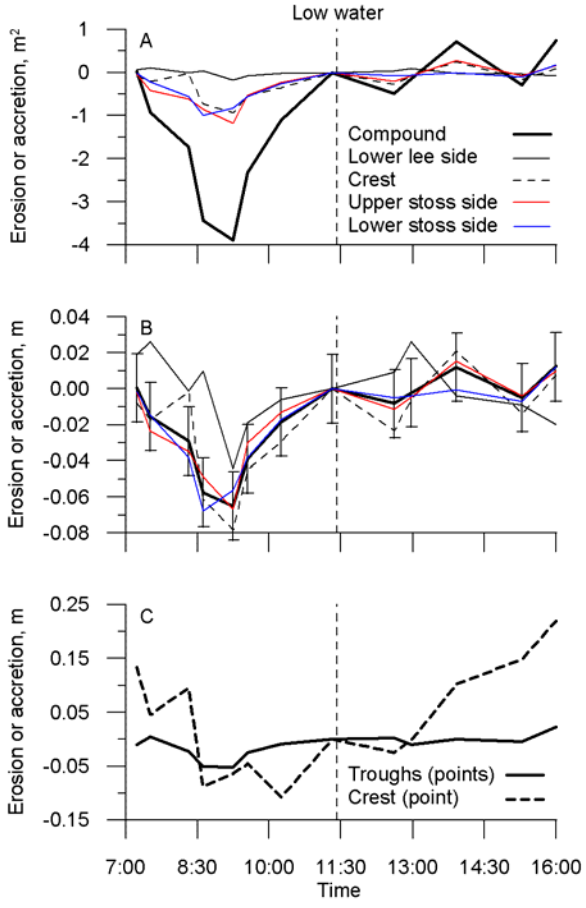

Fig. 5.9 (opposite page) Volumetric erosion and accretion per unit width (A) and per square meter (B) along the compound dune in relation to low water. Error bars mark the precision of the MBES system (±1.9 cm). C) Erosion and accretion of the troughs and the crest of the compound dune in relation to low water based on point measurements.

Dune dimensions

Despite a net decrease in length over the tidal cycle, the length of the compound dune is in general relatively stable (CV = 0%, Fig. 5.10 and Table 5.4). Overall, the lengths of the lower lee side dunes decrease during ebb tide and increase during flood tide, but display no net change over the tidal cycle (Fig. 5.10 and Table 5.4). The length of the crest dune generally decreases during the tidal cycle (Fig. 5.10 and Table 5.4). In general, upper stoss side dune lengths decrease during ebb tide and increase during flood tide, whereas the lengths of the lower stoss side dunes increase during ebb tide and decrease during flood tide (Fig. 5.10 and Table 5.4). However, the variations in length of the stoss side dunes are small (CV = 1-3%) and close to, or within the horizontal precision of the MBES system, i.e. ±13 cm, and are therefore not discussed any further (Fig. 5.10 and Table 5.4).

Table 5.4 Statistics (mean, standard deviation, SD, and coefficient of variation, CV) during the tidal cycle and variations with accelerating and decelerating flow during both ebb and flood tide of the length of the compound dune and the superimposed dunes.

				Ebb tide		Flood tide		Tidal cycle
	L_{mean} (m)	SD (m)	CV (%)	Acc. flow (m)	Dec. flow (m)	Acc. flow (m)	Dec. flow (m)	Net (m)
Compound	60.60	0.25	0	-0.18	-0.12	-0.47	+0.24	-0.54
Lower lee side	2.63	0.17	7	-0.09	-0.29	+0.12	+0.26	-
Crest	13.29	0.58	4	-0.51	-0.05	-0.47	-0.52	-1.55
Upper stoss side	3.22	0.09	3	-0.20	+0.05	+0.08	+0.14	+0.08
Lower stoss side	3.33	0.04	1	-	+0.09	-0.09	-0.06	-0.06

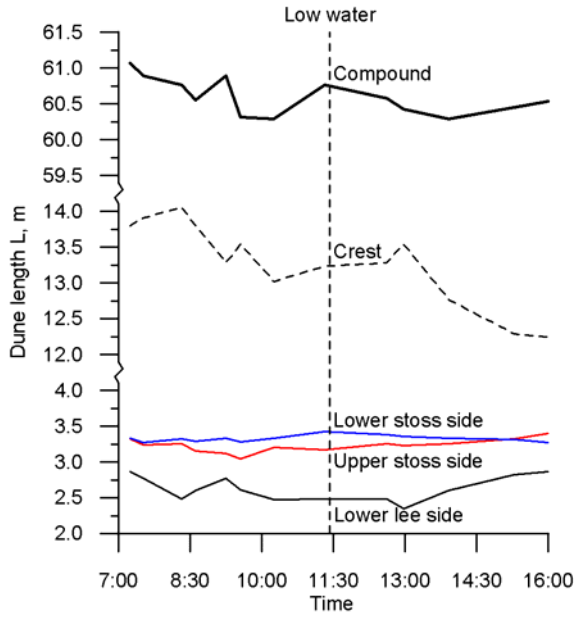

Fig. 5.10 Length of the compound dune and the superimposed dunes.

The height of the compound dune more or less shows the same pattern as the vertical crest movement, i.e. a general decrease during ebb tide and an increase during flood tide, with a local maximum around low water (Fig. 5.11). The lower lee side dunes display the largest relative variations in height (CV = 19%), but these are within the vertical precision of the MBES system, i.e. ±1.9 cm, and are therefore not discussed any further (Fig. 5.11 and Table 5.5). Overall, the height of the crest dune decreases during ebb tide, albeit with considerable scatter, before decreasing during the accelerating flow phase and increasing during the decelerating flow phase of the flood tide, resulting in a net decrease in height over the tidal cycle (Fig. 5.11 and Table 5.5). Upper stoss side dune heights increase with accelerating flow and decrease with decelerating flow during both ebb and flood tide, the decrease during the decelerating flood flow being insignificant though (Fig. 5.11 and Table 5.5). Lower stoss side dune heights display a similar pattern, with the exception of only a marginal decrease in dune height during the decelerating ebb flow (Fig. 5.11 and Table 5.5).

Table 5.5 Statistics (mean, standard deviation, SD, and coefficient of variation, CV) during the tidal cycle and variations with accelerating and decelerating flow during both ebb and flood tide of the height of the compound dune and the superimposed dunes.

				Ebb tide		Flood tide		Tidal cycle
	H_{mean} (m)	SD (m)	CV (%)	Acc. flow (m)	Dec. flow (m)	Acc. flow (m)	Dec. flow (m)	Net (m)
Compound	2.224	0.096	4	-0.15	-	+0.11	+0.11	0.07
Lower lee side	0.100	0.019	19	-0.018	+0.016	-0.014	+0.015	-0.001
Crest	1.404	0.057	4	-0.060	+0.001	-0.080	+0.037	-0.102
Upper stoss side	0.199	0.010	5	+0.021	-0.035	+0.023	-0.003	+0.007
Lower stoss side	0.252	0.017	7	+0.021	-0.004	+0.035	-0.024	+0.029

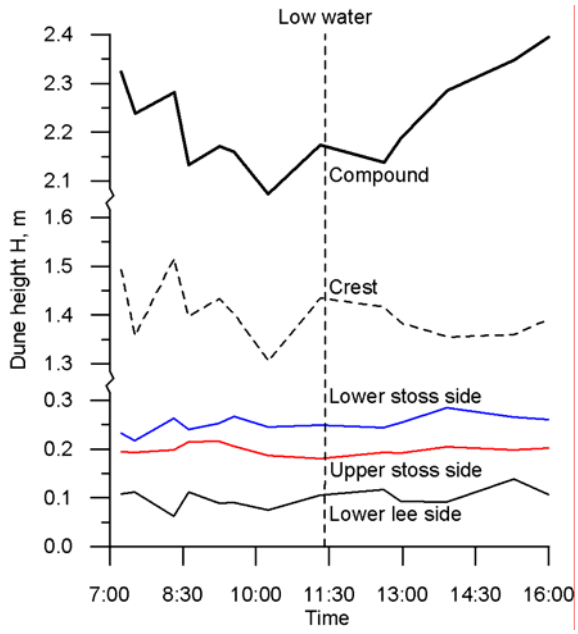

Fig. 5.11 Height of the compound dune and the superimposed dunes.

The flood side (i.e. the lee side of the compound dune exposed to the flood flow) slope angle of the crest dune generally increases during the ebb tide and decreases during the flood tide (Fig. 5.12) due to the displacement of the crest position (visualised in both Fig. 5.7B and Fig. 5.8). Maximum values reach 17.5° in the middle of the ebb tide and around low water (Fig. 5.8), which is still only about half of the angle of repose for sand-sized quartz grains, i.e. 35° [e.g. *van Rijn*, 1993; *Soulsby*, 1997]. The ebb side (i.e. the stoss side of the compound dune exposed to the ebb flow) slope angle of the crest dune displays exactly the opposite trend of the flood side slope angle, reaching a maximum of around 16° in the last survey towards high water (Fig. 5.12).

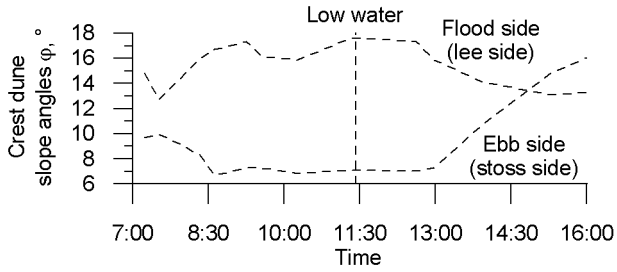

Fig. 5.12 Flood side (lee side of the compound dune) slope angle and ebb side (stoss side of the compound dune) slope angle of the crest dune during the tidal cycle.

5.5 Discussion

5.5.1 Dune migration

The spatially higher crest than trough displacement of the compound dune (Fig. 5.7B) is a result of the higher flow velocities at the crest relative to the troughs (Fig. 5.6). This non-uniform flow along the compound dune can be explained from flow continuity, i.e. in order to maintain uniform discharge along the compound dune, the flow velocity has to be higher over the crest than over the troughs. Likewise, the higher crest than trough displacement of the superimposed dunes is also suggested to be a result of flow continuity, although this cannot be demonstrated by the available ADCP measurements.

The temporal variation in migration rate of the superimposed dunes can primarily be explained by exposure to the flow. The most pronounced example is the extensive migration of the lower lee side dunes during the flood tide as compared to the ebb tide (Fig. 5.7B and Table 5.1) due to higher near-bed trough flow velocities during the flood tide (on average 0.62 m/s) as compared to the ebb tide (on average 0.57 m/s) (Fig. 5.6), the lee effect of the compound dune during the ebb tide being smaller during the flood tide. In addition, net migration is flood-directed over the tidal cycle (Fig. 5.7B and Table 5.1), despite the fact that annual net migration is ebb-directed [*Bartholdy et al.*, 2002 and *Ernstsen et al.*, 2005], a feature also emphasised by the ebb-directed asymmetry of the compound dune. This means that extrapolation of short-term migration rates is not possible.

The reversal of dune orientation during tidal semi cycles has already been observed by *Hawkins and Sebbage* [1972] from echo soundings in the Bristol Channel, UK; however, the dimensions of the dunes were not reported. *Boothroyd and Hubbard* [1974 and 1975] illustrated the reversal of superimposed small dunes ($L \approx 1.5$ m) based on diver observations in the Parker Estuary, USA. Recently, *Bastos et al.* [2004] reported the reversal of small dunes ($L \approx 3$ m, $H \approx 0.65$ m) on Shambles Bank in the English Channel, UK, based on side scan sonar images. Likewise, *Hoekstra et al.* [2004] recently observed a reversal in orientation of small dunes ($L = 0.6$-0.7 m, $H = 0.04$-0.05 m) during tidal semi cycles on Spratt Sand in the Teign Estuary, UK from measurements using an autonomous sand ripple profiler (ASRP). Hence, the reversal in orientation of small to medium dunes during tidal semi cycles, as also observed in this study (Fig. 5.7B and Fig. 5.8), is a common phenomenon in tidal environments.

Fenster and FitzGerald [1996] conducted echo soundings in the Kennebec River estuary, USA, over a tidal cycle, but observed no reversal in orientation of the large dunes (L = 50 m and H = 6.5 m); however, the echo sounder profiles (Fig. 5B and C, p. 108) reveal flood caps on the ebb-directed dunes. Already *Rubin and McCulloch* [1979 and 1980] observed large dunes (L =75-100 m, H ≈ 5 m) with reversed crests in the Central San Francisco Bay, USA, from side scan sonar images. Thus, large dunes (or at least in case of L > 50 m) do not appear to reverse their direction during tidal semi cycles, as was also observed in this study (Fig. 5.7B and Fig. 5.8), because of insufficient time to transport the required volume of sediment in the opposite direction.

Recently, *Knaapen* [2005] developed a dune migration predictor, determining dune migration from the change in crest position with time. In the Grådyb tidal inlet channel the variation in crest position of the large compound dune over a single tidal cycle (>3 m, Fig. 5.7B and Table 5.1) is substantial compared to the annual migration in the study area [9-31 m/y, *Ernstsen et al.*, 2005]. Consequently, in tidal environments it is recommended to determine long-term migration rates from the displacement of trough positions, or to make sure that crest positions at similar times in the tidal cycle are compared.

5.5.2 Bed erosion and accretion

During the ebb tide, bed material is eroded in the accelerating flow phase (Fig. 5.9A, B) and brought into suspension (Fig. 5.5). The decrease in erosion from the crest towards the troughs (Fig. 5.9 and Table 5.3) is a result of the higher near-bed flow velocities at the crest as compared to the troughs (Fig. 5.6). Subsequently, the moving bed material settles during the decelerating flow phase (Fig. 5.5), the bed accreting towards low water (Fig. 5.9A, B). The decrease in accretion from the crest towards the troughs (Fig. 5.9 and Table 5.3) is suggested to be due to a generally shorter settling distance to the crest of the compound dune. Very recently, *Kostaschuk and Best* [2005] observed somewhat similar dune and flow dynamics over a tidal cycle in the Fraser Estuary, Canada. Based on ADCP measurements and single beam echo sounding *Kostaschuk and Best* [2005] observed erosion of the troughs and crests of large dunes (L = 20-40 m, H = 1-2 m) during accelerating flow, accompanied by increased suspended sediment concentrations, the trough erosion being ascribed to increased turbulence resulting from development and expansion of the flow separation/deceleration zone. In addition, they observed deposition in the troughs and reported sand falling out of suspension and draping the dunes towards high water slacks. However, because of the limitations

imposed by the single beam echo sounder in combination with inadequate absolute positioning, *Kostaschuk and Best* [2005] were unable to quantify the observed dune dynamics. Bed accretion is also a possible reason for the increase in ripple height observed by *Hoekstra et al.* [2004] around high water slacks on Spratt Sand in the Teign Estuary, UK, from ASRP measurements. Based on ultrasonic depth profiler measurements in the laboratory, *Leclair* [2002] observed trough scouring, but, unfortunately, she did not relate the erosion to the flow.

During the flood tide, the patterns of erosion and accretion are not as clear as during the ebb tide. The initial accretion on the lower lee side of the compound dune (Fig. 5.9B) is suggested to occur because trough flow velocities are initially too low to bring bed material into suspension (Fig. 5.6). The subsequent erosion of the lower lee side (Fig. 5.9B) is considered to be partly due to a material transfer to the crest dune by bedload transport and partly the result of a significant increase in the near-bed flow velocity in the trough, sufficient to bring bed material into suspension (Fig. 5.6). This is supported by a simultaneous accretion of the crest dune (Fig. 5.9B) as well as an increase in suspended bed material (Fig. 5.5). The net erosion on the lower lee side of the compound dune and accretion on the crest and the stoss side (Fig. 5.9 and Table 5.3) is probably also related to flow continuity, yielding converging flow on the lee side, inducing erosion, as opposed to diverging flow on the stoss side, inducing deposition. However, the most significant pattern during the flood tide is the accretion of the crest of the compound dune (Fig. 5.9C). The overall erosion and accretion of the compound dune crest is related to the changing water depth. With decreasing water depth during the ebb tide (Fig. 5.6), the compound dune crest is generally lowered (Fig. 5.9C). This is reversed during the flood tide where the compound dune crest rebuilds (Fig. 5.9C) as water depth increases (Fig. 5.6). The minor accretion of the compound dune crest towards low water and erosion after low water (Fig. 5.9C) is ascribed to settling of the finer fractions of the bed material as the flow velocity decreases towards low water and subsequent resuspension of these easily eroded finer fractions as the flow picks up after low water. This initial erosion of the compound dune crest (Fig. 5.9C) is also observed in the volumetric erosion of the crest dune (Fig. 5.9B).

It has been well argued that water depth is not a primary control factor of dune dimensions [*Flemming*, 2000a; *Bartholdy et al.*, 2005], but that it merely acts as a limiting factor to dune growth [*Flemming*, 2000a; *Bartholdy et al.*, 2005]. This has been confirmed, e.g. by *Carling et al.* [2000a] in the River Rhine, Germany, and also in this study. With

increasing water depth during the flood tide, the near-bed crest flow velocities are slightly lower than during the ebb tide (Fig. 5.6), which enables the accretion of the compound dune crest. Hence, dune size is controlled by the interplay between flow velocity and grain size, but water depth can act as a limiting factor by controlling the near-bed flow velocity.

5.5.3 Dune dimensions

In the Fraser Estuary, the heights of large dunes change in the course of a tidal cycle, whereas their lengths remain stable [*Kostaschuk and Best*, 2005]. In a general way this is comparable to both the compound dune and the superimposed dunes in this study, with the exception of the crest dune (Fig. 5.10 and Table 5.4). *Kostaschuk and Best* [2005] found dune height to increase with increasing flow velocity due to trough scouring caused by increased turbulence resulting from the development and expansion of the flow separation/deceleration zone [*Kostaschuk and Best*, 2005]. In this study, the changing height of the compound dune is, as mentioned earlier, a result of water depth acting as a limiting factor to dune growth. The changes in height of the stoss side dunes (Fig. 5.11 and Table 5.5) follow the changes in flow velocity (Fig. 5.5) during both ebb and flood tide, but in two cases the degree of change is within the resolution limits of the MBES system. At this point in time it is not possible to determine whether the change in dune height is due to net trough or crest erosion. A lack of change in dune length or a prior change in dune height to dune length is due to the fact that the amount of sediment which has to be moved to raise or lower the height of a dune is smaller than the amount needed to change the length [*Dalrymple and Rhodes*, 1995]. This time lag in the adjustment of dune length relative to dune height caused by changing flow velocity has also been observed in the case of large to very large dunes over neap-spring tidal cycles [*Langhorne*, 1982; *Flemming and Davis*, 1992], large dunes in rivers during rising and falling stage [*Nasner*, 1978; *Wilbers and ten Brinke*, 2003], and even ripples in laboratory flumes [*Baas*, 1994 and 1999].

5.5.4 Flow separation

The increase in symmetry ratio of the lower lee side dunes in the middle of the ebb tide (Fig. 5.8), along with the simultaneous flood-directed displacement of the troughs of the compound dune (Fig. 5.7 and Table 5.1), indicate the potential existence of return flow in the trough and on the lower lee side of the compound dune. Such a return flow gyre would most likely be the product of flow separation at the crest and flow reattachment in the trough, generating a back-rolling vortex over the lee side/trough region of the compound dune, as

shown before in laboratory experiments [e.g. *Onslow et al.*, 1993; *Bennett and Best*, 1995; *Müller and Gyr*, 1996; *Ha and Chough*, 2003; *Best*, 2005]. Already thirty five years ago based *Terwindt* [1971] observed similar dune configurations of large compound dunes (L ≈ 300 m, H ≈ 5 m) with asymmetrical superimposed dunes on the lower lee sides on echo sounder profiles in the Dutch part of the North Sea, indicating sediment transport towards the crest; however, *Terwindt* [1971] did not comment on the orientation of the superimposed lower lee side dunes. In his model on the internal structure of dunes, *Allen* [1980] emphasizes that the bottom set of the lee side may display backflow ripples at high flow velocities. This is consistent with the fact that the crests of the lower lee side dunes and the troughs of the compound dune are displaced in the direction of flood when flow velocities are highest in the middle of the ebb period (Fig. 5.5). In addition, the flood-directed displacement coincides with a maximum flood side slope angle of the crest dune of 16-17.5° (Fig. 5.12), representative of the lee side slope angle of the compound dune, and a maximum in near-bed crest flow velocity of 1.2 m/s (Fig. 5.6). This also explains the low near-bed trough flow velocity of 0.4 m/s (Fig. 5.6), as this average velocity is based on values incorporating opposite flow directions. This suggests that flow separation occurs over lee side angles as low as ~16°, i.e. half the angle of repose (~35°), if the near-bed crest flow is strong enough, in this case ~1.2 m/s. The erosion in the troughs and on the lower lee side of the compound dune during ebb tide (Fig. 5.9B, C and Table 5.3) is thus also a result of flow separation, more specifically due to the generation of higher turbulence, as the near-bed trough flow velocities are generally low (Fig. 5.6). In addition, the flow is in general diverging which promotes deposition rather than erosion.

The horizontal resolution and ping rate of the ADCP measurements applied in this study are inadequate to resolve the flow pattern behind the crest as well as the near-bed reverse flow on the lower lee side. *Kostaschuk et al.* [2004] also argue that ADCPs cannot adequately measure flow velocity in dune troughs due to the beam geometry, which results in large sampling diameters close to the bed.

5.5.5 Sediment transport

Dune dynamics in the Grådyb tidal inlet channel appears to involve two transport modes: 1) Dune migration as a result of bedload transport (Fig. 5.7), and 2) erosion and accretion of the bed resulting from suspended load transport (Fig. 5.9A, B). At this point of the investigation it is not quite clear yet what effect the two transport modes have on the overall

sediment budget and morphology of the tidal inlet system. A major morphological element which can potentially be attributed to the pronounced erosion during the ebb tide (Fig. 5.9A, B) is the well-developed ebb tidal delta. It may be the result of a continuous contribution of sand from settling of suspended bed material during the ebb tide, which is promoted by the decreasing flow velocity as the tidal inlet widens, and, of course, a contribution from the net ebb-directed bedload transport.

5.6 Conclusions

On the basis of the analysis of bathymetry, water depth, flow velocity and echo intensity along a large compound dune with superimposed small to medium dunes during a semi-diurnal tidal cycle in the Grådyb tidal inlet channel in the Danish Wadden Sea, the following conclusions are reached:

1. Spatial variation in dune migration with dune crests displaying a larger displacement than dune troughs is due to higher flow velocities at the crests than in the troughs. This non-uniform flow over dunes can be explained by flow continuity.

2. Temporal variation in dune migration, e.g. with lower lee side dunes migrating more during the flood tide than during the ebb tide, is due to higher near-bed flow velocities in the troughs of the compound dune during the flood as compared to the ebb tide. This can be explained by flow exposure, i.e. the lee effect of the compound dune active during the ebb tide is negligible during the flood tide.

3. Net material displacement is flood-directed over the tidal cycle, despite the fact that annual net migration is ebb-directed [*Bartholdy et al.*, 2002 and *Ernstsen et al.*, 2005]. This means that extrapolation of short-term migration rates is not possible.

4. The superimposed dunes reverse direction during a tidal semi cycle, whereas the ebb-aligned compound dune merely develops a flood cap during the flood tide. The response time of the compound dune required to reverse its direction is thus longer than a tidal semi cycle, i.e. a half semi-diurnal tidal cycle is insufficient to move the required volume of sediment.

5. During the ebb tide, bed material is eroded and brought into suspension during the accelerating flow phase. Erosion decreases from the crest towards the troughs of the compound dune as a result of higher near-bed flow velocities at the crest relative to the troughs. Bed material settles during the decelerating flow phase, the bed accreting towards low water. The decrease in accretion rate from the crest towards the troughs of the compound

dune is suggested to be due to a generally decreasing settling distance towards the crest. The pronounced erosion of the crest of the compound dune is due to water depth acting as a limiting factor to dune growth.

6. During the flood tide, the bed of the compound dune is overall rather stable. Internally, bed material is eroded from the lower lee side, being partly transported to the crest in bedload and partly brought into suspension. The pronounced accretion of the crest of the compound dune is due to the fact that water depth no longer acts as a limiting factor to dune growth.

7. In general, dune height changes during a tidal cycle, whereas dune length remains stable. This is due to the fact that the amount of sediment that needs to be moved to change dune height is smaller than the amount needed to change dune length. The height of the compound dune follows the change in water depth (see point 6. and 7.), whereas the height of the stoss side dunes follows the change in flow velocity, i.e. the stoss side dunes are water depth-independent.

8. Flow separation at the crest of the compound dune with associated reverse flow in the trough lee side region is suggested to develop during the ebb tide as the troughs of the compound dune and the crests of the lower lee side dunes are displaced in the flood direction around maximum ebb flow. Flow separation is initiated over a lee side angle of ~16°, i.e. half the angle of repose (~35°) coupled with a near-bed crest flow velocity of ~1.2 m/s.

9. Long-term migration rates are recommended to be determined from trough positions in order to prevent erroneous calculations due to the high variability of crest positions during single tidal cycles.

Acknowledgements

This study was supported by the German Science Foundation. The captain and crew of the RV Senckenberg are thanked for their expertise and unfailing good spirits during the cruises. Also thanks to Erik Brenneche, Port of Esbjerg, for providing tide gauge data.

Paper V

Chapter 6: Paper V

Flow and grain size control of depth-independent simple subaqueous dunes

Jesper Bartholdy[1], Burg W. Flemming[2], Alex Bartholomä[2], Verner B. Ernstsen[3]

[1]*Institute of Geography, University of Copenhagen, Øster Voldgade 10, DK-1350 Copenhagen, Denmark*

[2]*Senckenberg Institute, Division of Marine Science, Suedstrand 40, D-26382 Wilhelmshaven, Germany*

[3]*Research Center Ocean Margins, University of Bremen, Leobener Str., P.O. Box 330 440, D-28359 Bremen, Germany*

Journal of Geophysical Research, 110(F04S16): 12 pp.

Abstract

In the Grådyb tidal inlet (Danish Wadden Sea) simple medium to large dunes, which are superimposed on large to very large dunes, increase in size with decreasing grain size under quasi-constant ebb dominated mean flow conditions. The mean height of the superimposed dunes increases from 0.1 m to 0.5 m and the mean dune length from 7 m to 12 m. This happens over a distance of 1.5 km from the inner to the outer part where mean depth (12 m) and the dominant ebb current (1.0 m/s) remain constant. Over this reach, the grain size changes from 0.6 mm in the inner part to 0.3 mm in the outer part. As the water depth is constant and more than one order of magnitude larger than the height of the dunes, these are regarded as being depth-independent. Relationships between dune dimensions and grain size established in previous studies are transformed into more general statements, bedform dimensions being directly related to the form-corrected Shields parameter (θ'). In this way, dune dimensions and flow strength/grain-size have, for the first time, been directly related to both bedload and free stream velocity in deeper flow systems. The former relationship is based on a recalibrated (form migration) version of the Meyer-Peter and Müller bedload formula. Four diagrams describing flow conditions and dune migration rates as a function of grain size and dune length are presented.

6.1 Introduction

Dunes and ripples are commonly distinguished on the basis of their scaling or non-scaling with flow depth as well as dimensional criteria such as wavelength [e.g. *Yalin*, 1977; *Allen*, 1982; *Ashley*, 1990] Ripples are defined as small bedforms (length, $L < 0.6$ m) which do not scale with water depth, whereas dunes are larger and generally considered to scale with water depth. The nomenclature used in this article follows that of *Ashley* [1990]. The common view that dunes scale with water depth consistently ignores numerous, well documented examples where dune dimensions were found to be independent of flow depth [e.g. *Jackson*, 1976; *Flemming*, 1978; *Dalrymple et al.*, 1978; *Dalrymple*, 1984; *Ashley*, 1990; *Harbor*, 1998; *Carling et al.*, 2000a and 2000b; *Idier et al.*, 2002]. The simple fact that compound dunes exist contradicts the depth-scaling argument. If the largest compound dunes scale with water depth, where does that leave the smaller, superimposed ones? Also, if these scale with water depth, how can the compound dunes be orders of magnitude larger?

To overcome this contradiction, it has sometimes been argued that the smaller, superimposed dunes scale with the newly developing boundary layer at the reattachment zone of the flow on the lower stoss-side of large dunes [e.g. *Southard*, 1991]. If this was true, then the contradiction is simply reversed, and the question must be asked, why large dunes should not also scale with boundary-layer thickness, in which case the scaling with water depth would merely represent a special case where a shallow flow imposes a depth limitation on dune growth. Indeed, this would explain why dunes in deep flows do not scale with water depth. The idea that the viscous depth (based on the turbulent viscosity concept) and the bed friction, rather than the depth itself, control bedform dimensions in tidal seas has been put forward by *Hulscher* [1996], *Komarova and Hulscher* [2000] and *Komarova and Newell* [2000]. At the other end of the scale, numerous experiments in small laboratory flumes the world over have demonstrated that ripples are not always independent of water depth. In terms of their size, all flow-transverse bedforms generated in small flumes are by definition ripples, in spite of the fact that they clearly scale with water depth, as revealed by contracting water surfaces over their crests. As a consequence, the criteria by which ripples and dunes are supposed to be distinguished are inherently suspect [*Flemming*, 2000a]. Based on stability analysis of flow at low Froude numbers over erodible beds *Richards* [1980] found two separate modes of instability. One with wavelengths related to the roughness of the bed and one with wavelengths related to the depth of the flow. *Richards* postulated that these two modes corresponded to ripples and dunes respectively. In his discussion, however, *Richards* stated that the model could be extended to predict a hierarchy of ripples with increasing wavelengths "until some limiting factor such as the depth of the flow becomes important" [*Richards*, 1980, p. 617]. Fact is that if flow depth is small enough, then any bedform will scale with it, simply because depth limitation forms a natural upper boundary, and serves as an upper limit for bedform growth of any kind. In most laboratory flumes, the maximum water depth is typically <0.5 m. As a result, dune heights will remain smaller than about 15 cm. It is therefore not surprising that the largest bedforms in flume studies are always found to scale with flow depth. By contrast, dunes observed on the ocean floor at depths of 10^s-1000^s of meters [e.g *Kenyon and Belderson*, 1973; *Lonsdale and Malfeit*, 1974; *Flemming*, 1978; *Kuijpers et al.*, 2002] exhibit a wide range of sizes. These must evidently be controlled by factors other than water depth. The only meaningful explanation is that dunes are not primarily scaled by water (or flow) depth but by the mutual relationship between flow conditions and form response. For obvious reasons this relationship should also be highly dependent on grain size. The dunes described in this paper are a case in point.

The bedforms recorded in the Grådyb tidal inlet on the west coast of Denmark (the northern part of the Wadden Sea) revealed that under virtually constant hydrodynamic conditions the height and length of both simple and compound dunes were essentially controlled by grain size [*Bartholdy et al.*, 2002]. The primary objectives of the present paper are: (1) to demonstrate, in a general way, that the dimensions of simple subaqueous dunes are controlled by flow strength and grain-size; (2) to stress the fact that simple dunes in deeper water are depth-independent, and to demonstrate that their variation with flow strength and grain size is similar to variations found for depth-dependent dunes in flumes; (3) to use the observed relationships for the construction of diagrams from which flow conditions and migration rates of simple subaqueous dunes can be predicted solely on the basis of grain size and dune length.

6.2 Flow conditions and physical setting of the study site

The Grådyb inlet is about 1000 m wide and on average 12 m deep (Fig. 6.1). The mean tidal range is close to 1.5 m. Mean grain size of the bed material along the center line of the inlet throat decreases from 0.6 mm in the inner part, to 0.3 mm in the outer part. Two dune size populations are present: large to very large compound dunes, and medium to large simple, superimposed dunes. Both dune populations are essentially two-dimensional with straight to slightly curved crest lines. The tidal currents are of similar magnitude along the entire study reach and vary little between spring and neap. Sediment transport occurs during both ebb and flood, the latter being less vigorous than the former. The centre line of the inlet has repeatedly been surveyed since January 1991 by the Harbour authorities in Esbjerg by means of echo-sounding coupled with a high-resolution navigation system.

The flow conditions in the inlet have been analysed by *Bartholdy et al.* [2002]. Based on detailed velocity measurements using an ADI 1.2 MHz Acoustic Doppler Current Profiler interfaced with a differential GPS navigation system, Niskin winged current meters (model 6011 MKII), and Marsh-McBirney® electromagnetic current meters fixed to a frame lowered onto the seabed, they concluded that the inlet as a whole was ebb dominated, the dominant ebb current reaching 1.0 m/s (4 m above the bed) at a mean water depth of about 12 m. The equivalent sand roughness of the bed (kt) varied from 0.08 m at the inner end to 0.34 m at the outer end of the survey line and, assuming a logarithmic velocity profile, the dominant friction velocities varied from 0.05 m/s to 0.07 m/s over the same reach. *Bartholdy et al.* [2002] defined the dominant velocity as the flow velocity above and below which half of the

sediment transport (using the total load formula of *Engelund and Hansen* [1972]) was achieved. The calculation of the dominant flow conditions was based on 6 weeks of continuously measured tidal currents at a fixed position in the inlet.

The downstream dimensional evolution of the large dunes is rather complex, switching from initial growth to progressive decline, followed by renewed growth in length but continued decline in height. This latter degradational phase begins at the centre of the survey reach and continues seaward until the large forms disappear completely. At the same time, the outer channel section becomes dominated by medium-sized simple dunes which grow in size with decreasing grain size. Both dune types are found to be in equilibrium with the dominant ebb flow, being solely controlled by the change in grain size along the study reach [*Bartholdy et al.*, 2002]. Since the simple dunes are more than one order of magnitude smaller in height than the flow depth, they are regarded as being "free" in the sense that they are not restricted by the flow depth. The equations shown in Fig. 6.2A and B link (sieve) grain size expressed in phi-units to dune height (H) and length (L) measured in meters [*Bartholdy et al.*, 2002]. The equations are empirically derived power regressions linking H and L to group mean values of grain size calculated at 1/8-phi intervals. The surveys during which the data were collected were carried out at low water with water temperatures averaging around 10^{o}C (8^{o}C +/-5^{o}C):

$$H = 0.17Md^{1.68} \quad (R^2 = 0.92) \tag{6.1}$$

$$L = 7.90Md^{0.68} \quad (R^2 = 0.83) \tag{6.2}$$

Dune heights (H) and lengths (L) are measured in meters and the median grain sizes (Md) are expressed in dimensionless phi-units [-$\log_{10}$(grain-size in mm)/$\log_{10}$(2 mm)]. Consequently the empirical constants have the dimension "meter".

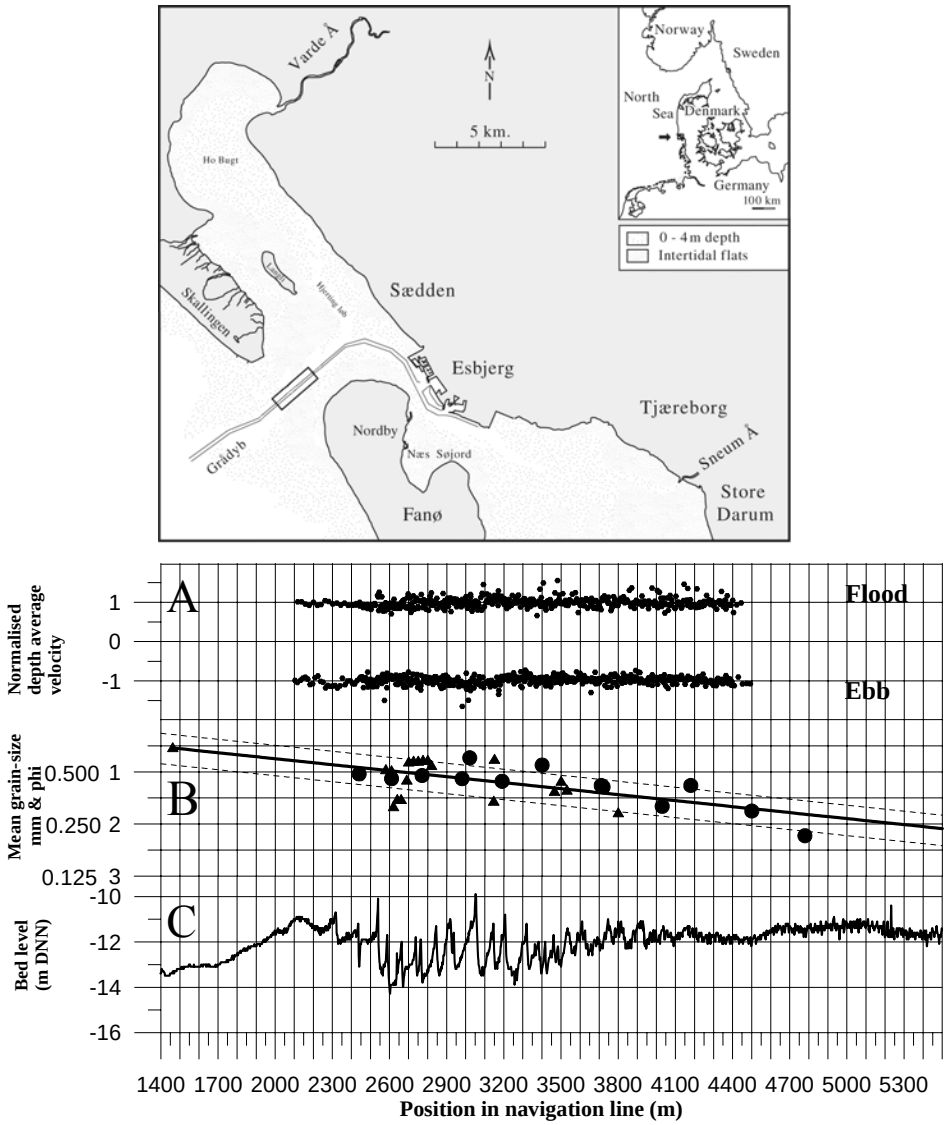

Fig. 6.1 Above: Location map of the investigated part of the Gråddyb tidal inlet. Beneath: A) Instantaneous normalised depth-averaged velocity along the centre line of the inlet. The data represents 5 ebb and 4 flood situations recorded by means of ADCP-equipment near peak flow conditions. Each velocity is normalised against the section mean velocity of the single data set. B) Mean grain size of bed samples along the study reach. Triangles correspond to samples collected in 1992, circles to samples from 1999. The full line represents the linear regression of mean grain size versus length in the navigation line, while the stippled lines indicate +/- one standard error of the estimate (equal to +/-0.292 phi). C) Topography along the study reach recorded on 19 May 1999. The ebb direction is from left to right. Modified after Bartholdy et al. [2002).

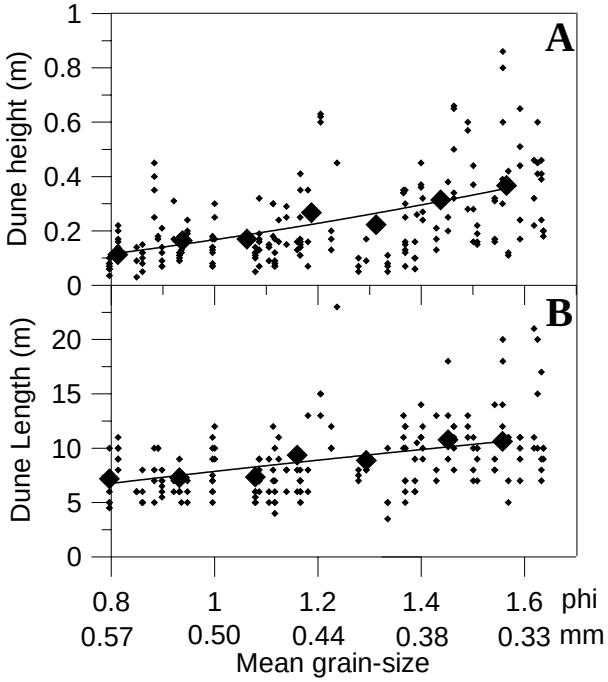

Fig. 6.2 A) Dune height and B) dune length of the simple dunes in the Grådyb inlet (low water situations in the spring seasons of 1991-1994) as a function of mean grain size. The mean grain size is calculated on the basis of the position along the survey line and the relation shown in Fig. 6.1. Only bedforms from the upper (¼) part of the large compound bedforms are included. The large symbols indicate the group mean values calculated at 1/8-phi intervals. Modified from Bartholdy et al. [2002].

6.3 Results

6.3.1 Dimensions of simple free dunes vs. grain size and flow strength

As bedform dimensions relate to transport conditions in general, a direct comparison based on grain size alone would be misleading in cases where flow conditions change. In order to compensate for this, the grain sizes in Equations (6.1) and (6.2) were used to calculate the form-corrected Shields parameter ($\theta' = uf'^2 / [(s\text{-}1)\ g\ d_{50}]$), based on the dominant friction velocity, where uf is the friction velocity, (s-1) the dimensionless submerged density of quarts, g the acceleration due to gravity, and d_{50} the median grain size (m). The Shields parameter expresses the dimensionless bed shear stress and represents the ratio between shear and gravity forces. The superscript (') indicates that the shear stress and the Shields parameter have been corrected for form drag (see below). By means of these equations it is possible to establish a local relationship between grain size (d_{50}) and the equivalent sand roughness of the bed (kt), following the model suggested by *van Rijn* [1982

and 1993], in which (in a slightly modified version) skin and form roughness are combined, and which add up to:

$$kt = 2.5d_{50} + 1.1H\left[1 - \exp\left(-25\,H/L\right)\right] \tag{6.3}$$

Originally, *van Rijn* suggested ks = $3 \cdot d_{90}$ for the skin roughness. Other results [see, e.g. *Yalin*, 1992] suggest that ks ≈ $2d_{50}$, which is in accordance with the *Engelund* and *Hansen* [1972] approach (ks = 2.5 d_{50}) used in Equation (6.3). *van Rijn* also suggested that the constant of 1.1 should be reduced to 0.77 when, under field conditions in rivers, the lee sides of the dunes did not reach the angle of repose [*Oginк*, 1988] (cited in *van Rijn* [1982]). In our experience, most simple dunes in the marine environment develop angles of repose, and there is thus no need to reduce the constant in Equation (6.3). Although the large to very large dunes (on the stoss-side of which the simple dunes occur) will also contribute to the hydraulic roughness, their effect is considered to be relatively small. *van Rijn* [1993] does not distinguish between bedform types in exactly the same manner as is done in the present paper. Thus, if – according to *van Rijn* - the largest bed features are sand waves with a low hydraulic roughness, then the hydraulic roughness values calculated for the superimposed dunes alone are absolutely realistic. If, on the other hand, the large bedforms are considered to be dunes and the smaller ones ripples, which according to *van Rijn* [1993] would be the other alternative, then the calculated hydraulic roughness values become unrealistically high, reaching values close to or over 1 m. Based on these considerations, L and H measures of the simple superimposed dunes (Equations (6.1) and (6.2)) have been used to produce a local Grådyb version of Equation (6.3):

$$\begin{aligned} kt &= 2.5d_{50} + 0.187Md^{1.68}\left[1 - \exp\left(-25 \cdot 0.17 \cdot Md^{1.68}/7.90 \cdot Md^{0.68}\right)\right] \\ &= 2.5d_{50} + 0.187Md^{1.68}\left[1 - \exp\left(-0.538Md\right)\right] \end{aligned} \tag{6.3'}$$

It is important to note here that, although d_{50} and Md represent the same parameter, they each have a different notation. Here d_{50} is expressed in meters and Md in dimensionless phi-units. Because of the empirical origin of the equation, both types of grain size notations have to be present. The empirical constant, -0.538, is dimensions less and the other, 0.187, has the dimension "meter". All grain-sizes used in these calculations were determined from the regression line shown in Fig. 6.1. Based on Equation (6.3'), the hydraulic roughness varies from 0.08 m in the inner part to 0.34 m in the outer part of the study reach.

In the following procedure, the dimensionless bed shear stress, θ (the Shields parameter),

$$\theta = \tau_0 / \left[(\rho_s - \rho) g d_{50} \right] = uf^2 / \left[(s-1) g d_{50} \right] \quad (6.4)$$

is transformed into the form-corrected Shields parameter, θ', which considers skin friction only. This was done in order to base the newly derived relationships on the single overriding dynamic factor, namely the dimensionless bed shear stress due to skin friction. The transformation was carried out by means of the method used by e.g. *Engelund and Hansen* [1972] and *Fredsøe and Daigaard* [1992],

$$\theta' = uf'^2 / \left[(s-1) g d_{50} \right] = 0.06 + 0.4\theta^2 \quad (6.5)$$

where τ_o is the bed shear stress (N/m^2), uf is the friction velocity (m/s), uf' is the form-corrected friction velocity (m/s), ρ_s is the density of quartz, ρ is the density of water (kg/m^3), (s-1) is the dimensionless submerged density of quartz (1.65), g is the acceleration due to gravity (9.82 m/s^2), and d_{50} is the mean grain size (m). Formula 6 was originally suggested by *Engelund* [1966] who derived it from similarity principles and calibrated the equation on the basis of the experimental work by *Guy et al.* [1966]. As θ' depends on θ alone, the following relations – if desired – can easily be recalculated to achieve dependence on θ instead of θ'. The form correction is derived from the currently used method originally suggested by *Einstein* [1950] and later modified as explained in *Engelund and Hansen* [1972]. The bed shear stress is split up into two components: τ' and τ'', the former being the effective shear stress, the latter that part of the total bed shear stress which is lost due to form drag on the bedforms.

The value of uf is found by means of the logarithmic velocity distribution [e.g. *Yalin*, 1977]:

$$uf = U_4 / \left[8.5 + 2.5 \ln (4/kt) \right] \quad (6.6)$$

where U_4 is the velocity 4 m above the bed (1.0 m s^{-1}) as defined earlier, and kt is found from Equation (6.3').

The resulting relationship between average dune heights and lengths and the form-corrected Shields parameter is illustrated in Fig. 6.3. A best fit relationship using polynomial relations between θ' and H and L resulted in Equations (6.7) and (6.8), both having an R^2 >0.99. A second-order equation was chosen for the bedform height as this is expected to decrease after reaching a maximum value when approaching the plane-bed phase of the upper flow regime at high values of θ'. A third-order equation was chosen for the bedform length

which is expected to continue to grow towards the upper-stage plane bed as suggested by *Fredsøe* [1982] and also implied by the trends in Fig. 6.4 (to follow).

$$H = -1.52\theta'^2 + 1.72\theta' \tag{6.7}$$

$$L = 100.30\theta'^3 - 116.89\theta'^2 + 50.60\theta' + 3.58 \tag{6.8}$$

H and L are measured in meters. As θ' is dimensions less all empirical constants in Equations (6.7) and (6.8) also have the dimension "meter". The advantage of using θ' as the independent variable is that this parameter is directly related to sediment transport [e.g. *Engelund and Hansen*, 1972, *Engelund and Fredsøe*, 1976, *Fredsøe and Daigaard*, 1992] which makes it the most obvious parameter to relate to bedform development. As the *Engelund and Hansen* [1972] method implies a direct relationship between θ and θ', H and L in Equations (6.7) and (6.8) can equally well be expressed as functions of θ:

$$H = -0.24\theta^4 + 0.61\theta^2 + 0.10 \tag{6.7'}$$

$$L = 6.42\theta^6 - 15.81\theta^4 + 15.06\theta^2 + 6.22 \tag{6.8'}$$

Again, all empirical constants have the dimension "meter".

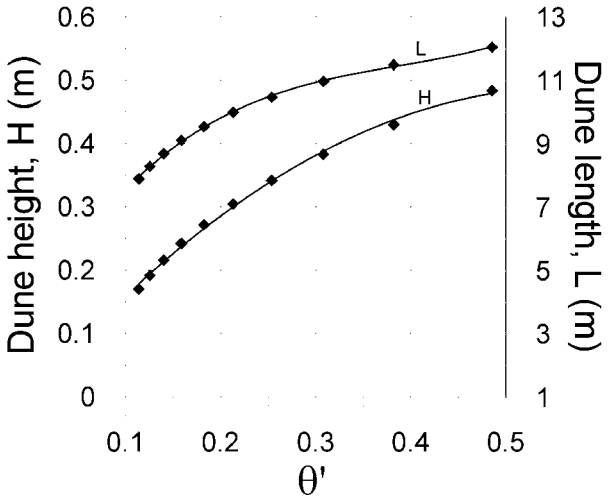

Fig. 6.3 Dune height (H) and length (L) of simple depth-independent dunes as a function of the form-corrected Shields parameter.

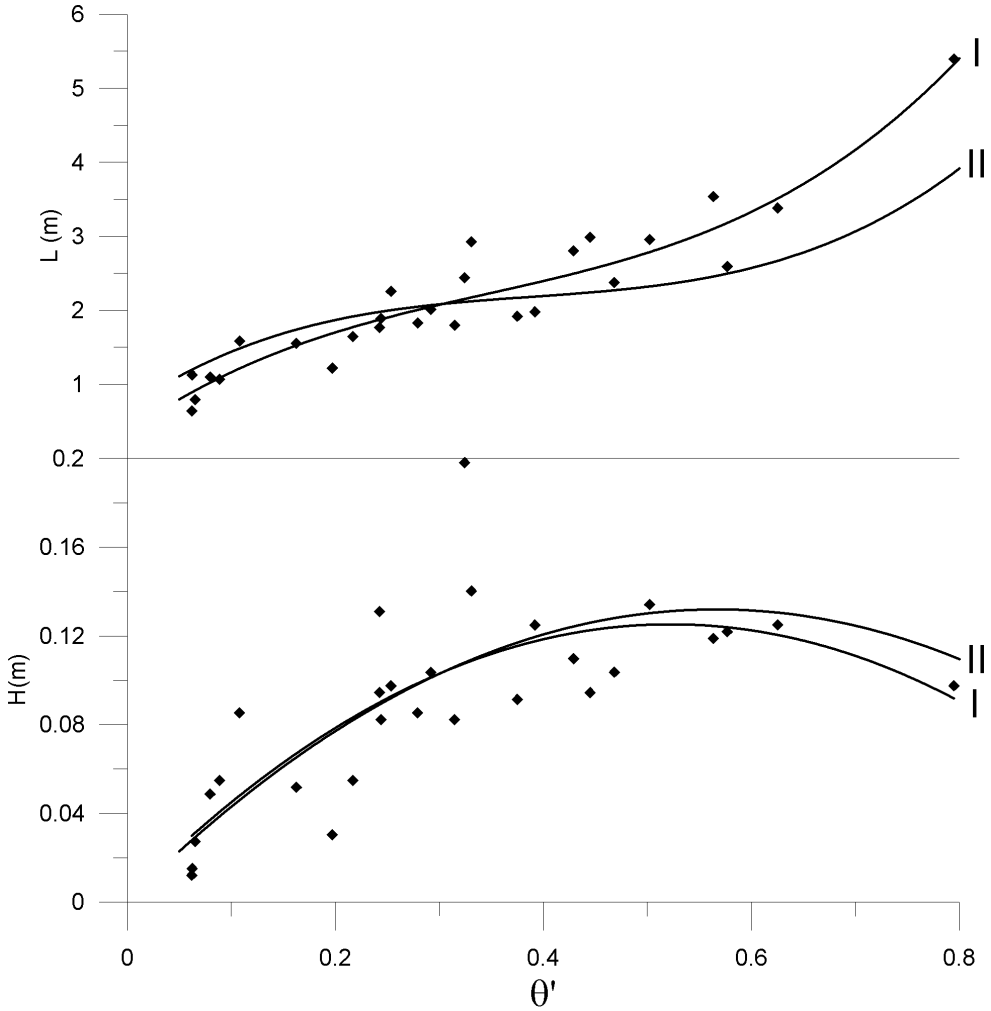

Fig. 6.4 Dune height (H) and length (L) as a function of the form-corrected Shields' parameter (θ') for all "8-foot flume" data in Guy et al. [1966] with water depth >0.28 m and dunes present on the bed. The average water depth is 0.31 m (+/- 1 standard deviation of 0.02 m). The lines labeled I are the polynomial regression lines based on the data set: $L = 18.75\ \theta'^3 - 19.50\ \theta'^2 + 9.92\ \theta' + 0.35$; $R^2 = 0.90$; $H = 0.45\ \theta'^2 - 0.47\ \theta'$; $R^2 = 0.60$. The lines labeled II are the regression lines from the Gådyb inlet (Equations (6.7) and (6.8)), multiplied by a factor: α_L and α_H, giving the smallest error compared to the flume data (these factors are found by means of a maximum likelihood procedure). α_L and α_H were found as 0.19 and 0.27 respectively.

6.3.2 Dune dimensions

For almost a century following the pioneering work of *Gilbert* [1914], studies of bedform development and sediment transport have primarily been carried out using flumes. The foremost reason for this was that the required precision of data on flow conditions, form shape and form migration could only be achieved under controlled laboratory conditions. However, the technological advances of the last two decades have now reached a point where field

studies also produce sufficiently precise data, especially after the development of integrated survey systems in which differential GPS positioning, acoustic Doppler current profiling and multi-beam echo sounding are combined [e.g. *Erntsen et al.*, 2004]. Most of our fundamental knowledge, however, is still based on flume studies. Of these, the work published by *Guy et al.* [1966] is in a class of its own. This outstanding detailed data report has functioned as the state of the art on which almost all models dealing with bedform development and sediment transport have been calibrated ever since it was published. When, as in the present paper, it is attempted to relate natural bedform conditions to plausible flow conditions at full scale, it is therefore only natural to test the derived relationships against the flume results. To keep the comparison as realistic as possible, only those data of *Guy et al.* [1966] have been considered which were least constrained by the laboratory conditions. Thus, only the data of the widest flume, namely the "8-foot flume" (2.4 m wide) with the largest water depth (>0.28 m) and with reported dunes on the bed, were used. A minimum water depth of 0.28 m was selected as a trade-off between a sufficiently large number of data sets and as great a water depth as possible. The average water depth in this case is 0.31 m (with a standard deviation of 0.02 m), the grain-size in this data set ranges from 0.19 mm to 1.00 mm, and θ' varies from 0.06 to 0.8 ($0.07 < \theta < 0.14$).

As flume data sets are depth limited, a comparison between free bedform dimensions and the flume bedforms is expected to reveal scale differences, even when only the largest water depths are used. This is indeed the case (Fig. 6.4). However, when the bedform lengths and heights have been adjusted (using a maximum likelihood procedure by means of a Fortran program which tests all possible reductions and chooses the one with the smallest cumulative error), the similarities are striking. A reduction of the dune heights to 27 % of that prescribed by Equation (6.7) produces a distribution which is practically identical to that obtained by a regression analysis of the flume data itself. Likewise, although with a somewhat greater variance, the dune lengths are found to be close to those of a direct regression analysis of the flume data, when the length prescribed by Equation (6.8) is reduced to 19 % of the prescribed lengths. The relationship thus produced has the same shape as the flume-regressions. The reason for using the second- and third-order regression equations for the flume data relationships between θ' and H and L, respectively, follows the arguments used for the generation of Equations (6.7) and (6.8) (see above). The peak value of $H = f(\theta')$ and the inflection points of $L = f(\theta')$ can be found by differentiation. It reveals that the largest bedform height is associated with $\theta' = 0.5$ to 0.6 ($\theta = 1.1$) for both equations, and that the

inflection point where L starts to increase again with increasing shear stress is associated with $\theta' = 0.4$ ($\theta = 0.9$) for both equations. Besides confirming a strong connection between the two relationships, it also implies that bedform development during accelerating flow reaches a general turning point when the form-corrected dimensionless shear stress reaches values close to 0.5 (θ close to 1.0). This is well above the criterion for suspension suggested by *van Rijn* [1993], but probably coincides with the condition where a naturally graded sediment becomes fully suspended. For the coarser part of the sand fraction, θ-values around 1 represent the suspension criterion suggested by *Bagnold* [1966]. It is conceivable that bedforms continue to grow until the coarsest part of the transported material goes into suspension, and that the bedform crests begins to erode when the flow strength increases further. The close correspondence between the field and the flume results is regarded as an indication for the validity of the equations, and suggests that scale differences for dunes range from about 70 % for H and 80 % for L in water depths of 0.3 m compared to free stream conditions.

To the best of our knowledge, only two earlier studies have linked bedform height to flow strength and grain size while acknowledging the fact that bedforms decrease in height when a certain flow strength is exceeded [*Fredsøe*, 1982; *van Rijn*, 1982]. *Fredsøe* [1982] based his method on theoretical considerations relating to the bedload formula of *Meyer-Peter and Müller* [1948]. In his approach, all suspended bed material is removed from bedform migration by means of the *Engelund and Fredsøe* [1976] sediment transport model. *van Rijn* [1982], on the other hand, used a purely empirical approach. He concluded that dune dimensions depend on grain size, water depth and a transport stage parameter, $T= (uf'^2 - uf_c^2)/uf_c^2$, in which (by means of his method) uf' and uf_c are the form-corrected friction velocity and critical friction velocity, respectively. He formulated an equation for which, when compared with flume and field data, "the best agreement was obtained" (*van Rijn* [1984b, p. 1738], also referring to *Report S 487-III* from Delft Hydraulic Laboratory). Both approaches determine the dune height in relation to flow depth, and are therefore restricted to depth-dependent dunes. The dune length is regarded by *van Rijn* [1984b] to be equal to 7.3 times the water depth, whereas *Fredsøe* [1982] suggested a method which accepts observed variations [e.g. those reported by *Fredsøe*, 1975; *Raudkivi*, 1976; *Yalin*, 1977; *Yalin and Karahan*, 1978] of increasing dune steepness with increasing bed shear stress for small bed shear stresses, and decreasing steepness with increasing shear stress for high shear stresses. *Fredsøe* explains the latter with increasing suspension transport, with references to *Kennedy* [1963] and *Engelund and Fredsøe* [1974].

In Fig. 6.5, the two approaches by *Fredsøe* [1982] and *van Rijn* [1984b] are compared with those shown in Fig. 6.4 (II) using the flume data mentioned above. Clearly, neither of the two approaches is able to reproduce the observed variation in bedform height and length, the regression lines being more or less horizontal. The mean errors of the reduced Equations (6.7) and (6.8), calculated as the relation between the summed errors and the summed heights and lengths, respectively, are 22% and 19%, whereas the corresponding percentages using the *Fredsøe* [1982]/*van Rijn* [1984b] methods are 62%/35% and 50% / 34%, respectively. It could be argued that, as the reduction of Equations (6.7) and (6.8) is made on the basis of the data set in question, the comparison is not fair. None of the two other approaches, however, can be changed in the same manner to correlate better than shown in Fig. 6.5. This is because their best fit lines are close to horizontal. Both predict the right order of magnitude for relatively small dune heights but substantially underestimate the larger ones. Using the two approaches on the data set from Grådyb, produces quite a different picture. In this case the measured heights change from 0.17 m to 0.49 m over the study reach, which is also predicted by Equation (6.7), whereas they produce a change from 2.4 m / 1.1 m and 0.84 m / 1.0 m in the case of *Fredsøe* / *van Rijn*, respectively. Thus, the predictions of the latter approaches produce much too large bedform heights and a decrease in bedform height over the study reach, which is incompatible with the observations and also contrary to the increase in height predicted by Equation (6.7). The reason for this, most likely, is that in this environment the two other approaches aim at the large-scale compound bedforms which decrease in height from about 3 m to about 1 m over the study reach. This is matched relatively well by the *Fredsøe* approach, whereas the *van Rijn* approach only predicts the right order of magnitude but misses the relatively rapid height decrease of the compound dunes.

At this stage, it is not clear what is happening in the transition zone from simple dunes (with heights on the order of 10 cm) to meter high compound dunes with superimposed simple dunes. Nevertheless, Equation (6.7) provides a realistic prediction of simple superimposed dune heights, and, if a proper way of determining a depth-dependent reduction for smaller water depths could be developed, it would also seem capable of predicting flow-strength associated changes under depth-restrained conditions. In accordance with the solution of *Fredsøe* [1982], also discussed in *Fredsøe and Daigaard* [1992], the reduction in dune height under dimensionless shear stresses higher than $\theta' = 0.5\text{-}0.6$ ($\theta = 1.1$) is interpreted here as the influence of increasing suspension transport. In *Fredsøe* [1982], the peak in dune height appears as early as $\theta' = 0.2$, which is probably a result of his interpretation of suspension as a

transport mode which is totally separated from bedform migration. As discussed in *Bartholdy et al.* [2002], increasing suspension transport is in fact regarded as the primary reason for the combined bedform change (simple and compound) in the outer part of the study reach in the Grådyb inlet.

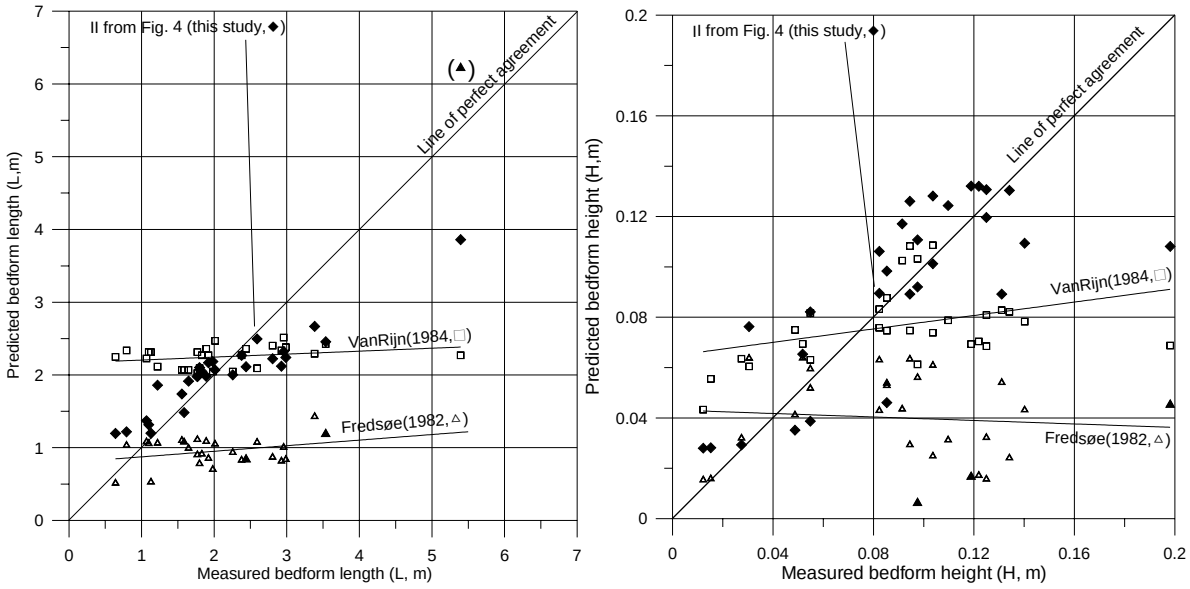

Fig. 6.5 Measured and predicted dune heights (H, left) and lengths (L, right) based on the data and relations shown in Fig. 6.4 (II, diamonds). Similar results based on the method proposed by Fredsøe [1982, p. 941, Fig. 6 and 8] (triangles) and van Rijn [1984b] (squares) are shown with their linear regression lines for comparison. The three filled triangles are extrapolated and the one in brackets were excluded from the regression.

The physical interpretation of the change in dune length is highly problematical. In the case of the Grådyb inlet, the approach suggested by *Fredsøe* [1982] predicts dune lengths in the range 46-35 m, whereas the observed range is 8-12 m. The suggestion by *van Rijn* [1982] of dune length being about 7.3 times the water depth (in accordance with *Yalin* [1977]) also produces much too large bedform lengths (about 88 m) in Grådyb. Again, the two approaches appear more appropriate for the prediction of the large compound features, although with the restriction of being unable to reproduce the length reduction from about 200 m to about 50 m observed along the study reach. Thus, both of these approaches fail to correctly predict the length of the simple depth-independent dunes, while also failing to predict the increase in length with decreasing height for θ' values over about 0.5. We are not aware of any theory which can explain the empirically based variations described by Equations (6.7) and (6.8).

6.3.3 Dune migration rate

An evaluation of the reported sediment transport values based on the 28 flume data sets mentioned earlier reveals a relatively close relationship (Fig. 6.6) between the sediment transport derived from bedform migration and that calculated by a slightly adjusted version of the bedload formula of *Meyer-Peter and Müller* [1948],

$$q_{stv} = 39.87\left[\left(\theta' - 0.047\right) d_{50}\right]^{3/2} \tag{6.9}$$

where q_{stv} ($m^3s^{-1}m^{-1}$) = ½ H Ub, is here defined as the volume of loosely packed sand transported per unit time and width, and calculated as the migration of triangular-shaped dunes where H is dune height and Ub is the dune migration rate. The empirical constant, 39.87, has the dimension, $m^{4/3}s^{-1}$. As evident from Fig. 6.6, the basic term of the *Meyer-Peter* and *Müller* formula, $((\theta'-0.047)d_{50})^{3/2}$ correlates relatively well with q_{stv} ($R^2 = 0.71$, $P<0.01$), and a regression forced through the origin produces a calibration constant of 39.87. This corresponds to a 20 % reduction of the calibration constant in the original work of *Meyer-Peter* and *Müller* if it is assumed that the bulk dry density of newly transported sand is roughly 1700 kg m^{-3} [e.g. *Bartholdy et al.*, 1991]. The calibration result can be regarded as being satisfactory when compared with results of other studies [e.g. *Yalin*, 1977]. It is generally accepted that when sediment transport takes place as bedload alone, the formula of *Meyer-Peter and Müller* [1948] is well suited to describe the sediment flux. Arriving from a different and much more sophisticated theoretical analysis, *Engelund and Fredsøe* [1976] developed an expression for bedload transport which, as later confirmed by e.g. *Fredsøe and Daigaard* [1992, p. 214], "becomes close to the widely used semi-empirical formula of *Meyer-Peter and Müller* [1948]". This formula was also the choice of *McLean et al.* [1994 and 1996] when they tried to relate the local boundary shear stress to local sediment flux on a bedform, and recently of *Colombini* [2004] when reanalyzing the instability mechanisms [*Kennedy*, 1963 and 1969] leading to the formation of bedforms.

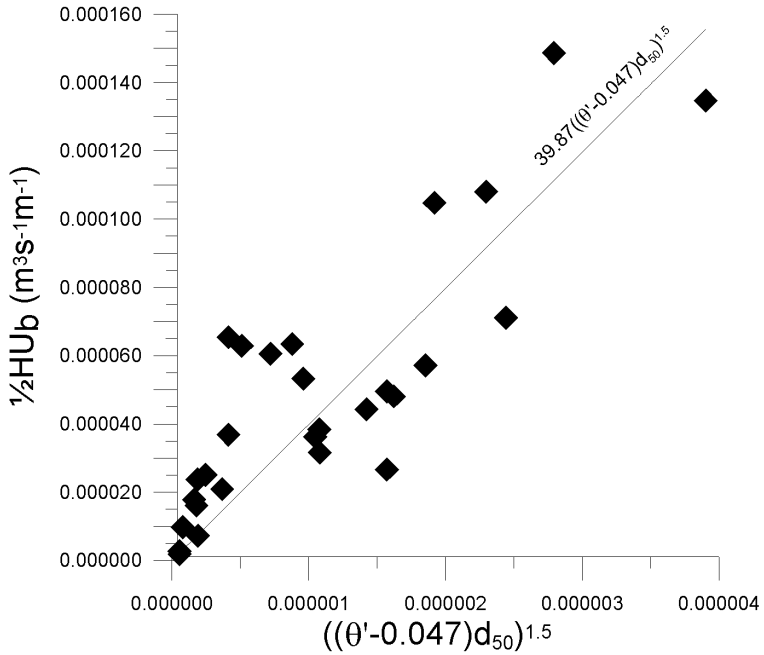

Fig. 6.6 Relation between the variable in the Meyer-Peter and Müller bedload equation and bedload data from the "8-foot flume" of Guy et al. [1966] with water depth >0.28 m and dunes present at the bed. The linear regression is forced through origin (R^2=0.87; P<0.01).

There is no exact borderline between bedload and suspended load when both transport modes are present. Describing a succession of grain jumps in terms of their trajectories, *Yalin* [1977, p 17] writes: "Indeed, there is no natural indicator to point out which among the transitional paths … should be the *border line* between the paths of the bedload and suspended load particles". Dealing with bedform behavior, the advantage of using a sediment transport formula based on bedform migration alone, is obvious. As the data sets plotted in Fig. 6.6 are associated with θ-values ranging from under 0.1 to over 1, the data series crosses the border between predominantly bedload and what must be regarded as fully developed suspended load [e.g. *Bagnold*, 1966, *van Rijn*, 1993]. Thus, the relatively successful calibration of Equation (6.9) suggests that bedform migration represents a continuum describing increasing bedform-related sediment transport as the shear stress increases even after the border line between predominantly "true" bedload and predominantly suspended load is exceeded.

Calibrating a model on the basis of laboratory results is of course not satisfactory when the aim is to evaluate depth-independent bedforms. For the moment, however, this employment of an existing model is the only possible way of interpreting our results, and

Equation (6.9) is believed to be the least feeble of available models which are able to describe bedform migration as a function of bed shear stress and grain-size.

6.3.4 Flow and transport parameters as a function of dune length

Equations (6.3), (6.4), (6.5), (6.7), (6.8) and (6.9) permit the formulation of direct relationships between dune dimensions and parameters describing flow strength and grain size. The easiest bedform parameter to obtain is the bedform length, L, (even from echo sounder profiles at large depths where the estimation of bedform heights may be problematical). Since Equation (6.8) relates L to θ' through a third-order polynomial equation, a solution with L as the entrance parameter requires an indirect iterative solution. In order to implement a more direct and less laborious procedure, regressions have been calculated between paired results of L and θ' (Equations (6.10a)-(6.10c)) as shown in Fig. 6.7. In order to obtain an adequate accuracy, it was necessary to split up the data set into different size classes,

4 m < L < 10 m: $$\theta' = 0.0044L^2 - 0.033L + 0.09 \quad (6.10a)$$

10 m < L < 12 m: $$\theta' = 0.0390L^2 - 0.719L + 3.50 \quad (6.10b)$$

12 m < L < 20 m: $$\theta' = 0.00074L^3 - 0.0389L^2 + 0.707L - 3.67 \quad (6.10c)$$

The empirical constants have the dimension m^x, where x is the reciprocal of the single power of L. Note that the experimentally obtained results from the Grådyb inlet are limited to 7 m < L <12 m. Equation (6.10c) has been included because the results presented in Fig. 6.4 imply a somewhat wider range of applicability because for dune lengths up to about 5 m, the depth-limited flume results correspond to depth-independent bedform lengths of about 25 m (compare Equation (6.8)). It must be stressed, however, that the results are currently still restricted to the range 7 m < L <12 m for which measurements in nature are available.

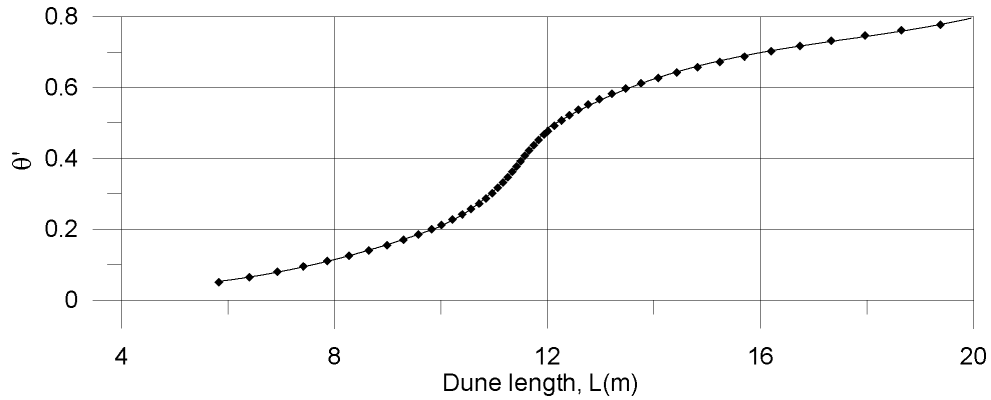

Fig. 6.7 Polynomial regressions (Equations (6.10a)-(6.10c)) between θ' and the simple depth-independent dune length, L, with L as the independent parameter.

The above relationships between the lengths of simple depth-independent dunes and the form-corrected Shields parameter enables the construction of additional relationships between dune length and grain size, and a large number of other relevant flow and transport parameters. Four examples are given in Fig. 6.8. Friction velocity can be calculated from dune length and grain size using Equations (6.10), (6.5) and (6.4). As clearly evident from Fig. 6.8A, a constant grain size and an increasing dune length indicates an increasing friction velocity. Furthermore, with a fixed dune length the friction velocity increases with grain size.

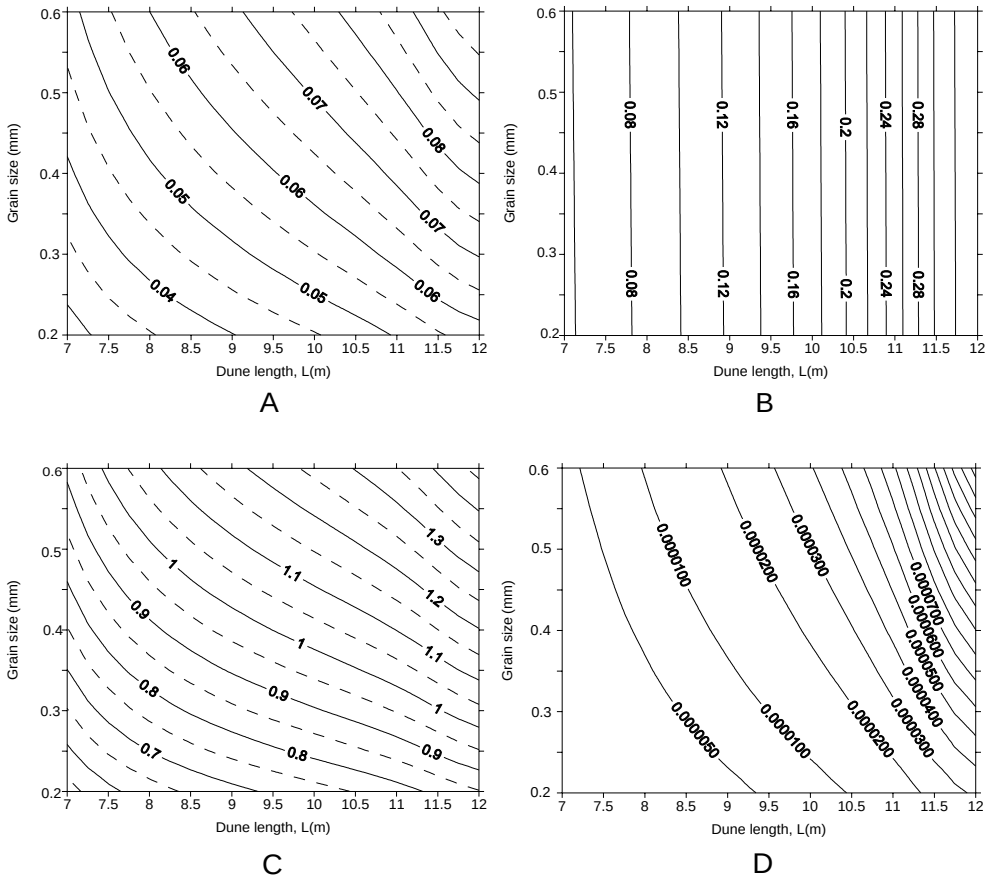

Fig. 6.8 Flow and transport parameters as a function of simple depth-independent dune length and grain size. A: Friction velocity (m s^{-1}); B: Total hydraulic roughness (m); C: Velocity 4 m above the bed (m s^{-1}); D: Bedload transport based on bedform migration (m^3 s^{-1} m^{-1}).

The same patterns emerge for the current velocity (U_{4m}, Fig. 6.8C) which can be found from dune length and grain size by using Equations (6.10), (6.7) and (6.3) to calculate kt, and Equations (6.5) and (6.4) to calculate uf. With these relationships at hand, the velocity at any height above the bed in the logarithmic layer can be calculated using Equation (6.6). In many deeper water situations the free stream velocity, which would be located well above the bed features, may be the only available indicator of flow conditions. Following the above arguments, dunes in deep flows having the same grain-size should adjust solely to the free stream velocity. It should thus be possible to predict the magnitude of free stream velocities from bedform dimensions and associated grain-sizes. According to the procedure suggested by *Soulsby* [1990], a reduction of the free stream velocity by 10% will transform it into the corresponding velocity at 4 m above the bed within an error of +/- 7 % for water depths greater than 10 m. Thus

$$U_{free} \approx U_{4m} / 0.9 \qquad (6.11)$$

The variations in the equivalent sand roughness of the bed associated with dune length are due to the fact that the hydraulic roughness changes only little with grain size, which gives almost parallel horizontal lines for the kt isolines in Fig. 6.8B. Grain size is of course part of kt (Equation (6.3)) but its influence is small compared to the hydraulic resistance of the bedforms. With increasing dune length, the kt-values grow fast (decreasing distance between the isolines) as long as the dune height grows more rapidly than the dune length. At dune lengths greater than about 12 m (on the border and outside the range of $\theta' < 0.5$ covered by Fig. 6.8C), dune heights – and therefore also kt – level out and decline with increasing flow strength. This is the prediction of Equation (6.7). However, since it lies outside the experimentally observed range, only the striking resemblance with the larger range flume data (Fig. 6.4) supports this trend. Unfortunately, few researchers have reported on the dimensions of superimposed bedforms, and often clear statements about whether a particular bedform is simple or compound are lacking. This makes it difficult to compare the present findings with other published data. Results published by *Harbor* [1998] from the Mississippi River and *Kostaschuk and Ilersich* [1995] from the Fraser River suggests that, under increasing flow strength, simple bedforms can grow higher than predicted by Equation (6.7).

The bedload transport can be obtained from dune length and grain size by calculating θ' from Equation (6.8), whereas the transport associated with bedform migration can be calculated from Equation (6.9), with θ' and grain size as the independent parameters. For a fixed grain size, the bedload transport increases with dune length, as it does with grain size for a fixed dune length.

Obviously, a field-based calibration of Equation (6.9) would improve the credibility of this approach. However, until that is achieved, the results presented here are claimed to represent the best possible way of expressing bedform migration as a function of flow strength and grain size, and to relate bedform dimensions – in form of bedform length – to a plausible bedload transport rate related to bedform migration. The procedure described in this paper for the first time presents a relationship between bedform dimensions and bedload transport which is based on transparent arguments based on accepted theory and which are in agreement with field (and flume) data. It should be kept in mind, however, that the bedload transport modeling in this case relates to quasi-stationary (dominant flow) conditions only.

It should also be noted that the algorithms presented above are calibrated for water temperatures of about 10 ^{o}C and grain sizes in the range of 0.3 - 0.6 mm. Deviations from

these conditions may change the calibration constants if other scaling effects than those represented by θ‘ (or θ) influence the result.

As the primary reason for the observed variations is suggested to be the proportion of suspension in the total transport, it would seem logical that temperature can play a role as one of the parameters controlling the sediment fall velocity. Following from the *π-theorem* analysis of *Yalin* [1977], four dimensionless parameters are sufficient to describe what he called “the two-phase phenomenon” of the motion of fluid and bed material. Omitting the dimensionless depth (as we are dealing with depth-independent bedforms) and mass (since only quartz and water are considered), only the grain Reynolds number remains in addition to the Shields parameter. The influence of this dimensionless number is important if variations in water viscosity affect the results. This is not important when the water temperature remains almost constant, as in the present study, but large changes in kinematic viscosity associated with seasonally changing water temperatures will probably have an effect [cf. *Krögel and Flemming*, 1998]. In fact, observations made in the Grådyb tidal channel suggest a tendency towards larger bedform heights during the summer season. The influence of water temperature should be an important concern of future research, but lies beyond the scope of the present paper. Unfortunately, since most studies involving compound bedforms concentrate on the larger features, only little has been published on free simple (superimposed) dunes with corresponding information on grain size and dominant flow conditions. A considerable amount of such data is probably available in the form of unpublished background information from various field studies dealing with bedforms. We are ourselves currently collecting such data and hereby invite interested colleagues to participate in building up a data base on free subaqueous dunes in order to improve our knowledge about bedform generation and its relation to flow conditions and grain size. Of particular interest would be the improvement of Equations (6.7) and (6.8) based on a wider range of data, and an examination of the extend to which shallow water depth affects the dune dimensions until they become depth independent.

6.4 Summary and Conclusions

Results from the Grådyb tidal inlet in the Danish Wadden Sea showed that, under near-constant dominant flow conditions, superimposed simple depth-independent subaqueous dunes vary in size according to grain-size.

For temperature conditions close to 10 ^{o}C, these results have been recalculated into two equations showing dune length (L) and height (H) as a function of the form-corrected Shields parameter (θ'). These equations show that dune length and height increase up to θ'-values of about 0.5-0.6 (θ ≈ 1), representing the experimental limits of the study. A comparison with flume data (depth ≈ 0.30 m) showed that a reduction of H and L by 70 and 80 %, respectively, gave almost identical results. This supports the main conclusion that bedform dimensions are primarily controlled by the flow strength and grain size, and that water depth can act as an additional limiting factor to dune growth.

The *Meyer-Peter and Müller* [1948] equation has been recalibrated expressing bedload transport in terms of bedform migration. The recalibrated bedload equation and the relations between H, L, and θ' permit the formulation of direct relationships between simple depth-independent dune dimensions and parameters describing flow condition and grain size.

Four diagrams have been constructed which relate grain size and length of simple depth-independent dunes to friction velocity, hydraulic roughness, velocity 4 m above the bed, and bedload transport at water temperatures close to 10^{o}C . The diagrams are restricted to θ' values under 0.5 (θ < 1.05) which form the empirical limitations of the calibrated equations.

From the diagrams it is shown that, with a constant grain size, the friction velocity and the velocity 4 m above the bed increase with increasing dune length. Furthermore, for a fixed dune length the friction velocity and the velocity 4 m above the bed increase with grain size. The hydraulic roughness changes only little with grain size but increases with dune length. For a fixed grain size, the bedload transport increases with dune length, as it does with increasing grain size for a fixed dune length. In studies where limited data on flow conditions are available (e.g. in many oceanographic surveys) these diagrams can be helpful as a first approximation of flow strength and transport parameters, as long as the available data contains information on grain size and wave length of simple dunes.

Acknowledgement

The study was supported by the Danish Science Research Council Grant # 21-01-0513.

Chapter 7: Concluding remarks and perspectives

The horizontal and vertical precision of the applied MBES system under normal field survey conditions is ±12.8 cm and ±3.4 cm, respectively, at a 95% confidence level. During individual surveys the vertical precision can be as high as ±1.9 cm at a 95% confidence level. However, the achieved precision probably does not correspond to the full potential of the MBES system, because an increase in coverage density (soundings/m^2), which can be achieved by reducing the survey speed of the vessel, would almost certainly further improve the precision. The precision achieved in this study is higher than that reported from earlier offshore tests but, of course, still lower than that attained onshore (Paper I).

The bed of the Grådyb tidal inlet channel is covered with large to very large ebb-directed barchanoid-shaped compound dunes. The barchanoid-shaped morphology develops due to an increase in dune migration from the centre (12 m/y) towards the sides (30 m/y) of the channel. This results from a decrease in dune height from the centre (3.1 m) towards the sides (1.4 m) of the channel, as smaller volumes of sediment have to be moved at the sides per unit time for equal dune celerity. The decrease in dune height is ascribed to an equivalent decrease in grain size from the centre (0.63 mm) towards the sides (0.36 mm) of the channel, as water depth and flow velocity are practically uniform across the channel (Paper II).

Annual net ebb-directed volumetric bedload transport rates (6-17 m^3/m/year), calculated from dune dimensions and migration, are significantly over-predicted by classical and widely applied bedload transport formulae (74-162 m^3/m/year) (Paper II).

During a single semi-diurnal tidal cycle, bedload transport rates are higher on the crest (~0.6 m^3/m per half tidal cycle) than in the troughs (~0.2 m^3/m per half tidal cycle) of the large to very large compound dunes (Paper III). This is due to near-bed flow velocities being higher at the crest (1.0-1.2 m/s) than in the trough (0.6-0.7 m/s) (Paper IV). Despite the fact that annual migration is ebb-directed, ~9-39 m (Paper II), net migration during single tidal cycles may even be flood-directed, ~0.39 m (Paper III and IV), which means that extrapolation of short-term migration rates (single tidal cycle) to long-term migration rates (annual) is not possible (Paper IV). Furthermore, bedload transport rates during single tidal cycles determined by classical and widely applied bedload transport formulae also deviate significantly from bedload transport rates calculated from dune dimensions and migration (Paper III).

Analysing dune dynamics in detail along a large compound dune during the same tidal cycle shows that the net bed level is practically constant at successive high waters, but changes considerably during ebb and flood tide. During ebb tide bed material goes into suspension with accelerating flow and settles with decelerating flow, resulting in an average erosion and accretion of the bed of 6.5 cm. The erosion decreases from the crest (~0.25 m) towards the troughs (≤0.05 m) of the compound dunes, the near-bed flow velocities being higher at the crests (1.2 m/s) than in the troughs (0.4-0.7 m/s). During flood tide the bed is practically stable. This results in a potential net export of sediment from the tidal inlet channel to the ebb tidal delta during every semi-diurnal tidal cycle, in addition to the sediment exported as bedload transport by dune migration (Paper IV).

The crests of the compound dunes migrate ~3 m during a half tidal cycle in the direction of the flow, developing a flood cap during the flood tide. The crests of the superimposed dunes on the stoss side are displaced by 1-2 m during a half tidal cycle, reversing direction. The superimposed dunes on the lower lee side remain flood-directed during the tidal cycle due to low migration and even reverse migration as a result of reverse flow in the trough/lee-side region due to flow separation. The flow separation is initiated at an upper lee-side slope angle of ~16° (half the angle of repose) and near-bed flow velocities at the crest of ~1.2 m/s (Paper IV).

Both in the case of the compound dunes and the superimposed dunes, the heights change during the tidal cycle, whereas lengths remain relatively constant, because the amount of sediment, which has to be moved to change dune height, is much smaller than the amount needed to change dune length. The height of the compound dune follows water depth, whereas the height of the stoss side dunes follows flow velocity, i.e. the stoss side dunes are water depth-independent (Paper IV).

General statements relating dune dimensions directly to the form-corrected Shields parameter are established from the depth-independent superimposed dunes, showing that dune dimensions are primarily controlled by flow strength and grain size; and that water depth can act as an additional limiting factor to dune growth (Paper V), as is the case with the compound dunes (Paper IV). Empirically derived diagrams describing flow conditions and bedload transport rates as a function of grain size and dune length are presented. These can be used, e.g., to give a first approximation of flow conditions in studies where limited data on flow conditions are available, as is often the case in oceanographic surveys, as long as the available data contain information on grain size and dune length (Paper V).

The introduction of high-resolution, high-accuracy swath bathymetry has truly revolutionised the study of bedform dynamics. The spatial depiction and the possibility to precisely quantify dimensions and dynamics have turned field studies into quasi laboratory experiments. Although it is impossible to steer the controlling parameters (flow velocity and grain size) and limiting factors (water depth), as can be done in flume studies, it is possible to precisely measure flow velocity, grain size and water depth as well as the related bedform dynamics. However, the new opportunities also raise new questions concerning certain processes, which have thus far been unable to be resolved.

One such process concerns secondary flow patterns in tidal channels, which induce changes in sediment dynamics and transport paths oblique to the main current direction. Processes oblique to the main current are an order of magnitude lower, but may play a significant role over longer time scales. Tracer studies, over and above measuring grain size, flow velocity and bathymetry, would be a very useful approach to determine transport directions and migration rates; and based on transport distances, tracer studies could reveal the transport modes, i.e. distinguish between bedload and suspended load, of the different fractions of the bed material.

In addition, quantification of sediment budgets in the different morphological units, e.g. along shore, in tidal inlet channels and on tidal deltas, could resolve large-scale, long-term morphodynamics and sediment transport paths. In the case of the ebb tidal delta in the Grådyb tidal inlet an annual volume in the order of 1 million m^3 is being dredged in order to maintain an adequate navigation depth of 10.3 m MLWS through the ebb tidal delta. Quantifying the sediment volumes transported from the different morphological units could form the basis for the consideration of alternative measures of dredging or changes in dredging/dumping strategy in order to reduce the very substantial maintenance costs. Finally, pre- and post-storm surveys in these morphological units could lead to a better understanding of the effects of extreme events and the influence of waves.

However, considerable limitations are still present in studies of bedform dynamics, e.g. the absolute quantification of suspended sediment in the water column as well as the determination of near-bed flow velocities without disturbing either the flow or the bed. Hopefully the hurdles can be surmounted in the near future.

References

Aagaard, T. (2002): Beach morphodynamics: two Danish case-studies. Meddelelser fra Skalling-Laboratoriet, XXXVII, 160 pp.

Aagaard, T., N. Nielsen, and J. Nielsen (1995): Skallingen – origin and evolution of a barrier spit. Meddelelser fra Skalling-Laboratoriet, XXXV, 85 pp.

Aagaard, T., J. Nielsen, R.G.D. Davidson-Arnott, B. Greenwood and N. Nielsen (1998): Coastal morphodynamics at Skallingen, SW Denmark: High energy conditions. Danish Journal of Geography, 98: 20-30.

Aagaard, T., K.P. Black and B. Greenwood (2002): Cross-shore suspended sediment transport in the surf zone: a field-based parameterization. Marine Geology, 185: 283-302.

Aagaard, T., R.G.D. Davidson-Arnott, B. Greenwood and J. Nielsen (2004a): Sediment supply from shoreface to dunes: linking sediment transport measurements and long term morphological evolution. Geomorphology, 60: 205-224.

Aagaard, T., J. Nielsen, S.G. Jensen and J. Friderichsen (2004b): Longshore sediment transport and coastal erosion at Skallingen, Denmark. Danish Journal of Geography, 104: 5-14.

Allen, J.R.L. (1968): Current Ripples. North Holland, Amsterdam, The Netherlands, 433 pp.

Allen, J.R.L. (1976): Conceptual models of dune time-lag: general ideas, difficulties and early results. Sedimentary Geology, 15: 1-53.

Allen J.R.L. (1980): Sand waves: A model of origin and internal structure. Sedimentary Geology, 26: 281-328.

Allen, J.R.L. (1982): Sedimentary structures: their character and physical basis, 1. Developments in Sedimentology, 30A, Elsevier, Amsterdam, The Netherlands, 593 pp.

Abraham, D. D. and T. Pratt (2002): Quantification of bed-load transport on the Upper Mississippi River using multibeam survey data and traditional methods. US Army Engineer Research and Development Center (ERDC)/Coastal and Hydraulics Laboratory (CHL), Coastal and Hydraulics Engineering Technical Note (CHETN): 9 pp.

Ardhuin, F., T.G. Drake and T.H.C. Herbers (2002): Observations of wave-generated vortex ripples on the North Carolina continental shelf. Journal of Geophysical Research, 107(C10): 14 pp.

Artilheiro, F.F. and F.M. Pimentel (2001): Multibeam accuracy tests at dry dock. Hydro International, 5(7): 29-31.

Ashley, G.M. (1990): Classification of large-scale subaqueous bedforms: A new look at an old problem. Journal of Sedimentary Petrology, 60(1): 160-172.

Baas, J.H. (1994): A flume study on the development and equilibrium morphology of current ripples in very fine sand. Sedimentology, 41: 185-209.

Baas, J.H. (1999): An empirical model for the development and equilibrium morphology of current ripples in fine sand. Sedimentology, 46: 123-138.

Bagnold, R.A. (1966): An approach to the sediment transport problem from general physics. U.S. Geological Survey Professional Paper, 422-I, 37 pp.

Bartholdy, J. (2000): Processes controlling import of fine-grained sediment to tidal areas: a simulation model. In: Pye, K. and J.R.L. Allen (editors) Coastal and Estuarine Environments: Sedimentology, geomorphology and geoarchaeology. Geological Society, London, Special Publications, 175, pp. 13-29.

Bartholdy, J. and S. Folving (1986): Sediment classification and surface type mapping in the Danih Wadden Sea by remote sensing. Netherlands Journal of Sea Research, 20(4): 337-345.

Bartholdy, J., B. Hasholt, M. Pejrup (1991): Sediment transport within the drainage area of River Ribe Å. Danish Journal of Geography, 91: 1-10.

Bartholdy, J. and D. Anthony (1998): Tidal dynamics and seasonal dependent import and export of fine-grained sediment through a backbarrier tidal channel of the Danish Wadden Sea. In: Alexander, C., R.A. Davis and V.J. Henry (editors) Tidalities: Processes and Products. SEPM Special Publication, 61, pp. 43-52.

Bartholdy, J, A. Bartholomae and B.W. Flemming (2002): Grain-size control of large compound flow-transverse bedforms in a tidal inlet of the Danish Wadden Sea. Marine Geology, 188: 391-413.

Bartholdy, J., C. Christiansen and H. Kunzendorf (2004): Long term variations in backbarrier salt marsh deposition on the Skallingen peninsula – the Danish Wadden Sea. Marine Geology, 203: 1-21.

Bartholdy, J., B.W. Flemming, A. Bartholomä, V.B. Ernstsen (2005): Flow and grain size control of depth-independent simple subaqueous dunes. Journal of Geophysical Research, 110(F04S16): 12 pp.

Bastos, A.C., D. Paphitis and M.B. Collins (2004): Short-term dynamics and maintenance processes of headland-associated sandbanks: Shambles Bank, English Channel, UK. Estuarine, Coastal and Shelf Science, 59(1): 33-47.

Bennett, S.J. and J.L. Best (1995): Mean flow and turbulence structure over fixed, two-dimensional dunes: implications for sediment transport and bedform stability. Sedimentology, 42: 491-513.

Berlijn, R.C. (2003): 'Tricolor' salvage using Long Range Kinematic GPS. Hydro International, 7(8): 39-41.

Best, J. (2005): Kinematics, topology and significance of dune-related macroturbulence: some observations from the laboratory and field. Special Publications International Association Sedimentology, 35: 41-60.

Boothroyd, J.C. and D.K. Hubbard (1974): Bed form Development and distribution pattern, Parker and Essex Estuaries, Massachusetts. Miscellaneous Paper 1-74, US Army, Corps of Engineers, Coastal Engineering Research Center, 39 pp.

Boothroyd, J.C. and D.K. Hubbard (1975): Genesis of bedforms in mesotidal estuaries. In: Cronin, L.E. (editor) Estuarine Research. Academic Press, New York, USA, pp. 217-234.

Brezina, J. (1979): Particle size and settling rate distributions of sand-sized materials. 2nd European Symposium on Particle Characterisation (PARTEC), Nürnberg, West Germany, 44 pp.

Carling, P.A., E. Gölz, H.G. Orr and A. Radecki-Pawlik (2000a): The morphodynamics of fluvial sand dunes in the River Rhine, near Mainz, Germany. I. Sedimentology and morphology. Sedimentology, 47: 227-252.

Carling, P.A., J.J. Williams, E. Gölz and A.D. Kelsey (2000b): The morphodynamics of fluvial sand dunes in the River Rhine, near Mainz, Germany. II. Hydrodynamics and sediment transport. Sedimentology, 47: 253-278.

Cartwright, D.E. and A.H. Stride (1958): Large sand waves near the edge of the continental shelf. Nature, 181(4601): 41.

Christiansen, C., J. Bartholdy and H. Kunzendorf (2002): Effects of morphological changes on metal accumulation in a salt marsh sediment of the Skallingen peninsula, Denmark. Wetlands Ecology and Management, 10: 11-23.

Christiansen, M.B. and R. Davidson-Arnott (2004): Rates of landward sand transport over the foredune at Skallingen, Denmark and the role of dune ramps. Danish Journal of Geography, 104: 31-43.

Colombini, M. (2004): Revisiting the linear theory of sand dune formation. Journal of Fluid Mechanics, 502: 1-16.

Dalrymple, R.W. (1984): Morphology and internal structure of sandwaves in the Bay of Fundy. Sedimentology, 31: 365-382.

Dalrymple, R.W., R.J. Knight and J.J. Lambiase (1978): Bedforms and their hydraulic stability relationships in a tidal environment, Bay of Fundy, Canade. Nature, 275: 100-104.

Dalrymple, R.W. and R.N. Rhodes (1995): Estuarine dunes and bars. In: Perillo, G.M.E. (editor) Geomorphology and Sedimentology of Estuaries. Developments in Sedimentology, 53, Elsevier Science, pp. 359-422.

Darwin, G. M (1883): On the formation of ripple-mark in sand. Proceedings of the Royal Society of London, 36, pp. 18-43.

Dinehart, R.L. (2002): Bedform movement recorded by sequential single-beam surveys in tidal rivers. Journal of Hydrology, 258: 25-39.

DSNP (1999): Aquarius 5000 Series USER'S MANUAL. Dassault Sercel Navigation Positioning (DSNP), 0311374 Rev B.

Edwards, S.J., P.A. Cross, J.B. Barnes and B. Betaille (1999): A methodology for benchmarking real-time kinematic GPS. Survey Review, 35(273): 163-174.

Eeg, J. (1998): On the estimation of standard deviations in multibeam soundings. The Hydrographic Journal, 89: 9-13.

Einstein, H.A. (1950): The bed-load function for sediment transportation in open channel flows. U.S. Department of Agriculture, Technical Bulletin, 1026, 71 pp.

Engel, P. and Y.L. Lau (1980): Computation of bedload using bathymetric data. Journal of the Hydraulics Division, 106: 369-380.

Engel, P. and Y.L. Lau (1981): Bed load discharge coefficient. Journal of the Hydraulics Division, 107: 1445-1454.

Engelund, F.A. (1966): Hydraulic resistance of alluvial streams. Journal of the Hydraulics Division, 92(HY2): 315-326.

Engelund, F.A. and E. Hansen (1972): A monograph on sediment transport in alluvial streams. Technical Press, Copenhagen, 62 pp.

Engelund, F. and J. Fredsøe (1974): Transition from dunes to plane bed in alluvial channels. Series Paper, 4, Technical University of Denmark, Copenhagen, Denmark, 56 pp.

Engelund, F.A. and J. Fredsøe (1976): A sediment transport model for straight alluvial channels. Nordic Hydrology, 7: 293-306.

Ernstsen, V. B., R. Noormets, C. Winter, A. Bartholomä, B.W. Flemming and J. Bartholdy (2004): Development of subaqueous barchan dunes due to lateral grain size variability. In: Hulscher, S., T. Garlan, and D. Idier (editors) Marine Sandwave and River Dune Dynamics, 2nd International Workshop, 1-2 April 2004, University of Twente, Enschede, the Netherlands, pp. 80-87.

Ernstsen V.B., R. Noormets, C. Winter, D. Hebbeln, A. Bartholomä, B.W. Flemming and J. Bartholdy (2005): Development of subaqueous barchanoid-shaped dunes due to lateral grain size variability in a tidal inlet channel of the Danish Wadden Sea. Journal of Geophysical Research, 110(F04S): 13 pp.

Ernstsen, V.B., R. Noormets, D. Hebbeln, A. Bartholomä and B.W. Flemming: On the state of the art of high-accuracy bathymetric surveys in shallow coastal water: Evaluation of high-resolution multibeam echo sounding coupled with high-accuracy positioning. Geo-Marine Letters (submitted).

Featherstone, W.E. and M.P. Stewart (2001): Combined analysis of Real-Time Kinematic GPS equipment and its users for height determination. Journal of Surveying Engineering, 127(2): 31-51.

Fenster, M.S. and D.M. FitzGerald (1996): Morphodynamics, stratigraphy, and sediment transport patterns of the Kennebec River estuary, Maine, USA. Sedimentary Geology, 107: 99-120.

Flemming, B.W. (1978): Underwater sand dunes along the southeast African continental margin – observations and implications. Marine Geology, 26: 177-198.

Flemming, B.W. (1988): Zur Klassifikation subaquatischer, strömungstransversaler Transportkörper. Bochumer geologische und geotechnische Arbeiten, 29: 44-47.

Flemming, B.W. and R.A. Davis Jr. (1992): Dimensional adjustment of subaqueous dunes in the course of a spring-neap semicycle in a mesotidal backbarrier channel environment (German Wadden Sea, southern North Sea). In: Flemming, B.W. (editor) Tidal Clastics 93, Courier Forschungsinstitut Senckenberg, 151, pp. 28-30.

Flemming, B.W. (2000a): The role of grain size, water depth and flow velocity as scaling factors controlling the size of subaqueous dunes. In Trentesaux, A. and T. Garlan (editors) Marine Sandwave Dynamics, Proceedings of an international workshop held in Lille, France, 23 and 24 March 2000, pp. 55-60.

Flemming, B.W. (2000b): On the dimensional adjustment of subaqueous dunes in response to changing flow conditions: a conceptual process model. In Trentesaux, A. and T. Garlan

(editors) Marine Sandwave Dynamics, Proceedings of an international workshop held in Lille, France, 23 and 24 March 2000, pp. 61-67.

Folk, R.L. (1974): Petrology of sedimentary rocks. Hemphill, 182 pp.

Folk, R.L. and W.C. Ward (1957): Brazos river bar: a study in the significance of grain size parameters. Journal of Sedimentary Petrology, 27(1): 3-26.

Fredsøe, J. (1975): The friction factor and height-length relationships in flow over dune-covered bed. Progress Report, 37, Technical University of Denmark, Copenhagen, Denmark, pp. 31-36.

Fredsøe, J. (1982): Shape and dimensions of stationary dunes in rivers. Journal of the Hydraulics Division, 108(HY8): 932-947.

Fredsøe, J. and R. Deigaard (1992): Mechanics of Coastal Sediment Transport. Advanced Series on Ocean Engineering, 3, World Scientific, 369 pp.

General Oceanics Inc. (2000): Model 6011 MK II Niskin winged current meter, operating manual, ram memory. General Oceanics Inc., Miami, Florida, USA, 33 pp.

Gilbert, K.G. (1914): Transportation of débris by running water. United States Geological Survey, Professional Paper, 86, 263 pp.

Gounon, R. and F. Erceau (1998): The LRK® real-time kinematic technique for a centimetre accuracy domain up to 40km. The Hydrographic Journal, 88: 3-6.

Graham, N., E.G. Jones and D.G. Reid (2004): Review of technological advances for the study of fish behaviour in relation to demersal fishing trawls. ICES Journal of Marine Science, 61: 1036-1043.

Guy, H.P., D.B. Simons and E.V. Richardson (1966): Summary of alluvial channel data from flume experiments, 1956-61. United States Geological Survey, Professional Paper 462-I, 96 pp.

Ha, H.K. and S.K. Chough (2003): Intermittent turbulent events over sandy current ripples: a motion-picture analysis of flume experiments. Sedimentary Geology, 161: 295-308.

Haga, K.H., F. Pøhner and K. Nielsen (2003): Testing multibeam echo sounders versus IHO S-44 Requirements. International Hydrographic Review, 4(2): 31-40.

Harbor, D.J. (1998): Dynamics of bedforms in the lower Mississippi River. Journal of Sedimentary Research, 68(5): 750-762.

Hare, R., B. Calder and L. Alexander (2004): Multi-beam error management – New data processing trends in hydrography. Hydro International, 8(8): 6-9.

Harris, P.T. and M.R. Jones (1988): Bedform movement in a marine delta: air photo interpretations. Geological Magazine, 125(1): 31-49.

Harris, P.T., C.B. Pattiaratchi, A.R. Cole and J.B. Keene (1992): Evolution of subtidal sandbanks in Moreton Bay, eastern Australia. Marine Geology, 103: 225-247.

Hawkins, A.B. and M.J. Sebbage (1972): The reversal of sand waves in the Bristol Channel. Marine Geology, 12: M7-M9.

Heaps, W. (2004): Standards for the calibration of multibeam echosounders, are new standards required? The Hydrographic Journal, 111: 26-27.

Hennings, I, D. Herbers, K. Prinz and F. Ziemer (2004): On waterspouts related to marine sandwaves. In: Hulscher, S., T. Garlan, and D. Idier (editors) Marine Sandwave and River Dune Dynamics, 2nd International Workshop, 1-2 April 2004, University of Twente, Enschede, the Netherlands, pp. 88-95.

Hine, A.C. (1975): Bedform distribution and migration patterns on tidal deltas in the Chatham Harbor estuary, Cape Cod, Massachusettes. In: Cronin, L.E. (editor) Estuarine Research, 2, Geology and Engineering. Academic Press, New York, pp. 235-252.

Hoekstra, P., P. Bell, P. van Santen, N. Roode, F. Levoy and R. Whitehouse (2004): Bedform migration and bedload transport on an intertidal shoal. Continental Shelf Research, 24(11): 1249-1269.

Hughes-Clarke, J.E., L.A. Mayer and D.E. Wells (1996): Shallow-water imaging multibeam sonars: A new tool for investigating seafloor processes in the coastal zone and on the continental shelf. Marine Geophysical Researches, 18: 607-629.

Hulscher, S.J.M.H. (1996): Tidal-induced large-scale regular bed form patterns in a three-dimensional shallow water model. Journal of Geophysical Research, 101(C9): 20727-20744.

Hulscher, S.J.M.H. and C.M. Dohmen-Janssen (2005): Introduction to special section on marine sand wave and river dune dynamics. Journal of Geophysical Research, F04(S01): 6 pp.

Idier, D., A. Ehrhold and T. Garlan (2002): Morphodynamique d'une dune sous-marine du detroit du pas de Calais: Morphodynamics of an undersea sandwave of the Dover Straits. Comptes Rendus Geosciences 334(15): 1079-1085.

International Hydrographic Organization (1998): IHO standards for hydrographic surveys, Special Publication, 44, 4th Edition, 23 pp.

IXSEA OCEANO (2003): User guide OCTANS SURFACE. February 2003, MU/OCTS/003, Edition F.

Jackson, R.G. (1976): Large scale ripples of the lower Wabash River. Sedimentology, 23: 593-623.

Kennedy, J. F. (1963): The mechanics of dunes and antidunes in erodible-bed channels. Journal of Fluid Mechanics, 16(4): 521-544.

Kennedy, J.F. (1969): The formation of sediment ripples, dunes, and antidunes. Annual Review of Fluid Mechanics, 1: 147-168.

Kenyon, N.H. and R.H. Belderson (1973): Bed forms of the Mediterranean undercurrent observed with side-scan sonar. Sedimentary Geology, 9: 77-99.

Knaapen, M.A.F. (2005): Sandwave migration predictor based on shape information. Journal of Geophysical Research, 110(F04S11): 9 pp.

Knaapen, M.A.F. and S.J.M.H. Hulscher (2002): Regeneration of sand waves after dredging. Coastal Engineering, 46: 277-289.

Knebel, H.J. (1989): Modern sedimentary environments in a large tidal estuary, Delaware Bay. Marine Geology, 86: 119-136.

Komarova, N.L. and S.J.M.H. Hulscher (2000): Linear instability mechanisms for sand wave formation. Journal of Fluid Mechanics, 413: 219-246.

Komarova, N.L. and A.C. Newell (2000): Nonlinear dynamics of sand banks and sand waves. Journal of Fluid Mechanics, 415: 285-321.

Kostaschuk, R., M.A. Church and J.L. Luternauer (1989): Bed-material, bedforms and bed load in a salt-wedge estuary – Fraser River, British Columbia. Canadian Journal of Earth Science, 26: 1440-1452.

Kostaschuk, R.A. and S.A. Ilersich (1995): Dune geometry and sediment transport: Fraser River, British Columbia. In: Hickin, E.J. (editor) River Geomorphology, Wiley, pp. 19-36.

Kostaschuk, R. and P. Villard (1996): Flow and sediment transport over large subaqueous dunes: Fraser River, Canada. Sedimentology, 43: 849-863.

Kostaschuk, R., P. Villard and J. Best (2004): Measuring velocity and shear stress over dunes with acoustic Doppler profiler. Journal of Hydraulic Engineering, 130(9): 932-936.

Kostaschuk, R. and J. Best (2005): Response of sand dunes to variations in tidal flow: Fraser Estuary, Canada. Journal of Geophysical Research, 110(F4S04): 11 pp.

Kostaschuk, R.A., J.L. Best, P.V. Villard, J. Peakall and M. Franklin (2005): Measuring flow velocity and sediment transport with an acoustic Doppler current profiler. Geomorphology, 65: 25-37.

Krögel, F. and B.W. Flemming (1998): Evidence for temperature-adjusted grain-size distributions in the back barrier tidal flats of the East Frisian Waddensea (southern

North Sea). In: Alexander, C., R.A. Davis and V.J. Henry (editors) Tidalities: Processes and Products. SEPM Special Publication, 61, pp. 31-44.

Kuijpers, A., B. Hansen, V. Hühnerbach, B. Larsen, T. Nielsen and F. Werner (2002): Norwegian Sea overflow through the Faroe Shetland gateway as documented by bedforms. Marine Geology, 188: 147-164.

Langhorne, D.N. (1982): A study of the dynamics of a marine sandwave. Sedimentology, 29: 571-594.

Leclair, S.F. (2002): Preservation of cross-strata due to the migration of subaqueous dunes: an experimental investigation. Sedimentology, 49: 1157-1180.

Lonsdale, P. and B. Malfait (1974): Abyssal dunes of foraminiferal sand on the Carnegie Ridge. Geological Society of America Bulletin, 85: 1697-1712.

Ludwick, J. C. (1972). Migration of tidal sand waves in ChesapeakeBay Entrance. In: Swift, D.J.P., D.B. Duane and O.H. Pilkey (editors) Shelf Sediment Transport: Process and Pattern. Dowden, Hutchinson & Ross, Inc., Stroudsburg, Pennsylvania, USA, pp. 377-410.

Lund-Hansen, L.C., E. Larsen, T.K. Jensen, K. Mouritsen, C. Christiansen, T.J. Andersen, and G. Vølund (2004): A new video and digital camera system for studies of the dynamics of microtopographic features on tidal flats. Marine Georesources and Geotechnology, 22: 115-122.

Lutz, P. and R. Gounon (2001): THALES Navigation's LRK®, an improved RTK solution for long baselines: technique, applications and field results. Paper presented at The Satellite Division of the Institute of Navigation 14th International Technical Meeting.

Maddux, T.B., J.M. Nelson and S.R. McLaren (2003a): Turbulent flow over three-dimensional dunes: 1. Free surface and flow response. Journal of Geophysical Research, 108(F1): 20 pp.

Maddux, T.B., J.M. Nelson and S.R. McLaren (2003b): Turbulent flow over three-dimensional dunes: 2. Fluid and bed stresses. Journal of Geophysical Research, 108(F1): 17 pp.

McLaren, P. (1981): An interpretation of trends in grain size measures. Journal of Sedimentary Petrology, 51(2): 0611-0624.

McLaren, P. and D. Bowles (1985): Bed-load transport. Report 2nd Meeting, International Association of Hydraulic Structures Research, Stockholm, pp. 39-64.

McLean, S.R., J.M. Nelson and S.R. Wolfe (1994): Turbulence structure over two-dimensional bed forms: Implications for sediment transport. Journal of Geophysical Research, 99: 12729-12747.

McLean, S.R., J.M. Nelson and R.L. Shreve (1996): Flow-sediment interactions in separating Flows over Bedforms. In: Ashworth, P.J., S.J. Bennett, J.L. Best and S.J. McLelland (editors) Coherent flow structures in open channels. John Wiley & Sons Ltd., pp. 203-227.

Meyer-Peter, E. and R. Müller (1948): Formula for bed-load transport. Proceedings International Association Hydraulic Structures Research, Stockholm, pp. 39-64.

Müller, A. and A. Gyr (1996): Geometrical analysis of the feedback between flow, bedforms and sediment transport. In: Ashworth, P.J., S.J. Bennett, J.L. Best and S.J. McLelland (editors) Coherent flow structures in open channels. John Wiley & Sons Ltd., pp. 237-247.

Nasner, H. (1978): Time-lag of dunes for unsteady flow conditions. In: Proceedings of the 16th International Conference on Coastal Engineering (ICCE), American Society of Civil Engineers (ASCE), Hamburg, Germany, pp. 1801-1817.

Nielsen, N. (1935): Eine Methode zur exakten Sedimentationsmessung. Meddelelser fra Skalling Laboratoriet, I, 97 pp.

Nielsen, P. (1992): Coastal Bottom Boundary Layers and Sediment Transport. Advanced Series on Ocean Engineering, 3, World Scientific, 352 pp.

Nielsen, N. and J. Nielsen (2002): Vertical Growth of a Young Back Barrier Salt Marsh, Skallingen, SW Denmark. Journal of Coastal Research, 18(2): 287-299.

Ogink, H. (1988): Hydraulic roughness of bedforms. Delft Hydraulics, Report M2017, Delft, The Netherlands.

Onslow, R.J., N.H. Thomas, R.J.S. Whitehouse (1993): Vorticity and sandwaves: the dynamics of ripples and dunes. In: Clifford, N.J., J.R. French and J. Hardisty (editors) Turbulence: Perspectives on flow and sediment transport. John Wiley & Sons Ltd., pp. 279-293.

Pickrill, R.A. and B.J. Todd (2003): The multiple roles of acoustic mapping in integrated ocean management, Canadian Atlantic continental margin. Ocean & Coastal Management, 46: 601-614.

Raudkivi, A.J. (1976): Loose Boundary Hydraulics. Elsevier, New York, USA, 397 pp.

RDI (1996) Acoustic Doppler Current Profiler, Principles of Operation, A Practical Primer, Second Edition for Broadband ADCPs. RD Instruments, San Diego, California, USA, 57 pp.

Reichel G (1998) Suspended sediment monitoring: use of acoustic Doppler current profiler. In: Herschy, R.W. and R.W. Fairbridge (editors) Encyclopaedia of Hydrology and Water Resource. Springer, New York, pp. 638-644.

Reineck, H.-E. (1963). Sedimentgefüge im Bereich der südlichen Nordsee. Abhandlungen der Senckenbergischen Naturforschenden Gesellschaft, 505: 5-61.

RESON Inc. (1999): RESON Patch Test OPERATOR'S HANDBOOK Version 1.21.

RESON Inc. (2000a): RESON PPS Box OPERATORS'S HANDBOOK Version 1.00.

RESON Inc. (2000b): 6042 Version 7 QuickStart Handbook (Version 9.00).

RESON Inc. (2001): SeaBat 8125 Ultra High Resolution Focused Multibeam Echosounder System OPERATOR'S MANUAL Version 2.20.

Richards, K.J. (1980): The formation of ripples and dunes on an erodible bed. Journal of Fluid Mechanics, 99: 597-618.

Rubin, D.M. and D.S. McCulloch (1979): The movement and equilibrium of bedforms in Central San Francisco Bay. Proceedings of the 58th Annual Meting of the Pacific Division of the American Association for the Advancement of Science, San Francisco State University, San Francisco, California, USA, p. 97-113.

Rubin, D.M. and D.S. McCulloch (1980): Single and superimposed bedforms: A synthesis of San Francisco Bay and flume observations. Sedimentary Geology, 26: 207-231.

Salsman, G.G., W.H. Tolbert and R.G. Villars (1966): Sand ridge migration in St. Andrews Bay, Florida. Marine Geology, 4: 11-19.

Satalich, J. and R. Ricketson (1998): Field test of Trimble 4000 Real-Time Kinematic GPS survey system. Journal of Surveying Engineering, 124(1): 40-48.

Scarfe, B. (2002): Measuring water level corrections (WLC) using RTK GPS. The Hydrographic Journal, 104: 18 pp.

Seibt-Winckler, A., M. Heineke and R. Riethmüller (2002): Suitability of multibeam echosounder for underwater bottom topography mapping in shallow waters. The Hydrologic Society, Hydro 2002 Proceedings, 13th Biennial International Hydrographic Symposium, Kiel Germany, 8-10 October 2002, pp. 350-366.

Simons, D.B. and E.V. Richardson (1961): Forms of bed roughness in alluvial channels. Journal of the Hydraulics Division, 87(HY3): 87-105.

Simons, D.B., E.V. Richardson and C.F. Nordin Jr. (1965): Bedload equation for ripples and dunes. US Goelogical Survey Professional Paper, 462-H, 9 pp.

Soulsby, R.L. (1990): Tidal-current boundary layers. In: LeMehautè, B. and D.M. Hanes (editors) The Sea, Vol. 9B, Ocean Engineering Science, Wiley, New York.

Soulsby, R. (1997): Dynamics of Marine Sands: A Manual for Practical Applications. Thomas Telford, London, UK, 249 pp.

Soulsby, R. and R.J.S.W. Whitehouse (1997): Threshold of sediment motion in coastal environments. Proceedings of the Pacific Coasts and Ports '97 Conference, Christchurch, 1, University of Canterbury, New Zealand, pp. 149-154.

Southard, J.B. (1991): Experimental determination of bed-form stability. An Annual Review of Earth and Planetary Sciences, 19: 423-455.

Sukhodolov, A., M. Thiele and H. Bungartz (1998): Turbulence structure in a river reach with sand bed. Water Resources Research, 34(5): 1317-1334.

Terwindt, J.H.J. (1971): Sand waves in the Southern Bight of the North Sea. Marine Geology, 10: 51-67.

van den Berg, J.H. (1987): Bedform migration and bed-load transport in some rivers and tidal environments. Sedimentology, 34: 681-698.

van den Berg, J.H. and A. van Gelder (1993): A new bedform stability diagram, with emphasis on the transition of ripples to plane bed in flows over fine sand and silt. Special Publications International Association Sedimentology, 17: 11-21.

van Rijn, L.C. (1982): Equivalent roughness of alluvial bed. Journal of the Hydraulics Division, 108(HY10): 1215-1218.

van Rijn, L.C. (1984a): Sediment transport, part I: Bed load transport. Journal of Hydraulic Engineering, 110(10): 1431-1456.

van Rijn, L.C. (1984b): Sediment transport, part III: Bed forms and alluvial roughness. Journal of Hydraulic Engineering, 110(12): 1733-1754.

van Rijn, L.C. (1993): Principles of sediment transport in rivers, estuaries and coastal seas. Aqua Publications, Amsterdam, The Netherlands.

Villard, P.V. and M. Church (2003): Dunes and associated sand transport in a tidally influenced sand-bed channel: Fraser River, British Columbia. Canadian Journal of Earth Science, 40: 115-130.

Vinther, N., J. Nielsen and T. Aagaard (2004): Cyclic sand bar migration on a spit-platform in the Danish Wadden Sea – spit-platform morphology related to variations in water level. Journal of Coastal Research, 20(3): 672–679.

Wells, D.E. and D. Monahan (2002): IHO S44 standards for hydrographic surveys and the variety of requirements for bathymetric data. The Hydrographic Journal, 104: 9-16.

Wienberg, C., J. Dannenberg and D. Hebbeln (2004): The fate of dumped sediments monitored by a high-resolution multibeam echosounder system, Weser Estuary, German Bight. Geo-Marine Letters, 24: 22-31.

Wilbers, A.W.E. and W.B.M. ten Brinke (2003): The response of subaqueous dunes to floods in sand and gravel bed reaches of the Dutch Rhine. Sedimentology, 50: 1013-1034.

Williams, J.J., P.S. Bell, J.D. Humphery, P.J. Hardcastle and P.D. Thorne (2003a): New approach to measurement of sediment processes in a tidal inlet. Continental Shelf Research, 23: 1239-1254.

Williams, J.J., P.S. Bell and P.D. Thorne (2003b): Field measurements of flow fields and sediment transport above mobile bed forms. Journal of Geophysical Research, 108(C4): 36 pp.

Yalin, M.S. (1977): Mechanics of Sediment Transport. Pergamon Press, Oxford, UK, 298 pp.

Yalin, M.S. (1992): River Mechanics. Pergamon Press, Oxford, UK, 220 pp.

Yalin, M.S. and E. Karahan (1979): Inception of sediment transport, Journal of the Hydraulics Division, 105: 1433-1443.